Modeling and Fault Diagnosis of Automotive Lead-Acid Batteries

Submitted to:
The Engineering Honors Committee
119 Hitchcock Hall
College of Engineering
The Ohio State University
Columbus, OH 43210

by

Ahmed Fasih

222 W Lane Avenue, #1007
Columbus, OH 43201

Dr Giorgio Rizzoni, Advisor

April 2, 2006

Abstract

In a bid to perform model-based diagnostics on the electrical network of an automobile, experimental work and analysis was conducted to model an automotive lead-acid battery over the domain in which one is expected to operate. First, a thorough literature review discusses past attempts at modeling, as well as state and parameter estimation. Also, the literature on the aging and failure modes of batteries is presented. Next, the model selected is described, consisting of a locally linear time-invariant system approximation of a globally nonlinear time-variant battery. To obtain the parameters best enabling this approximation, a series of experiments were performed on a battery, the methodologies of which are detailed. Finally, the details of parameter extraction are also presented, along with their results.

Acknowledgments

Many warm thanks to Drs Rizzoni and Guezennec for their support and inspiration. To Jim Shively, Annalisa Scacchioli, Pierluigi Pisu, and Shawn Midlam-Mohler, and all the research staff and faculty at the Center for Automotive Research. Also to fellow students and colleagues, Zakaria Chehab, Weiwu Li, John Neal, and Lorenzo Serrao. And Don Butler, Frank Ohlemacher, and Darrin Orr. And of course Drs Moses, Cruz, and Utkin for one heck of an Autumn quarter.

And naturally, many thanks to family, and the friends made over the course of this project, especially in ECE and Challenge X.

Datastore

All the data and programs used in this thesis will be collected and placed on a CD-ROM or a USB drive. This will be referred to as the thesis datastore through this work, and will be deposited with the Battery group at the Center for Automotive Research (CAR), at The Ohio State University. The thesis will refer to directories in this datastore, and will serve as a lengthy user manual to the software and data.

Table of contents

1 Introduction

This chapter will provide background on the topic of research, present its motivation and scope, and summarize its current state with a literature review.

1.1 The automotive electrical network

An automobile's electrical network consists of an alternator, a battery, a voltage regulator, and several electrical and electronic loads (fans, computers, motors, gages, etc.). The alternator is an electric generator that is physically coupled to the engine and can be controlled by the voltage regulator to convert mechanical engine power to electric power for on-board electrical loads, as they switch on and off. Standard modern consumer vehicles ship with alternators that can provide up to 80 to 100 A; it may therefore be understood that these vehicles are designed to adequately power loads that in total draw this much current.

The primary function of the battery in this network is to buffer the output of the alternator by absorbing any high-frequency pulses it may generate and by meeting transients in current draw while the alternator readjusts to meet such a new load. Furthermore, the battery powers the starter motor that cranks the engine to start it.

The average driving cycle therefore consists of: the battery providing very high current (more than 600 A) for less than a second to drive the starter motor to start the engine and immediately thereafter powers all electrical loads. The alternator, in a matter of seconds, begins to generate the current drawn by these loads and the battery's discharge current decreases. As the vehicle is driven, the battery lapses to a quiescent state where it discharges only to meet transients in current requested (for example, when the air conditioner is turned on, it will take the alternator a few seconds to meet this large load; meanwhile, the battery will provide the current needed to power it) but otherwise is steadily recharged.

1.2 Lead-acid battery principles of operation

The battery as described has been an integral part of the automotive electrical network for many decades and the fundamental lead-acid technology has not changed. It consists of essentially two electrodes immersed in sulfuric acid electrolyte. Some modern advances include adding of valves to the battery and immobilizing the electrolyte (either by being absorbed by an absorbent glass mat, AGM, or by gelling using silicon dioxide [1]), allowing it to be used in any orientation, and also allowing it to be "sealed," making it maintenance-free. They cannot be hermetically sealed because by necessity they have vents to allow discharge of gas during faults, and so these batteries are called sealed valve-regulated lead-acid (VRLA) and are the kind generally used in automotive starting, lighting, and ignition (SLI) applications.

It may be said that the main purpose of the battery in a car is to start the engine; only after this has been accomplished can the battery's secondary roles of providing power during high transient loads and maintaining charge be fulfilled. Therefore, the design of lead-acid batteries for orthodox automotive SLI applications (i.e., not for hybrid electric vehicles, forklifts, or golfcarts, etc.) maximizes power density, cycle life, and ease of manufacture. Ability to perform at high levels of discharge is not important, and therefore it is considered unhealthy to leave a battery at any level of discharge. [2] details these design and construction tradeoffs, but an important resultant consideration is that plates and separators must be thin and porous to maximize the amount of current that can be delivered during cranking.

Returning to the general operating principles: the negative terminal is the electrode attached to lead-containing spongy active mass, whereas the positive terminal is attached to a porous grid containing granules of metallic lead dioxide. These two materials are arranged in a matrix and are separated and immersed in concentrated sulfuric acid electrolyte to provide the mobile positive and negative charges. The matrix comprises a cell, several of which are placed in series to form the battery [6]. Modern SLI batteries contain six cells, each with a nominal voltage

of 2.1 V [5].

The redox reactions occurring at the two electrodes during *discharge* are given below [2]. The charging reactions are exactly reversed.

- Positive electrode:
  - $PbO_2 + 4H^+ + 2e^- \rightarrow Pb^{2+} + 2H_2O$
  - $Pb^{2+} + SO_4^{2-} \rightarrow PbSO_4$
- Negative electrode:
  - $Pb \rightarrow Pb^{2+} + 2e^-$
  - $Pb^{2+} + SO_4^{2-} \rightarrow PbSO_4$

(1)

In words, during discharge, the positive electrode accepts electrons that the negative one gives up (recalling that electric current is the flow of hypothetical positive charges). In this discharge case, the positive electrode is the anode because it is being oxidized; the negative electrode is the cathode because it is doing the oxidization, i.e., being reduced. By convention, then, this is reversed for the charging case. It may be noted that the movement of charge clearly uses the dissolving and precipitating of charge-carrying ions through the electrolyte.

From this electrochemical view of the battery, we examine some of the higher-level characteristics of batteries that are used to describe their behavior.

1.3 Overview of battery characteristics

This section will discuss the parameters and characteristics of all batteries, and specific idiosyncrasies of lead-acid batteries, as they impact the modeling process. All the modeling performed is done with these characteristics and behaviors in mind.

1.3.1 Rechargeable vs. non-rechargeable

A battery designed to allow the charging chemical reaction efficiently is called a secondary battery, as it may be recharged by applying current. A primary battery is one that is not rechargeable. All automotive batteries are, therefore, secondary batteries.

1.3.2 Capacity

The amount of capacity that a battery pack can store is measured in units of Ampere-hours (A-h). This unit of measure is the amount of electricity delivered at one Ampere over one hour, and a capacity defined as such indicates the amount of charge that can be drawn for some length of time before the battery is considered discharged. There is a fair amount of flexibility in what constitutes “completely discharged” and most manufacturers do not conform to any standard. Theoretically, for a battery rated at 10 A-h, a discharge current of 1 A should deplete the battery in 10 hours, much as a 10 A discharge would in 1 hour. However, these expectations can be extremely inaccurate due to the nonlinear behavior of available capacity as a function of discharge current (see Section 1.3.5 below; in short, the higher the discharge current, the less apparent capacity). This, in addition to the variability between manufacturers' definitions of capacity, make total capacity (and therefore, remaining capacity in a partially discharged battery) a tricky thing to measure.

In the world of automotive batteries, manufacturers will specify a *reserve capacity*, in units of minutes during which a fully-charged battery can be discharged at 25 A without the terminal voltage dropping below 10.5 V [8]. At this voltage, the battery is treated as completely discharged. Conventions like this are more often battery manufacturer-specific rather than battery type-specific, but we are fortunate to have a uniform method for automotive batteries. Therefore, a battery rated at 90 minutes reserve capacity is defined to have a capacity of 37.5 A-h: 25 Amperes · (90 minutes / 60) hours.

In research settings, a capacity test is done to quantify a battery's capacity. Such a test depends on the manufacturer to indicate how to best charge the battery to full capacity and for a minimum voltage under load. The battery is discharged at 10% of its rated capacity (.1 C, e.g., 5 A for a 50 A-h battery) until the voltage reaches this minimum voltage (which may be designated fully discharged). The low current enables the capacity to be determined by simple multiplication

of the current with discharge time because it precludes the majority of nonlinear effects such as internal heating. Figure 1 gives an example.

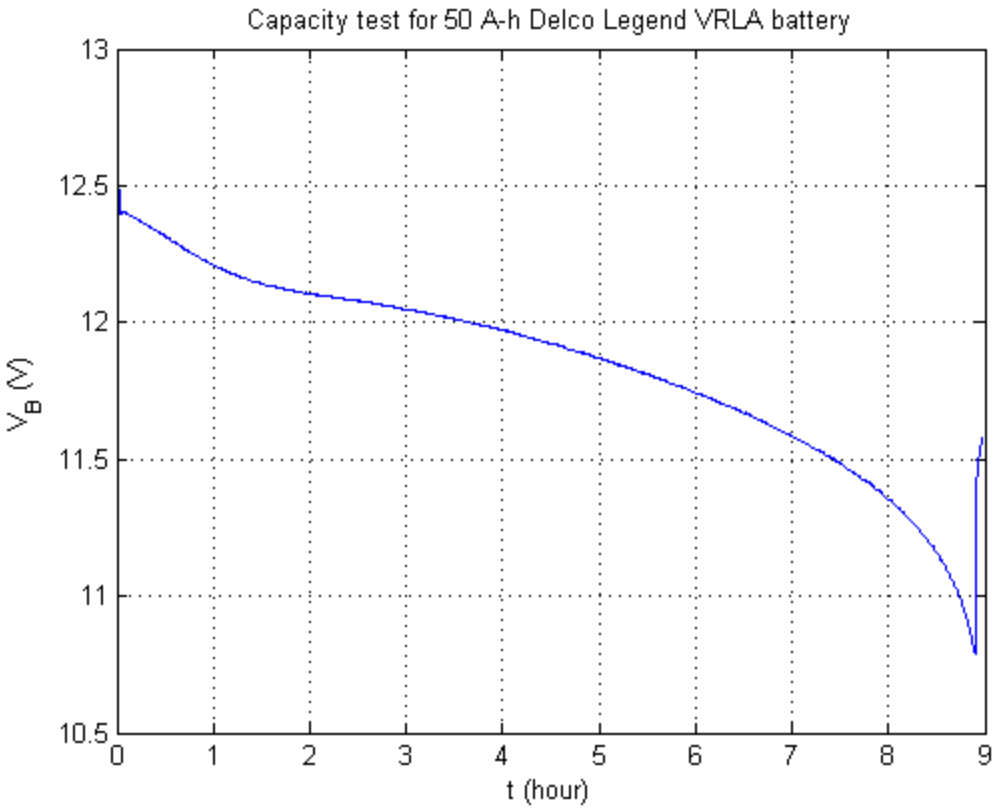

Figure 1: Example curve obtained from a laboratory capacity test

The voltage curve obtained by this test proves useful in understanding other battery effects because it represents how the battery's open-circuit voltage, the amount of potential-carrying ions saturating the electrodes, evolves as the battery is discharged.

Notice the rebound in voltage that happens when the discharge current is cut off; this will be explained below.

1.3.3 State of charge

State of charge (SOC) is simply a measure of how much current the battery can deliver after partial discharge or charge. It is an extremely difficult quantity to determine reliably and precisely due to the many nonlinear effects that exist in batteries. A major topic of research in the field is accurate and precise state of charge estimation and much theoretical and experimental

work has been done, without the problem being completely resolved. The term is introduced here, and will be brought up in subsequent sections as these nonlinearities are discussed, and a thorough literature review detailing its definition and estimation will be given in Section 2.2.

A major result of battery research has been, however, that a lead-acid battery' open-circuit voltage (no-load voltage in a relaxed state) is a linear function of its SOC [3]. Therefore, one of the most important aspects of a battery's operational behavior, the terminal voltage, is strongly influenced by state of charge, as is the amount of charge it can deliver before some threshold capacity is reached.

State of charge is a unitless number between 0 and 1, corresponding to percent. Note again that 0% SOC does not mean that the battery can no longer deliver any amount of current, only that the battery cannot go below this value without causing some kind of (possibly reversible) damage.

1.3.4 Surface charge

This is a major cause of nonlinearity in lead-acid batteries that does not exist in modern battery technologies such as nickel-metal hydrides. Surface charge refers to the phenomenon resulting from the plates comprising the positive and negative electrodes being of finite thickness; it causes a recently discharged battery to incorrectly appear to be dead (as indicated by terminal voltage) and a recently but incompletely charged battery to be fully charged ([9]).

The electrochemical reactions that store or produce electricity happen only at the interface of the electrode material and the electrolyte. Therefore, when the battery is being charged, charge is accumulating at the surface of the electrodes, and must diffuse into the plates of the electrodes. This diffusion process is much slower than diffusion of charge-carrying ions through the electrolyte that separates the electrodes because it happens in a solid.

Therefore, as a battery is charged, more and more surface charge accumulates; the higher

the charging current, the more surface charge accumulates. This causes the terminals of the battery to quickly reach a very high voltage, indicating that it is fully charged. Further charging will cause the battery to overcharge: the electrolyte will boil, the battery will vent, and the case may burst. However, if one allows the battery to relax for anywhere between 4 and 12 hours (we cite conventional mechanic wisdom here) and renew charging, the exact same pattern will repeat at the terminals of the battery. This is because the surface charge diffuses throughout the plate.

Conventionally, when a mechanic goes to check a battery's state of charge, she will allow it to relax for 4 to 12 hours, and then remove any surface charge by discharging the battery at approximately 33% of its rated capacity (or just 10 A) for 5 minutes. This will reduce the absolute SOC by 2% to 3%, but only the surfaces of the plates are discharged by this process. The majority of the charge remains locked inside the plates, after several hours of diffusion. Then she will allow the battery to relax for some 10 minutes and then take a terminal voltage reading and referring to a table. It is only after this process is done does the battery's open-circuit voltage linearly correlate to its state of charge.

Note that the relaxation time required for surface charge to disappear is much longer than the time conventionally given to a battery to reach open-circuit (hours instead of minutes). Surface charge will be important when modeling the charging behavior of SLI batteries, but based on discussion with nickel-metal hydride battery researchers, does not appear in different chemistries and technologies. Be this due to more advanced design or different design requirements remains an open question.

The existence of surface charge explains why smart battery chargers will taper down the charging voltage as the battery approaches higher states of charge. Some will in fact cycle down (stop charging) before resuming charging at low currents to attain the last few percent of charge.

There exists after discharge the same effect, but in reverse. Immediately following

discharge, the surface layers of the plates have a much lower concentration of charged chemical species than deeper in the plate. It may take several before charge is evenly distributed through the electrode, and so a voltage measured just after discharge will sag lower than actual open-circuit. This is sometimes called surface discharge.

Surface charge is not the only current-related nonlinearity of automotive lead-acid batteries. Another major effect is called the Peukert relationship between the battery discharge current and its remaining capacity.

1.3.5 Discharge current and the Peukert curve

The Peukert equation gives a relationship between immediately available capacity deliverable as a function of current. It is commonly modeled as

$$Q = K \cdot I^{1-n} \tag{2}$$

where Q, capacity, is measured in Ampere-hours, K and n are the Peukert constant and exponent (characteristic battery constant and the battery discharge rate sensitivity exponent), respectively, and I the current in Amperes. In words, it states that as the discharge current increases, the total capacity of the battery (in Ampere-hours), or the total energy delivered by the battery, decreases disproportionately.

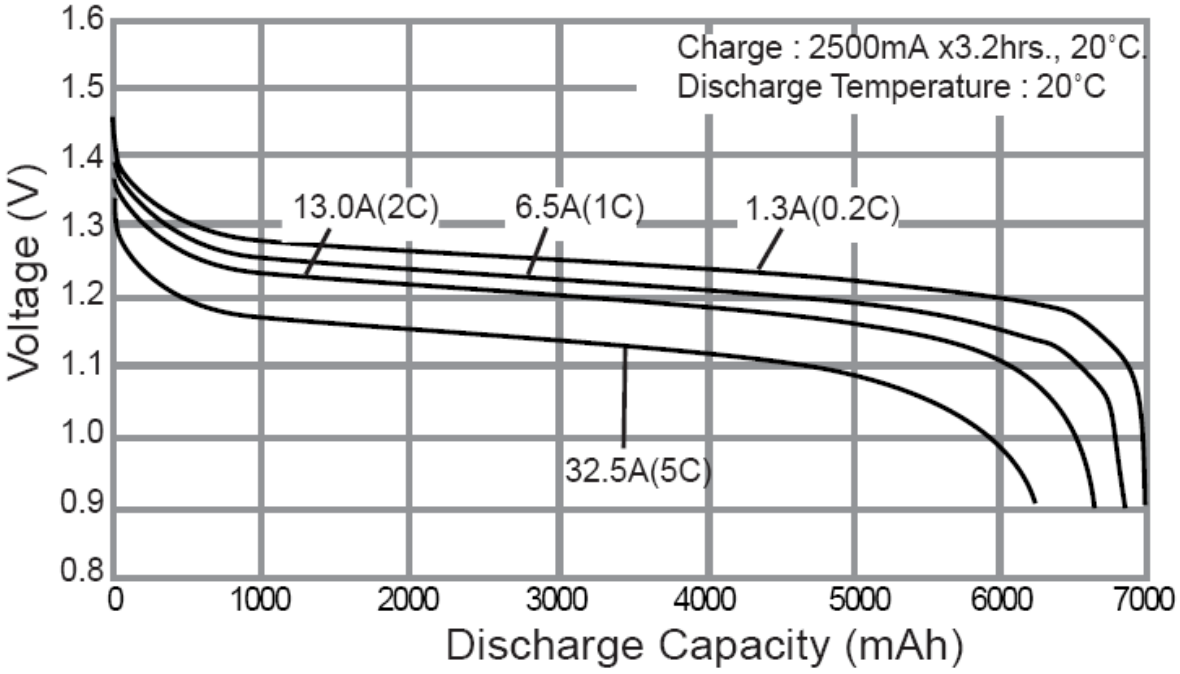

Figure 2: The Peukert effect in Panasonic nickel-metal hydride batteries [11]

The Peukert equation is a simple empirical curve-fit, and the exponential does not model any physical phenomenon. An example set of curves for Panasonic's nickel-metal hydride batteries is given in Figure 2 to illustrate this effect. The higher the discharge rate, the less total capacity could be withdrawn from the battery.

The Peukert effect is attributed to lower reactivity of the lead-containing active mass at higher discharge currents at lower states of charge by [3], but has also also been traditionally attributed to increased inefficiency caused by thermal effects at lower SOCs, e.g., by [7].

An important connection may be drawn between the Peukert effect and the voltage curve obtained from a capacity test (Section 1.3.2). When one is operating a battery at some state of charge between 0 and 1, the steady-state voltage at the terminals of the battery will follow a curve similar to the capacity test's curve: a sharp nonlinear initial drop followed by piecewise linear decreases and finally a sharp knee at complete discharge. If one loads the battery at high currents, the Peukert effect will cause the *apparent capacity to decrease*, and in effect *shift one's*

position on the capacity curve to the right. This happens even at high states of charge, and must be accounted for if one hopes to estimate battery parameters from during discharge. This may be best illustrated by a picture, Figure 3. Note that the horizontal axis, time, can also mean for this curve state of charge.

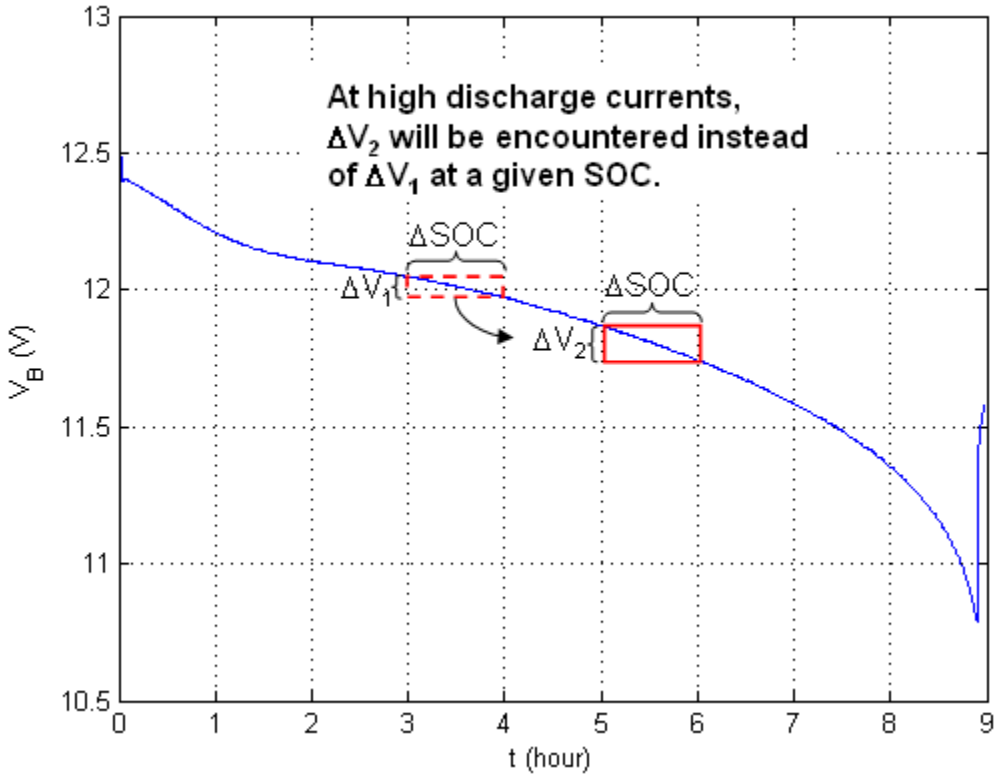

Figure 3: Effect of the Peukert relationship on steady-state discharge voltage

It is conventional to cite a current in proportion to a battery's capacity, where a current equal to the magnitude of the rated capacity is called 1C, and a current twice, or half, the rated capacity is 2C and 0.5C respectively. The 'C' indicates the rated capacity (but will not be used as a variable below to avoid confusion).

1.3.6 Temperature effects

It is conventional wisdom that battery operation has a strong dependency on temperature. The chemical reactions of charging and discharging can be greatly affected by increased or decreased energy available in the form of heat. In Figure 4, [2] (p. 24.37) illustrates that higher temperatures result in greater terminal voltages as well as higher capacities (thereby indicating that there is a Peukert-like relationship between temperature and capacity as well).

Several numerical approximations for this relationship exist. One given in [3] is

$$Q_0 = Q_{0,25} \cdot \left(1 - \alpha (25 - T)\right) \tag{3}$$

where $Q_{0,25}$ is nominal capacity at 25 °C in A-h, Q_0 the adjusted capacity, α the battery's temperature coefficient, and T temperature in °C. However, with experimental data needed for every battery type, the usefulness of such empirical fits is limited; one may as well do capacity tests on one's battery type and fit the data to arbitrary precision or use a manufacturer's set of curves.

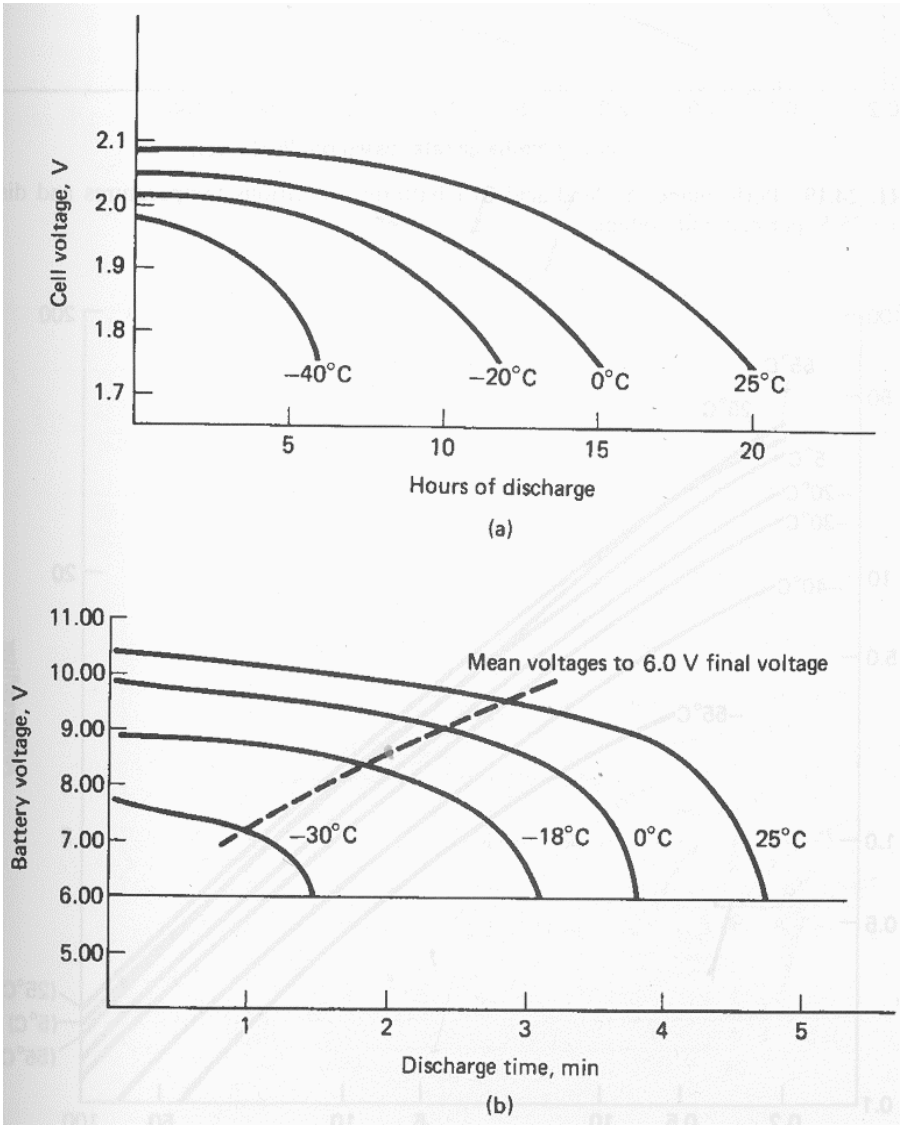

Figure 4: Effects of temperature on lead-acid batteries' discharge profiles, (a) at C/20 rate, (b) at 340 A. 12 V 60 A-h SLI battery [2].

A more important facet of temperature effects is that, during charge or discharge operation, a battery will generate heat. This is due to the heat losses as current travels through non-superconducting electrolyte and conducting plates. Thermal runaway is a major fault mode in all batteries, where the internal battery temperature rises very quickly, damaging the battery and potentially its surroundings. This is more often than not caused during overcharging. The cell plate surfaces are fully saturated with charged ions and current forced into the battery by a dumb charger (versus a “smart” charger, with voltage-controlled current) simply heats the plates

and electrolyte. As shown next, this has an effect on how much one must recharge a battery after discharging it.

1.3.7 Efficiency

A battery, as an electrothermal system, encounters the same efficiency losses as all systems that deal with the laws of thermodynamics. When a battery is being discharged, the current seen at its terminals is downstream of all the electrothermal losses encountered, starting from the charge migration from deep inside the plates, to the plate-electrolyte interface, through the electrolyte to the terminals, and out through wire of a certain gage. Therefore, to have the battery reach the same state of charge as before one started, one must put back more current than one pulled out.

Conventional wisdom (such that comes from mechanics and mechanic-oriented websites) states that automotive batteries should be recharged with 110% as much charge, in Ampere-hours, for the battery to reach the original state of charge. This efficiency that penalizes charging current from fully contributing to state of charge is called the Coulombic or calorimetric efficiency [12]. It is, however, sometimes neglected in computation if a reliable method to determine state of charge is not extant to determine this value empirically, and if it has not been provided by the manufacturer. (See Section 2.2, which presents a review of state of charge estimation techniques.)

1.3.8 Aging effects

As may be expected, two fully charged batteries of the same make and model will have separate behavior under load (charging and discharging) depending on how they have been treated in the past. Quantifying the result of battery history on its present operation is a complicated matter, but one that has become an active field of research, both for older technologies such as lead-acid batteries (as automobile manufacturers attempt to reduce warranty

costs due to electrical system malfunctions) as well as newer ones, such as nickel-metal hydride batteries that are rapidly gaining importance due to their widespread application in hybrid electric and fuel cell vehicles.

The research done for this thesis was a part of a larger thrust to perform diagnostics and prognostics on automotive lead-acid batteries; this lent itself very naturally to studying the aging effects of batteries. We will thus discuss the background of the present research task in order to understand what aspects of battery operation remained to be better understood, and then we will provide an overview of current literature on these subjects.

1.4 Motivations for research

Modern *On-board diagnostics* (OBD) involves the monitoring of the components and systems that are directly or indirectly impacting automobile emissions levels. Components that allow the diagnostics computer to monitor the states of other components are also themselves monitored. For example, if a catalyst monitor only activates in a certain engine speed range, the sensor that detects the engine speed must also be monitored for faults [13].

The sensors involved usually operate via thresholds or continuity (binary). Monitoring is done on a component-by-component basis. When faults are detected in individual components by measurements indicating deviations from certain pre-programmed acceptable ranges, [14] indicates that traditionally logic equations implemented using logic gate circuits or PLCs are utilized to: 1) generate a Diagnostic Trouble Code (DTC) and record it to OBD memory, and 2) turn on the Malfunction Indicator Light (MIL) on the dashboard.

These DTC codes are meant to subsequently be read by any repair technician with a standardized connector and off-board computer. However, *the causes of any single DTC are myriad*. A code has limited use in diagnosing the problem with the intent of fixing it. For example, if an oxygen sensor code is registered, it is deducible that it was caused by an off-

voltage-range reading of an oxygen sensor in the exhaust process. However, it is not trivial to determine the cause of this, which may be something as unrelated as a vacuum leak. In another example, going over a pothole may briefly dislodge a weak battery connection experiencing corrosion or insulation fraying, registering an undervoltage. The problem is not reproducible by going over another pothole.

Also, an automobile mechanic cannot verify the proper functioning of any sort of integrated solid-state component. She can only ensure that the component is receiving a reliable voltage and has a good ground [15]. Therefore, repair shops or dealerships sometimes must resort to resetting the MIL, with the hope that the code was an isolated event, or begin replacing components in a bid to divine the cause of the repeating failure codes. This latter process of replacing parts is done at the expense of the auto manufacturers and comprises a significant portion of their short-term reducible losses.

Model-based diagnostics presents another method to monitor the overall state of a complex system such as the electrical network of a car. This involves accurately modeling the subsystems' dynamics and setting up a network of sensors that are conducive to the design of observers and estimators (of the Luenberger and Kalman variety) that determine the internal (non-measured) states of the plant while in operation [16]. A model of operation can therefore be built and refined continuously, adding a dimension of thoroughness and accuracy for diagnostics beyond rule-based OBD. This would allow the auto mechanic to determine not only what test failed but also from where within the system the failure originated.

Aging models and capacity sensing for automotive lead-acid batteries can, in conjunction with observers and Kalman filters, add a further element of prognostics in automotive electrical systems, providing a car owner with information that may lead to preventative maintenance that prolongs the life and health of the battery. Therefore, model-based diagnostics and subsequent

prognostics are a bid to cut costs of automobile manufacturers, increase reliability of vehicles, and reduce ownership costs of consumers.

At the Center for Automotive Research (CAR), much industry-supported battery and vehicle management research is conducted, including characterization of batteries for use in conventional passenger vehicles, hybrid electric and fuel cell vehicles, as well as specialized vehicles such as garbage collection trucks or military vehicle platforms. It is therefore natural that the agglomeration of expertise in battery systems would be extended to automotive lead-acid batteries in passenger vehicles.

In order to bring the wealth of theoretical knowledge of model-based diagnostics to bear on these batteries, a robust model for the battery that captures all the elements to diagnose must be available. In the next sections and chapters, the effort to build this model will be detailed.

1.5 Thesis outline

This chapter has served to provide a broad outline of the characteristics of batteries that are well-known and relevant to the task at hand (outlined in the previous section). In the next chapter, the results of a literature review on battery modeling and fault diagnosis will be presented. Much of the chemistry involved will be restricted to this chapter, and so physiochemical bases of the models involved are scattered across it.

Chapter 3 begins with a section detailing the model structure chosen for this work, and outlines the experimentation required to complete the model. It then details the hardware and software setup that was brought to bear on construction of this complete battery model. This will serve as a manual to the entire methodology used for this study: software control of hardware, the data acquisition, filtering and analysis of acquired data, and parameter estimation and final curve fitting.

Next, the actual results of this whole process will be provided in Chapter 4. Flaws and

discrepancies in the results will be discussed.

The final chapter will contain some concluding thoughts, some guidelines for future work in this field, as well as a compilation of the nomenclature used in the thesis. This will be followed by the references in Chapter 6.

2 Literature review

The research review in the area of battery diagnostics and prognostics identified three main topics.

The construction of a battery model to reflect all the characteristics of battery behavior is the foundational step in understanding what one can do theoretically for model-based diagnostics. Therefore, a review of models was made.

The estimation of state of charge remained a difficult task, and numerous attempts have been made to reliably construct a single method to do this. However, a single estimation structure does not exist that works for all battery chemistries and applications. Therefore, a review of state of charge estimation for lead-acid batteries is included here.

Finally, it becomes important to understand how batteries age in automotive vehicles today. The natural aging and fault modes were investigated and reviewed.

2.1 Battery modeling

The main approaches taken to battery modeling are:

- chemical modeling of the electrochemistry directly,
- a machine-learning approach traditionally involving a neural network, and
- modeling with an electrical circuit with varying circuit parameters.

These models need to minimally provide an estimate of the terminal voltage, but to be at all useful, should give also state of charge, available capacity, and possibly some measure of state of health (that takes into account the aging of the battery).

2.1.1 Chemical modeling

As the totality of battery behavior is the result of myriad fairly well-understood electrochemical reactions at a molecular level, it should be possible to quantify each each of these reactions with an equation and derive, bottom-up, a hyperfine description of the battery.

Such a model would use experimental data to identify the static parameters that it needs, and would subsequently derive all dynamic variables; this would not be a phenomenological description of the battery that one might build.

Some of the chemical effects that would be modeled include [17] polarization, the voltage developed beyond the open-circuit voltage when the battery is charged or discharged. It comprises of the voltage potentials developed in the plates (activation polarization), across the resistive paths in the battery (ohmic polarization), and due to the transport of chemical species through the electrolyte (concentration polarization).

The amount of charge extractable from an electrode depends on its activation rate, which may or may not be uniform, depending on state of charge, temperature, and current levels. If concentration of the charge-exchanging chemical species cannot be approximated as uniform, there are mass transport effects that must be accounted for. At all times, a measure of the capacity of the battery must be maintained, based on how much charge is stored in the plates.

As an example, [18] builds a physics-based model for nickel-hydrogen batteries that includes the majority of these chemical effects. The model requires *twenty-nine* parameters and constants to accurately represent relevant electrothermal effects, and reaches very high levels of accuracy.

The primary disadvantage of this approach is that very few applications warrant the time and resources to empirically determine the many parameters and coefficients that such a physics-based model needs, and indeed many of them (such as average specific heat of electrolyte) cannot be determined for sealed lead-acid batteries in a lab, let alone in a vehicle for battery diagnostics purposes. Therefore, this approach for *modeling* is rare in literature.

However, the insights that a strong understanding of the chemical foundations of battery operation are extremely valuable in the development of equivalent models that do not model the

entirety of its chemical behavior. These insights are discussed in subsequent sections and are considered when choosing a battery model.

2.1.2 Computational intelligence-based modeling

An opposite school of thought holds that a battery comprises processes too complicated and interrelated to model individually, and seeks a data-driven heuristic approach to predicting battery behavior and state. To this end, computational intelligence techniques such as artificial neural networks and particle swarm optimization may be applied to experimental data to fabricate a nonlinear function that can describe the outputs of the battery.

An artificial neural network (ANN) is generally the cornerstone of a computational intelligence model because this is the tool that can be trained on experimental data. The acquisition and selection of this training data is generally the most difficult process in utilizing an ANN. When training has been completed, ANNs' extrapolation and interpolation abilities outside and within its training set can vary due to its design (number of layers and neurons, local weighting function, etc.), which is another dimension of their use, beyond selection of training data.

In [19], however, where the goal was to aid the design of batteries, the results were excellent. Given current-voltage profiles, the neural network was able to give excellent interpolation results.

For some applications, such as design of batteries, or control of partially or fully electric vehicles, such a result is very worth having. For others, such as model-based diagnostics, a neural-network solution to battery modeling is less than ideal because it necessarily cannot describe the separate internal processes of the battery. For diagnostics and prognostics, we do not need to predict what the system will do, because we can observe this directly. We need to know why it is doing what it is doing, and therefore must seek out alternative modeling approaches.

2.1.3 Equivalent circuit models

Between the low-level chemical modeling and the input-output heuristic-level modeling exists a compromise. It is possible to understand the chemical processes in the battery, and approximate their effects as the behavior of a lumped-model network of higher-level physical systems. In this section, we review a number of ways to reduce complex chemical phenomena to well-understood and well-behaved electrical-level circuit elements in creating a model.

In [21], many of the short-time and long-time processes inside batteries are identified and modeled. Figure 5 both lists the major dynamic processes inside batteries, and shows typical time scales on which they operate. An appreciation of these scales will be very useful when creating and using battery models.

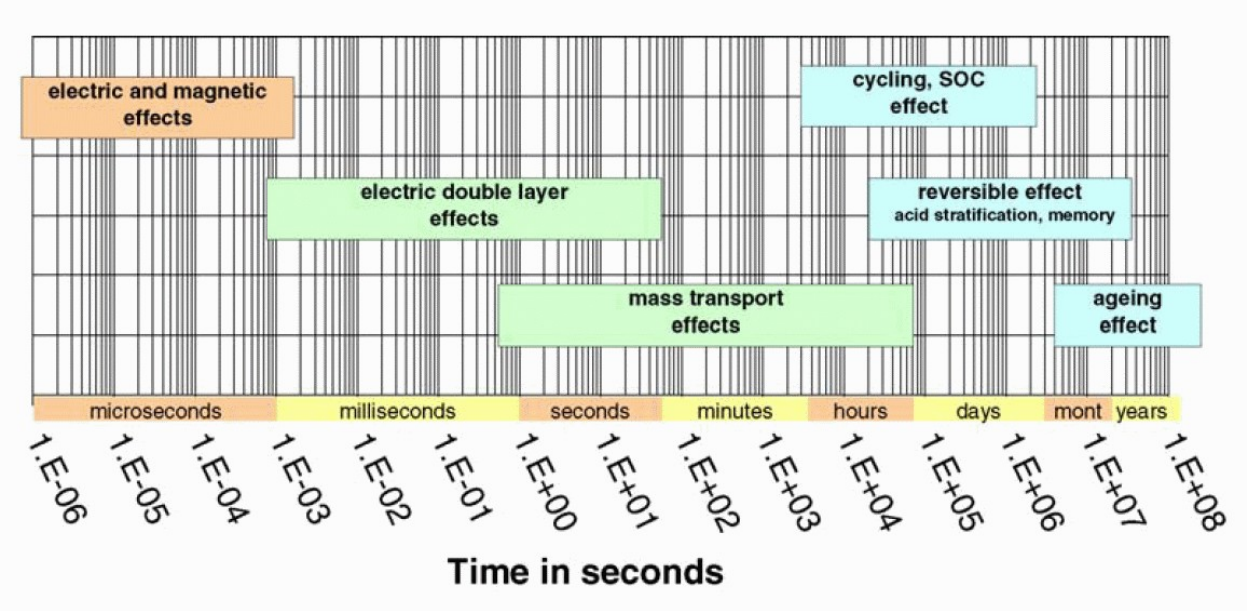

Figure 5: A listing of the major dynamic processes in batteries and their average time constants [21]

The long-term processes such as irreversible aging, some reversible effects such as minor sulfation or acid stratification, and cycling processes vary greatly from battery to battery due to their dependence on how the battery is used. These effects are desired to be quantified for aging and prognostics studies of batteries and therefore must be domain-specific. The model proposed,

however, is not directly intended to model these effects but instead the shorter-time processes of mass transport, electric double-layering and charge storage, and electromagnetic processes.

The technique of electrochemical impedance spectroscopy (EIS) was used here to observe these processes. This technique is another major topic of ongoing research for it may yield not only excellent battery models but may also allow predictive estimation of the states of the battery with respect to aging and other extremely long-term effects (viz., [22]). The technique has excellent primers elsewhere ([23]), but a briefly, the technique involves performing a frequency sweep of a complex system to compute its complex impedances using the amplitude and phase differences of the input and output signals. These complex impedances are then fit to a number of possible circuit models using least-squares, etc.

On the time scale of seconds to hours (that is, from requesting current to dissipation of surface charge, Section 1.3.4) are mass transport effects. There exist two modes of transport for chemical species: diffusion due to chemical gradients is the more important one, but migration due to electrical fields also plays a secondary role. It is at this level that temperature plays a key role, by determining diffusion rates.

At a semi-infinite diffusion layer, such that is formed by a planar electrode surrounded by electrolyte in a lead-acid battery, the impedance is a Warburg impedance, a term whose popularity is growing with EIS'. The Warburg circuit element has a complex nonlinear impedance given by:

$$Z_W = \frac{\sigma}{\sqrt{\omega}} - j\frac{\sigma}{\sqrt{\omega}} \tag{4}$$

where σ is the Warburg coefficient, and ω the angular frequency.

Diffusion processes occur in the active mass, the porous electrode, and in free electrolyte. They can be modeled using RLC elements either as a series of T-circuit ladders, as shown in

Figure 6 and whose mathematics can grow unwieldy, or can be lumped into a Warburg impedance.

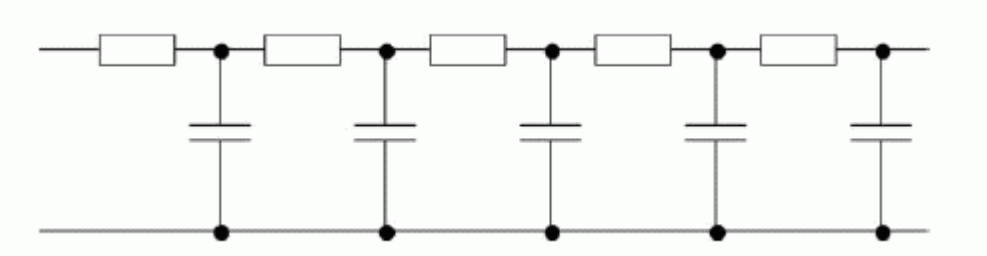

Figure 6: The RLC equivalent circuit needed to model diffusion effects [21]

On a faster level is the double-layer capacitive effect, which many models stop at. This useful idea derives from the fact that charge must move from the solid electrode to the liquid electrolyte by crossing a charge-free region. This naturally warrants a capacitive description. A single layer turns out to be overly simplistic, as generally more than one of these capacitive layers form side-by-side: one right at the electrode-electrolyte interface and another beyond it. Figure 7 shows that this effect can be reduced to a simple electrical equivalent circuit. The parallel circuit parameters vary by state of charge and temperature, and even battery age and current levels. (The series element is an ohmic resistance, discussed shortly.) Additional effects happen in this range when an electrode is porous (to maximize surface area, as is the case in automotive lead-acid batteries).

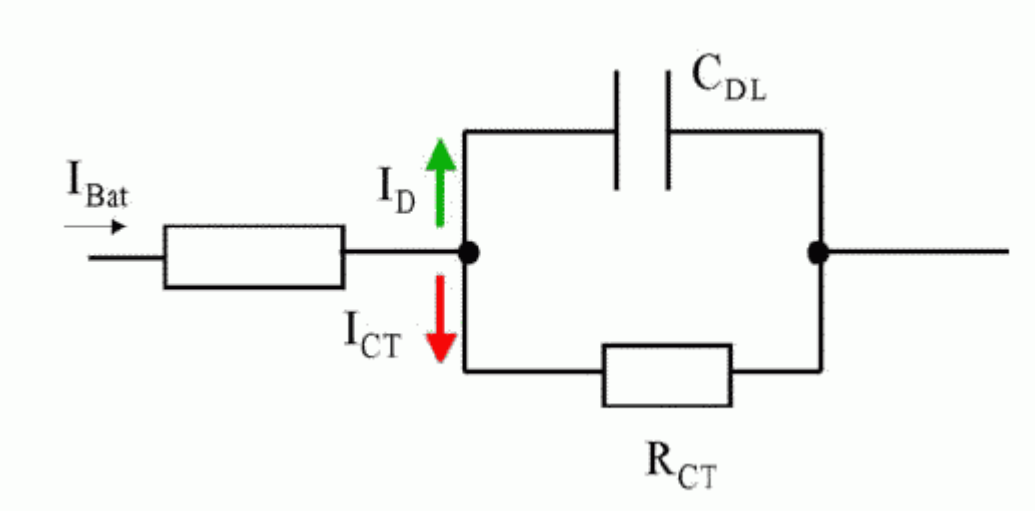

Figure 7: Equivalent circuit modeling double-layer capacitive effects [21]

The highest frequencies are the ranges at which electric and magnetic effects manifest themselves. Here, ohmic losses cause instantaneous voltage responses when current is applied to the battery. These are modeled by resistances. Furthermore, the battery is comprised of individual cells connected in series, which can be modeled as series inductances. There can also be an interelectrode capacitance, all of which are shown in Figure 8, an equivalent circuit model of the high-frequency effects of the battery.

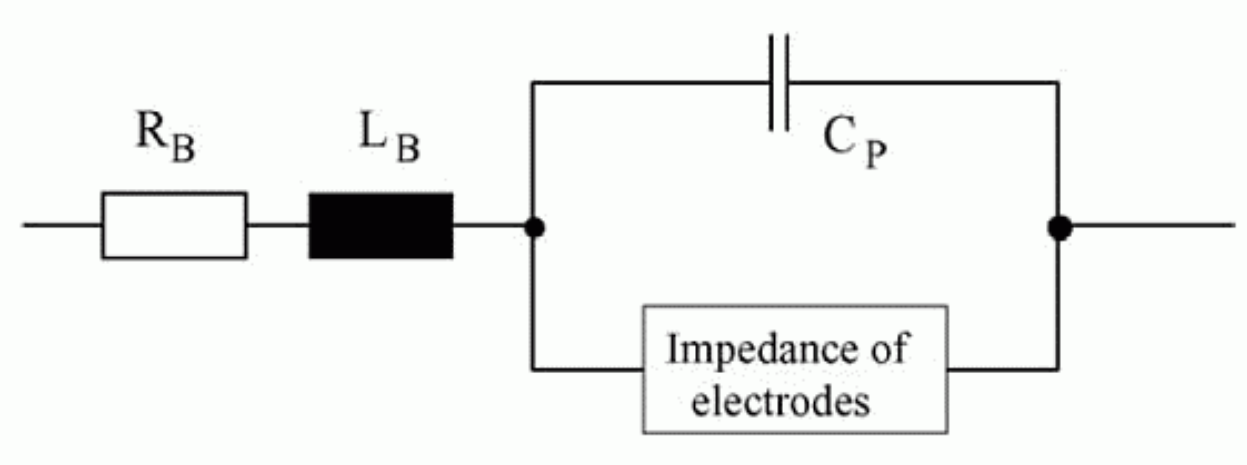

Figure 8: Equivalent circuit modeling high-frequency effects

All these equivalent circuit models were derived from a first-principles understanding of the physiochemical processes occurring inside the battery. They lend themselves very naturally to be fleshed out, and their circuit element values identified, using EIS. The model is more useful in its theoretical depth than practical implementation, and is considered in this section on electrical circuit equivalents instead of a previous one on chemical modeling only because the circuit parameters can be quickly identified by EIS software in the laboratory. However, such software and hardware is not available aboard a vehicle.

In [20], on the other hand, three lumpable chemical processes are identified as the primary ones for battery dynamics:

1. ionic charge and electronic charge conduction, the former through the electrolyte in the pores of the active mass and the latter through the active mass itself,
2. electrochemical reaction at the interface of active mass, including electron transfer, and
3. movement of charged or uncharged chemical species via diffusion into and out of the reaction zone.

These processes combine in a manner that are described by partial nonlinear differential equations. However, it is pointed out that each of the physical processes can be modeled for a certain state of the battery using lumped circuit elements such as resistors and capacitors, and transmission lines for distributed ones. If the parameters of these circuit elements, and the steady-state open-circuit voltage, are identified for a variety of discharge states (making them nonlinear), then the model may be subjected to arbitrary current loads and yield good results at acceptable computational expense.

The final circuit model is reproduced in Figure 9, where: R_{ser} is the resistance of the separator and current collectors, ρ is the distributed resistance of the transmission line modeling electronic and ionic resistance of the active mass, Z_s is the combined impedance at the surface of the active mass where the reaction is occurring, and includes the sub-elements associated with

charge transfer and passivation layer resistances R_{ct}, the double layer capacitance C_{dl}, diffusion and charge storage inside particles of active mass represented as a generalized Warburg impedance modeled as a finite-length transmission line, and C_s representing additional charge storage.

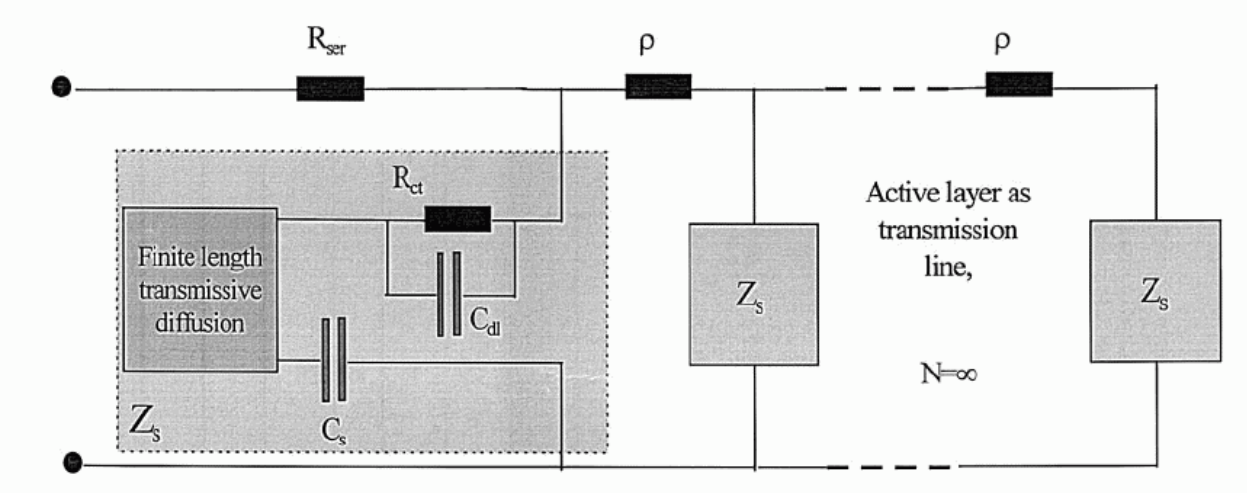

Figure 9: Universal battery model equivalent circuit [20]

The identification of these circuit parameters at varying states of charge is done using electrochemical impedance spectroscopy, and further nonlinear least-squares fitting to separate some variables.

The two circuit models presented here represent a very large number of possible effects to model and a variety of ways to model slightly different and distributed processes. Between these and the simplest model, comprising a static voltage source and resistor, many others can be derived, consisting of many circuit elements offering to model this or that effect. Excellent overviews of such models are available in [10] and [3]. From the latter is Figure 10, showing some common ones. One element that is missing from these circuits, however, is an open-circuit voltage source (see Section 2.2.5 for some real-world models used for battery state estimation). This represents the stiff center voltage of the battery around which all charging and discharging terminal voltages oscillate around.

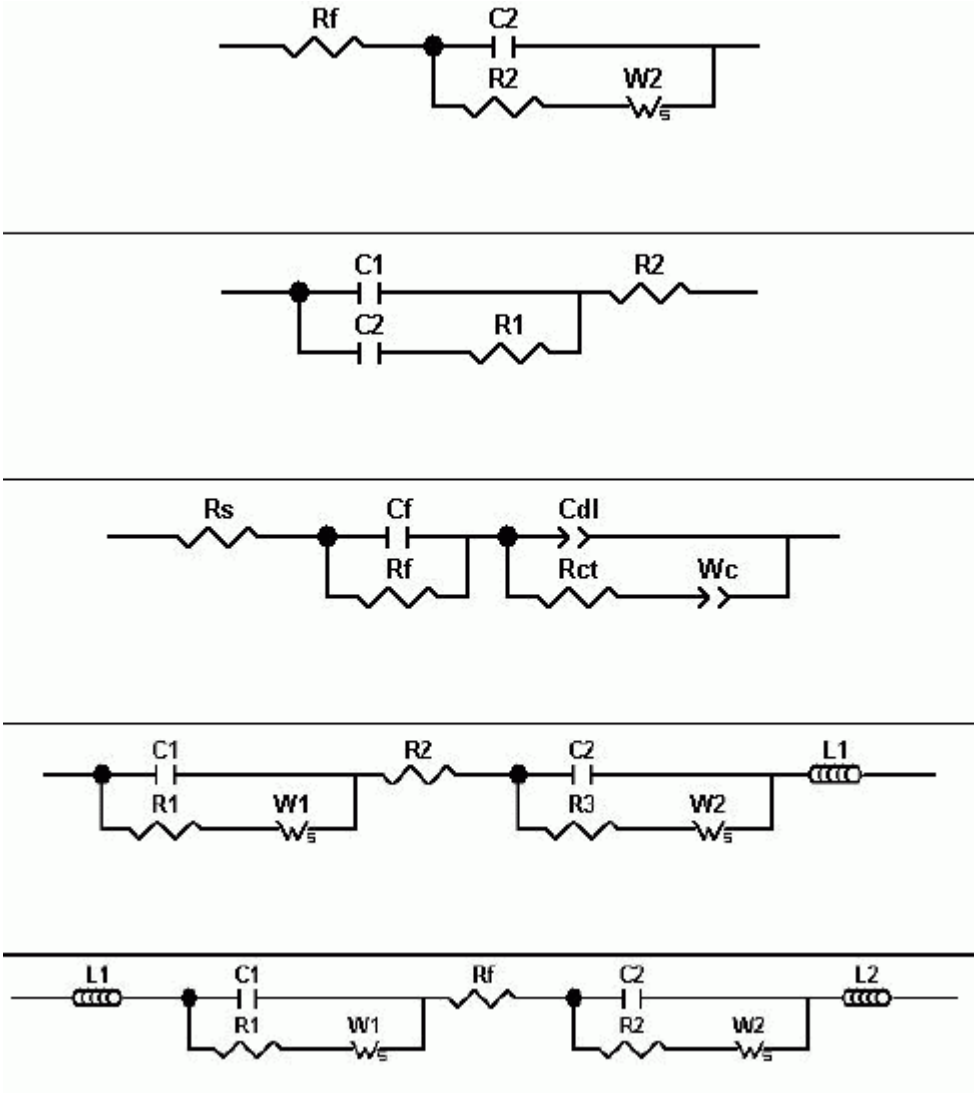

Figure 10: Several electrical circuit equivalent battery models

In the end, one must consider the battery in question, its chemistry, design parameters, and intended use, perform necessary experimental validation and choose a model (or turn to previous work done for the same type of battery). When one intends to do vehicle-based model-based diagnostics, a model that can provide the information needed with minimal measurements is needed. One such piece of quantity that is always valuable in battery diagnostics is state of charge estimation. Some of the copious amounts of literature on this topic will be reviewed next

2.2 State of charge estimation

[24] presents a fairly complete overview of the various methods of SOC estimation that

have been reported. Many of these techniques are easy to understand, and others are more theoretical (such as the Kalman filter) or involved (EIS). However, all but the most simple utilize some kind of model, specially constructed with the hope that some of its parameters or outputs will have some bearing on the battery's state of charge.

The subject has received much research interest because of its importance in diagnostics as well as hybrid electric and fuel cell vehicles. Batteries are designed to be operated at specific states of charge, and permanent damage can result due to improper management. Although automotive SLI batteries cost between US$70 and $100, HEV batteries cost several thousands of dollars and care must be taken to monitor their SOC under operation.

2.2.1 Discharge test

The only fully reliable method to measure a partially discharged battery's state of charge is to discharge it until it reaches 0% SOC. The problems with this method are obvious, but this is the only way to perform capacity tests (Section 1.3.2), etc.

2.2.2 Current integration

The next approach uses the definition of capacity, the Ampere-hour. Counting the amount of current that enters or leaves the battery should allow good estimation of SOC, one would think, according to the equation:

$$Q(t) = Q(0) - \frac{\eta}{Q_0} \int_0^t I_B(t)\, dt \tag{5}$$

with Q being the variable for SOC, Q_0 the nominal capacity in Ampere-hours, t the indepdent time variable in hours, η the Coulombic efficiency (Section 1.3.7), and I_B the battery current, with negative defined as discharge.

There are two main drawbacks to this method. First, measurement error will invariably cause drift in estimation unless one is very certain of what one's loads are, at all times. Secondly,

the charging efficiency η must be determined for the battery, and may be a function of any number of parameters, and minimally the direction of current. [24] gives an alternative form of the above equation:

$$Q(t) = Q(0) - \frac{1}{Q_0}\int_0^t \left(I_B(\tau) - I_{loss}(\tau) \right) d\tau \quad (6)$$

I_{loss} here is taken to be known: the amount of current that does not reach the electrodes due to path losses.

2.2.3 Open-circuit voltage

It is well-known by mechanics that the battery's open-circuit voltage is a linear function of its SOC, and manufacturers have long disseminated tables identifying this trend. However, there are two caveats accompanying this satisfying result: open-circuit voltage must be read without surface charge (Section 1.3.4), and after the battery has relaxed from any charging or discharging activities.

2.2.4 Measurement of electrolyte specific gravity

Another (formerly) very common method of determining a car battery's state of charge was to use a hydrometer and measure the electrolyte specific gravity. Recall that the battery discharge equations consume sulfuric acid and convert it to H_2O, and so the electrolyte in a highly discharged battery is almost entirely water (which is why one must never leave a lead-acid battery at deep levels of discharge: not only will the lead sulfate crystallize, but the water will corrode the metallic grids and electrodes).

Water has a specific gravity of 1.0, whereas sulfuric acid is about 1.280 [37]. The relationship between the electrolyte specific gravity and SOC is also linear, but the usefulness of this for a sealed maintenance-free battery is nil.

2.2.5 State estimation (Kalman filtering)

The majority of literature on state of charge estimation perform some sort of state estimation based on a model to identify battery SOC. (E.g., [25], [26], [27], [28], [29], etc.) It is in this approach that the selection of a model becomes of vital importance. Conventional methods of state estimation rely on the theory of Kalman filtering (KF).

These approaches rely on there being a linear or nonlinear model of the system's states and outputs. Linear systems may contain states that are unmeasurable but nonetheless estimated based on the system's measurable outputs and inputs. Kalman filtering theory presents a method of constructing such state observers which minimizes the mean-squared error between estimates. The same applies to nonlinear systems, but the theory becomes less rigorous and one must go to an extended Kalman filter (EKF) or to a totally different approach to state estimation, such as particle filtering. One may consider parameters of a system “states” if one goes to a nonlinear model, and thus extended Kalman filtering may be used to do both state and parameter estimation. Copious details of the glorious topic of estimation are available in [30] and [31].

[25] utilizes a circuit model shown in Figure 11 and constructs an observer to estimate the open-circuit voltage of the battery, given measurements of battery current and terminal voltages. The estimated open-circuit voltage is used to provide a SOC measurement, due to the linear relationship between the two. The nonlinear time-varying (NLTV) circuit model was reduced to a linear time-varying (LTV) system that depends on only one state variable, and furthermore the work proves that the open-circuit voltage's estimate will asymptotically converge to the actual value *without* requiring estimation of the circuit parameters. For purely SOC estimation, the procedure serves very adequately, but is no complete solution for diagnostics precisely because it avoids estimation of any other parameter of the battery.

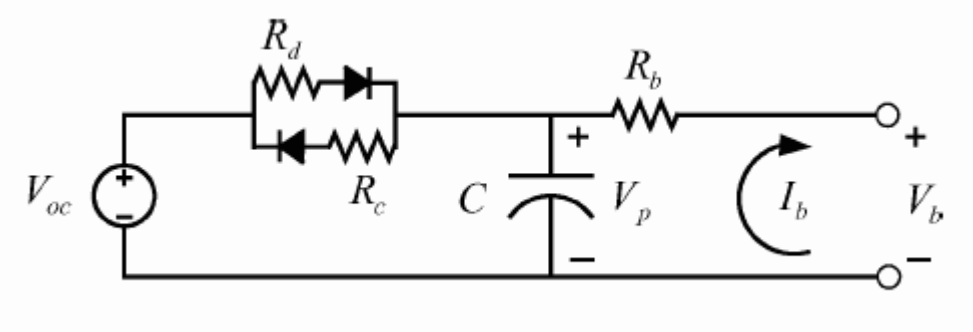

Figure 11: Circuit model utilized in [25]

In [26], however, a set of observer are designed to estimate both state of charge as well as state of health (SOH) by modeling the charge-storage functionality of the battery as a bulk capacitor. The way this bulk capacitor's value varies with time can yield insight into the battery's state of health, or how much charge it can generally store.

The equivalent circuit model is shown in Figure 12. The SOC is estimated, similar to [25], by utilizing a Kalman filter to estimate the voltage across the bulk capacitor, V_{Cb}. The state of health quantification comes from utilizing an extended Kalman filter to estimate the actual value of this bulk capacitance, C_{bulk}.

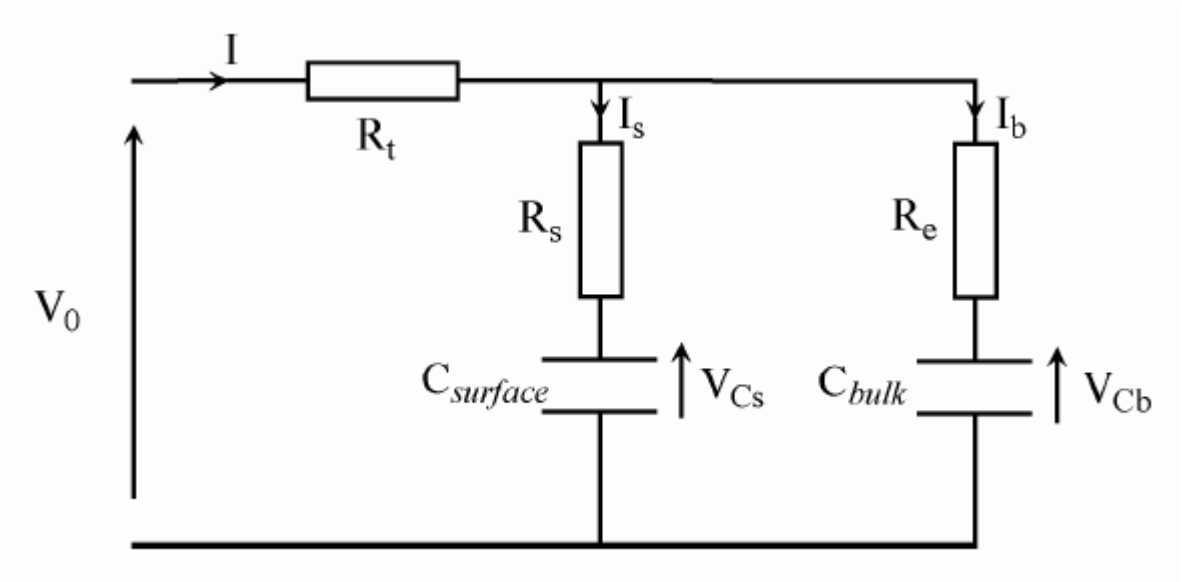

Figure 12: Equivalent circuit model built by [26]

This work, unlike the [25], does need parameter values for the remaining circuit elements, and these were experimentally determined. However, beyond the states being

estimated, all other circuit parameters remain static. Therefore, the method does not allow for online determination of the other states of the system other than SOC and SOH.

However, one can clearly imagine combining some of the methods outlined in the previous section on battery modeling (Section 2.1) with some of the state estimators that are available in literature in order to obtain both accurate representation of the battery's behavior as well as some internal parameters such as SOC and SOH. This thesis will utilize an equivalent circuit similar to, but simpler, than these (detailed in the next chapter), but first we will discuss further ways of doing SOC estimation.

2.2.6 Electrochemical impedance spectroscopy

Many results of attempting to use EIS to measure state of charge have been gathered in [24], and need not be repeated here because of the great variability in the reports of success. The issue with using a Nyquist plot for this narrow purpose is that one must interpret it correctly. The interpretation is necessarily correlative. The problem may be further clarified by showing what the results of EIS look like. In Figure 13, Nyquist plots of a polymer lithium ion battery at various states of charge are shown. There has been no clear way to interpret these curves to yield useful SOC information. This is contrasted to state estimation, whereby a state that was closely related to SOC could be estimated.

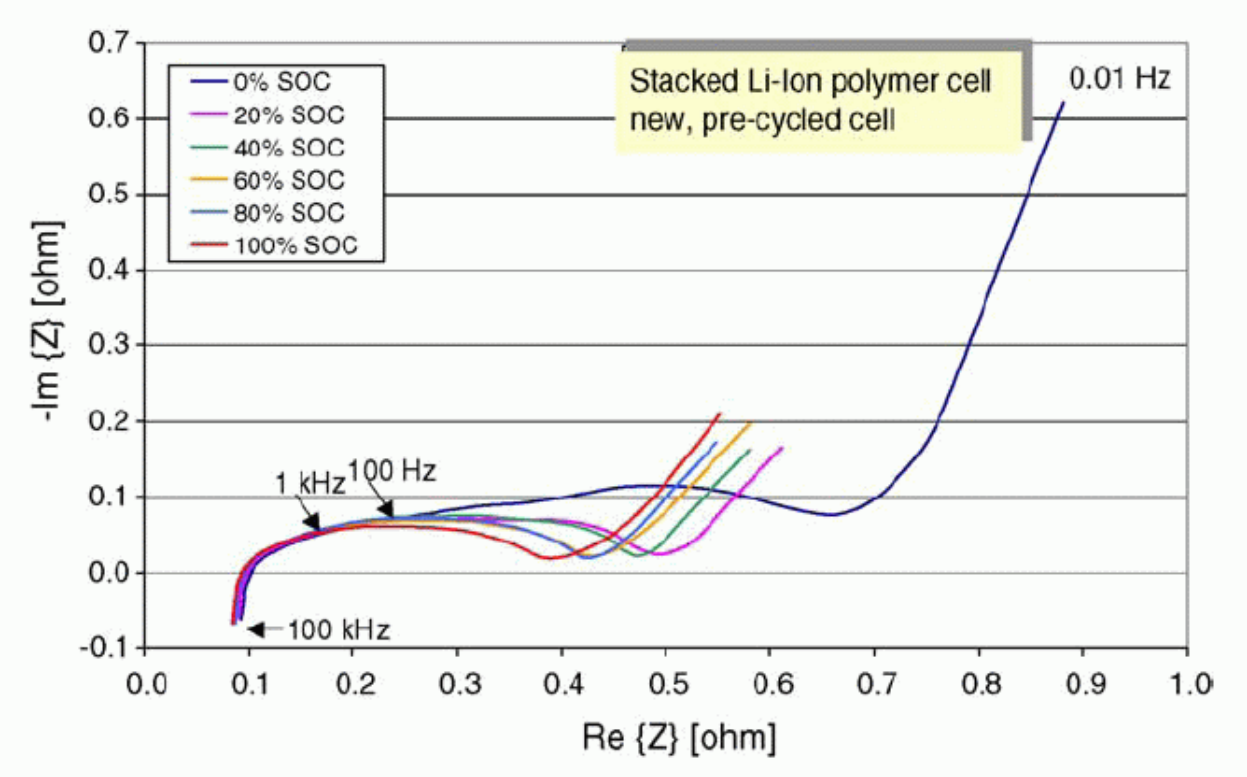

Figure 13: Nyquist plot of a battery subjected to EIS analysis [21]

2.2.7 Coup de fouet

There exists for lead-acid batteries only a phenomenon that causes the terminal voltage to dip in the first few minutes of a discharge that follows a full charge. This dip is called the coup de fouet, and is shown in Figure 14, [32]. Although the effect was explained at least by the mid-60s [33], only in the late 90s was it realized that one could determine reserve capacity of a battery using the coup de fouet, and much research was sponsored in the area by telecommunications companies. (A major use of batteries is backup power supplies for telecom and datacom installations.)

The coup de fouet may be applicable to automotive batteries as well, but has not seen much use because, although in general a car battery can be said to be at full charge after being driven for some time, a constant discharge current is not practical in a car. The engine will be started with a very high current pulse lasting less than a second, there will be an inrush as the alternator reaches steady state, and then the battery will reach a quiescent state of charging; not

much time for a discharge test as required by the coup de fouet. However, the technique may still be applicable in the lab to test for aging and other state of health parameters.

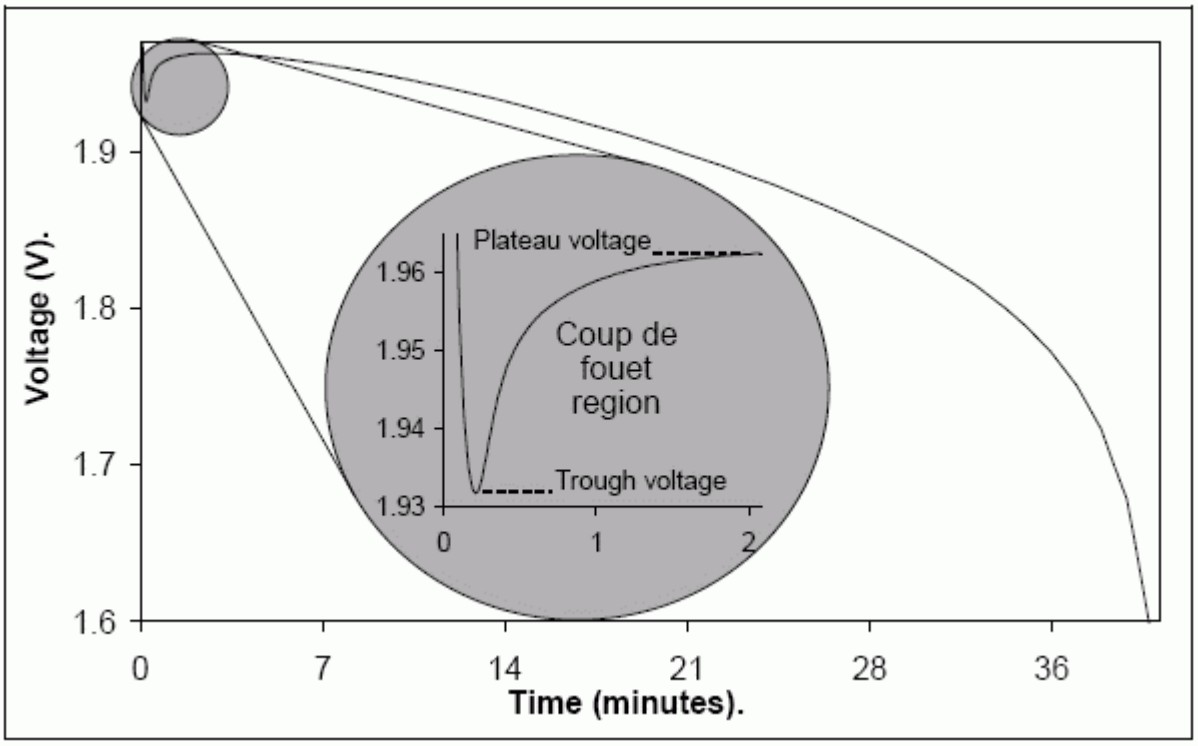

Figure 14: The coup de fouet in a Hawker 2HI275 cell discharged at 275 A at 20 °C [32]

2.2.8 Conclusion

A review of state of charge estimation allows us to gain a further dimension in understanding battery modeling for various applications, as well as a chance to see some models at work, such as those presented in state estimation. Some of the concerns regarding the practical utilization of these models can be appreciated as they need to be implemented online in various environments.

The last major topic that was reviewed pertains directly to battery diagnostics and prognostics and involves the aging and fault modes specifically present in automotive lead-acid batteries.

2.3 Aging and failure modes

This section will discuss the findings of a review of literature on the ways batteries age

with use. These involve natural fault modes that can be avoided only by not using the battery and so are always present, as well as service life faults that are caused by misuse of the battery. There will be almost no mathematical equations in this section; there is very little quantitative analysis done on the subject, as this would require a large sample of partially aged and failed batteries, and this is not feasible for the many chemistries and usage environments that exist.

A battery is conventionally considered to be dead if its available capacity drops below 80% of its nominal capacity (presumably when it was new). Recall that such a capacity is measured by a capacity test (Section 1.3.2), which involves nominally a 10 hour discharge at 0.1C. Such a test may not properly reflect some fault modes such as sagging voltage, but will adequately measure the most important characteristic of the battery: its ability to store and deliver charge.

While the literature on battery aging identifies numerous fault modes, that is, internal changes to the battery caused by (mis)usage, according to [34], all of them manifest themselves to the external user as one of two effects:

1. Decrease in capacity, and
2. Decrease in power delivery due to internal resistance.

With these two indicators in mind, we can examine some of the most common aging effects in lead-acid batteries.

The primary unavoidable aging effect is *corrosion of the positive grid*, composed initially of metallic PbO_2, and is probably the most important factor for calendar life [1]. This effect is also called *grid growth* because the electrode physically expands. [35] gives details on how the design of VRLA batteries can impact this fault mode, and [36] on the chemistry of the process. In a nutshell, although we say that the positive electrode is composed of PbO_2, this lead dioxide forms a dense corrosion layer around the metallic lead in the positive electrode when fully charged. This layer shrinks and expands during discharge and charge, and as it becomes fixed in

a state of permanent corrosion, the grid is said to be corroded.

When this fault mode is activated, the life of the battery may be terminated by complete oxidation, or more often by the positive grid making contact with the negative top-bar of the battery, forming a short circuit. Through either of these two specific modes, grid corrosion is usually the cause of death in SLI batteries [36], because they are usually kept at float charge, and manifests itself as the second fault effect, that of increased internal resistance. However, another fault mode, the deterioration of the active mass on the positive electrode, is active in vehicles that experience heavy cycling.

Degradation of the positive active mass is due to the precipitation of $PbSO_4$ back to PbO_2 during charging will cause a morphological shape change in the latter because $PbSO_4$ crystals have much higher volume than PbO_2 [36]. As this shape change becomes more and more pronounced, the lead dioxide particles lose coherence and shed from the positive plate. This is more aggravated in batteries experiencing heavy cycling, and manifests itself as a decrease in capacity. (Interestingly, the negative plates are generally immune to corrosion and active mass deterioration [35].)

A third major aging mechanism is *sulfation*, and has many meanings among the user community, such that it is the sole topic of [37]. Recalling that the active mass at both electrodes reacts and becomes $PbSO_4$ during discharge, the danger of it crystallizing into an electrochemically inactive form (not reversible to form lead and lead oxide) is always present. This used to be the scourge of battery designers and users for years but as charging regimes become more streamlined in vehicles, the occurrence rate has also declined.

This fault mode strikes when the battery is either allowed to remain at open-circuit for long periods of time, or at a deep level of discharge. It is aggravated by elevated temperatures. Appropriate charging rates and intervals can keep this problem at bay, but when it occurs, it

reduces the capacity of the battery. There exist numerous commercially-available products that claim to reverse sulfation [38]–[40], by applying a distinctive sinusoidal or pulsed current charging profile, but there is only scattered evidence that they actually work.

There exist several other fault modes that operate ancillary to these three prime ones. They have been detailed in the papers cited here, and include:

1. Agglomeration of fine lead particles at the negative electrode.
2. Loss of electrolyte.
3. Loss of water (hydrogen evolution at the negative electrode, accompanies gassing during overcharge).
4. Inter-cell connector failure.
5. Short-circuiting.
6. Electrolyte stratification.

However, all these effects seem to manifest themselves as some form of capacity reduction or resistance increase. With this in mind, and with the models and state estimation techniques studied in this chapter, we may move on and discuss the equivalent model chosen for this study, and the experimental methodologies to characterize the battery.

3 Battery model and experimental methodology

In this chapter, the dynamic battery model that was used will be introduced and explored. It has been used in some of the work presented in literature (e.g., [29]) as well as much of the battery research done at the Center for Automotive Research (CAR).

With the model chosen, the need for experimental characterization remains and a fairly thorough overview of the experimental bench that now exists at CAR and that was used for this study will be given. This will include the hardware as well as software control and some analysis.

The methodology utilized in modeling 12 V lead-acid batteries will then be detailed. As all practitioners of battery engineering know, the equations and values provided by models have great variability. Data obtained from one battery test will yield parameters that may differ greatly from data obtained from a slightly different test. Therefore, exact methodology is very important to give end-users of battery models sufficient insight into the domain of their models and when they may no longer apply, and to compare variations in models.

3.1 First-order triple-state dynamic equivalent circuit model

An equivalent circuit model is the only type of model that is amenable to both simulation as well as fault diagnosis and dynamic system analysis. However, as the three major variables that pervade and strongly influence battery behavior are terminal voltage, state of charge (SOC), and temperature, and only one of these is a strictly electrical value, the model must include dynamic state equations for SOC and temperature.

This is however a non-issue because, 1) thermal system dynamics are extremely similar to electrical ones (the differential equations have the exact same form), and 2) it is possible to express SOC as an integral equation. The latter, however, requires that we use current integration

as our SOC estimator. For much of the simulation and diagnostic work in the lab, this was deemed acceptable.[1]

The model therefore comprises three subsystems: the electrical system, the thermal system, and the SOC estimator. Figure 15 gives a schematic of this.

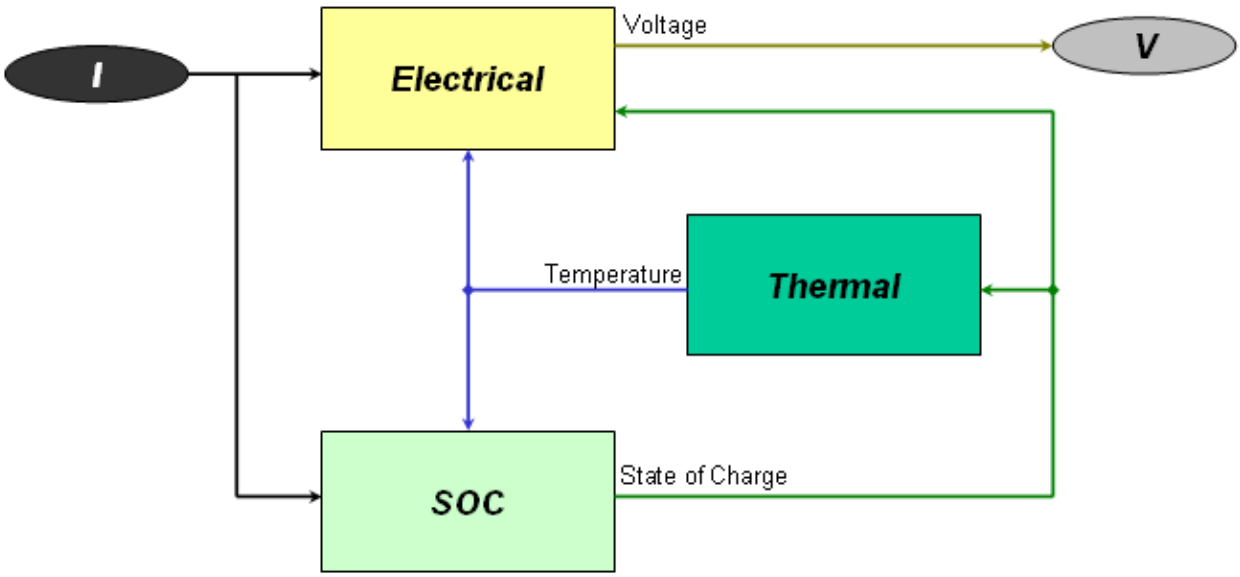

Figure 15: Triple-state battery model with three distinct subsystems

Inputs to the model are the battery current, and the output is voltage. This model was very useful for stand-alone simulation purposes. However, as work progressed, it was realized that diagnostic work would be made much simpler, given an unrestricted sensor set, if the temperature of the battery could be measured. This yields a model with once again three states but with an additional input and one less subsystem, as in Figure 16.

1 However, it is of vital importance to appreciate the low probability that one could get a current sensor in a production vehicle: there are problems whether one imagines a current shunt (a precision resistor, the voltage drop across which is measured) or a current clamp (a Hall effect sensor) approach given today's stratified auto production procedures.

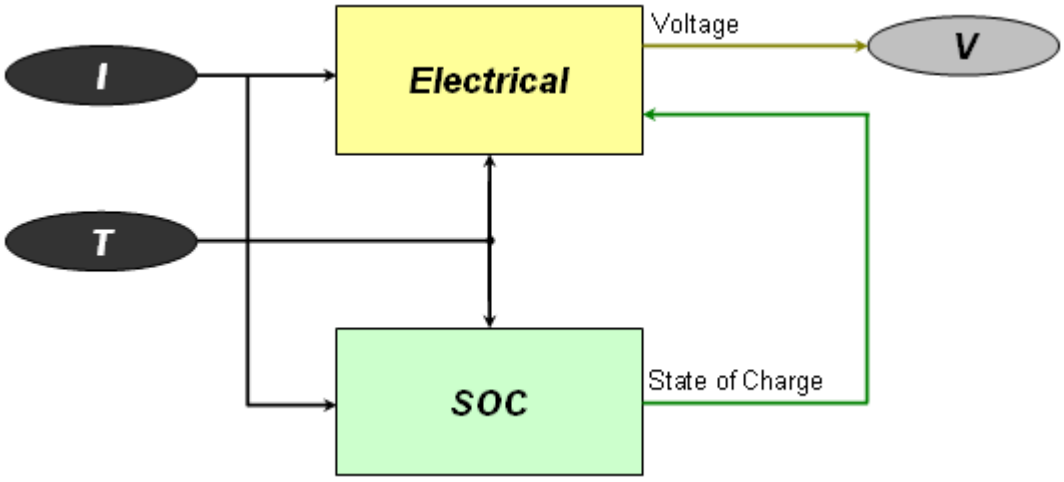

Figure 16: Triple-state battery model with two inputs and two distinct subsystems

3.1.1 Electrical model

Whether temperature is considered an external input (for diagnosing other internal parameters) or a state variable (during stand-alone simulation of battery behavior), we cannot describe it quantitatively without discussing the electrical model, which is presented in Figure 17. The electrical model captures first-order dynamics of the battery under load because of one memory element, the capacitor.

Some notes:

- All the circuit elements in the equivalent circuit model are assumed to vary as some function of: SOC, temperature, current magnitude (which includes direction of current, charging or discharging), unless they are found experimentally not to vary.
- Current direction is in the circuit shown in Figure 17 defined to be *negative for charging*, and *positive for discharging*.
- The capacitor voltage V_c is the only state of the electrical submodel. The input is the current I_B and the estimated circuit element values; the output is the terminal voltage V_B.

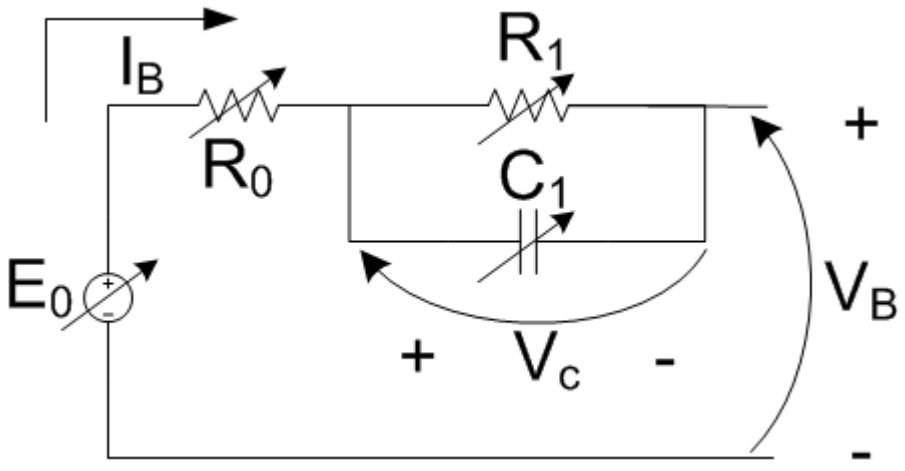

Figure 17: Equivalent circuit model of electrical system with variable parameters

For this first-order electrical model, Kirchoff's current rule yields:

$$E_0 - I_B R_0 - V_c - V_B = 0 \tag{7}$$

Capacitor voltage V_c is a state with the following differential equation:

$$\dot{V}_c = \frac{1}{C_1} I_B - \frac{1}{R_1 C_1} V_c \tag{8}$$

which is an ordinary first-order differential equation with the solution being

$$V_c(t) = V_c(0) e^{-\frac{t}{R_1 C_1}} + R_1 I_B (1 - e^{-\frac{t}{R_1 C_1}}) \tag{9}$$

Combining this result with the battery terminal equation yields the following for terminal voltage:

$$V_B = E_0 - I_B (R_0 + R_1) + (I_B R_1 - V_c(0)) e^{-\frac{t}{R_1 C_1}} \tag{10}$$

This equation may be applied to four different situations, which can be referenced against an example current-voltage profile shown in Figure 18. These relationships become important when performing parameter estimation based on experimentally obtained input-output current-voltage curves.

- $t \to \infty$, $I_B = 0$

$$V_B(t \to \infty) = E_0 \tag{11}$$

$$V_c(t \to \infty) = 0 \tag{12}$$

- $t \neq \infty$, $I_B = 0$

$$V_B(t) = E_0 - V_c(0)\,\mathrm{e}^{-\frac{t}{R_1 C_1}} \tag{13}$$

- $t \neq \infty$, $I_B \neq 0$, $V_c(0) = 0$

$$V_B = E_0 - I_B(R_0 + R_1) + I_B R_1\,\mathrm{e}^{-\frac{t}{R_1 C_1}} \tag{14}$$

- $t \neq \infty$, $I_B \neq 0$, $V_c(0) \neq 0$: the complete equation returns.

$$V_B = E_0 - I_B(R_0 + R_1) + \left(I_B R_1 - V_c(0)\right)\mathrm{e}^{-\frac{t}{R_1 C_1}} \tag{15}$$

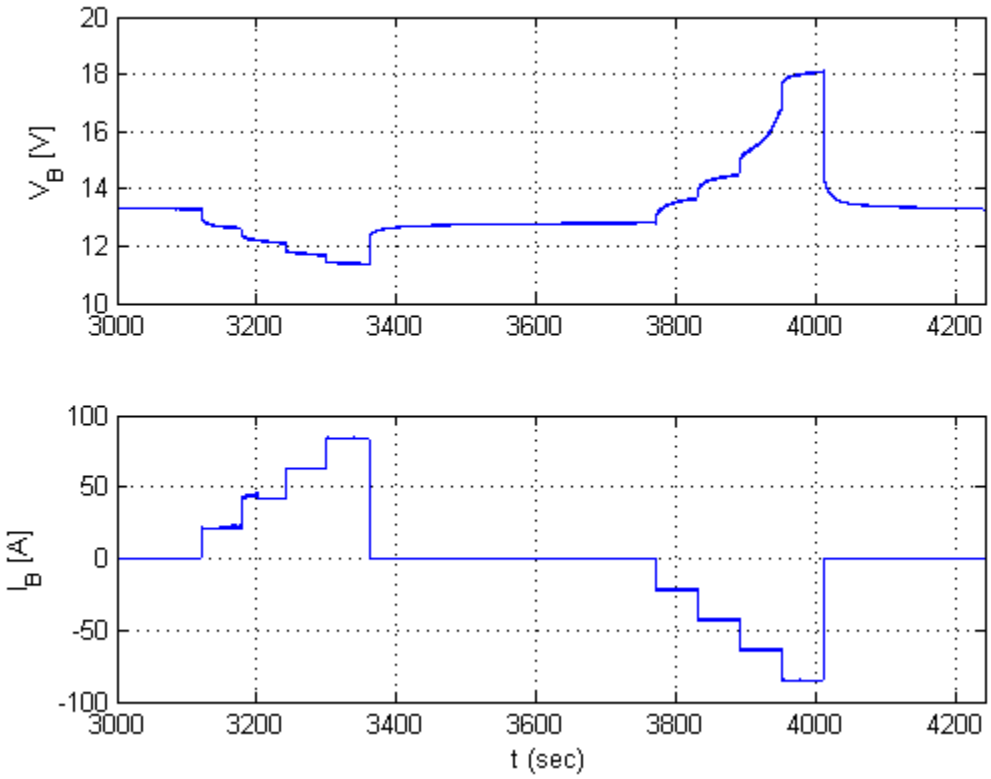

Figure 18: Example of a discharge-charge test cycle

3.1.2 Thermal model

With an electrical model, it becomes easy to construct a first-order thermal model. Heat is produced by current flowing through the lumped resistors, and is dissipated by a simple first-order term representing convection out of the battery or into a cooler electrolyte. The differential equation representing heat flow is:

$$mc\frac{d\Delta T}{dt} = (R_0 \cdot I_B^2 + R_1 \cdot I_{B,R_1}^2) - h_A(T - T_\infty) \tag{16}$$

with *mc* being the battery's specific heat in J/°C, h_A the heat transfer rate in W/°C, and $I_{B,R1}$ being the current through the R_1-leg of the parallel branch.

The thermal parameters are obviously extremely difficult to precisely quantify, but a benefit of using a lumped thermal model such as this is that overall effects can be approximated to a first-order exponential. Nominal values of both the specific heat and heat transfer rate can be obtained by looking at sample values of resistance and temperature changes accompanying currents. With experimental data, more exact values can be obtained.

3.1.3 State of charge model

As explained above, the SOC estimation method for the model chosen was current integration. This method simply counts the charge entering and leaving the battery:

$$Q(t) = Q(0) - \frac{\eta}{Q_0}\int_0^t I_B(t)\,dt \tag{17}$$

The calorimetric efficiency η may be determined by discharging the battery a known amount, recharging it at the same current level for the same amount of time, and measuring state of charge using open-circuit voltage. It will be necessary to account for surface charge after charging to ensure that the open-circuit voltage will correctly reflect the SOC.

3.1.4 Complete model

Over the window of time that the circuit element values remain constant, this presents a

linear time-invariant system that is easily analyzed using ordinary methods of system theory. Now, after we have presented a literature review as well as the final model chosen to characterize the battery for, the main work of *this* thesis, parameterizing these circuit elements, will be elucidated.. The design and execution of experiments, as well as data analysis procedures, will be detailed shortly. First, the equipment available will be described.

3.2 Experimental equipment

The experimental tasks for battery modeling involve placing current profiles upon the battery, and measuring the temperature and voltage responses. An experimental test bench had been previously assembled for the study of supercapacitors at CAR in 2004 [4], and this setup was enhanced for the present study.

3.2.1 Hardware

The experimental hardware setup comprises of the following:

- Environmental chamber capable of maintaining temperatures between -40 and 100 °C.
- Chroma 63201 2.6 kW programmable electronic load, capable of drawing 300 A at 80 V.
- PowerTen 10 kW electronic supply (source), capable of delivering200 A at 50 V.
- A custom-built signal conditioning box to scale and filter analog signals.
- National Instruments SCXI chassis containing a thermocouple amplifier board and a feedthrough module for analog and digital I/O.
- National Instruments PCI DAQ card (in a desktop PC) that interfaced all digital and analog I/O to
- the desktop PC, which samples sensor data and outputs all electronic control commands to the supply and load.

There are three sets of sensors that monitor the state of the battery and hardware:

- a voltage sensor takes a reading from cables connected to the terminals of the battery, and is normalized to be between 0 and 50 V in the signal conditioning box.
- A 500 A Hall effect current sensor that measures the current through the cable connected to the positive battery terminal, and
- connections for up to 40 thermistor temperature sensors, three of which were employed to

measure the temperatures of the positive and negative terminals and of ambient air.

Temperature measurements in an automotive lead-acid battery may be problematic as all of them today are valve-regulated batteries, and are sealed and maintenance-free. Usually a fairly thick plastic container forms the outer shell of the battery, making it somewhat unclear what exactly comprises a lumped battery temperature. Noting, however, that the construction of a battery involves thermally conductive materials connected to its terminals, the terminal temperature may be taken as a valid temperature.

Figure 19 shows the electrical circuit of the assembly, and Figure 20 explains the flow of both control signals and data. Component and connection details (especially regarding the signal conditioning box) have been thoroughly elucidated in [4].

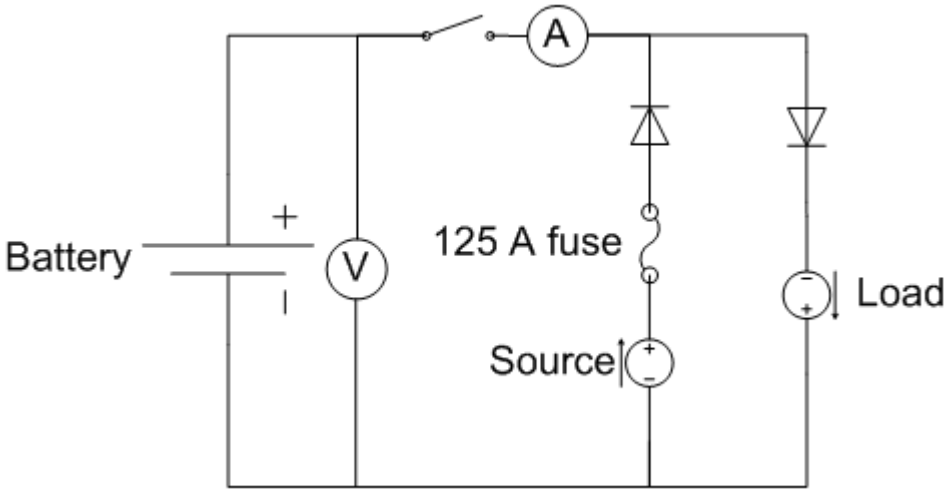

Figure 19: Electrical schematic for experimental setup (note the battery isolation relay, added for the present work)

The major hardware additions to the setup from [4] are the more powerful *Chroma load with RS232 control* (the previous one was limited to 600 W and used analog voltage control), and a *battery isolation relay-controlled contactor* to isolate the battery. The latter was done because when 0 A was commanded from the load and the supply, the load would draw 0.15 A and the source would inject between 0.15 and 0.4 A into the battery. The solid-state relay is controlled via a digital output from the PC, and triggers the high-current electromechanical

contactor switch upon request.

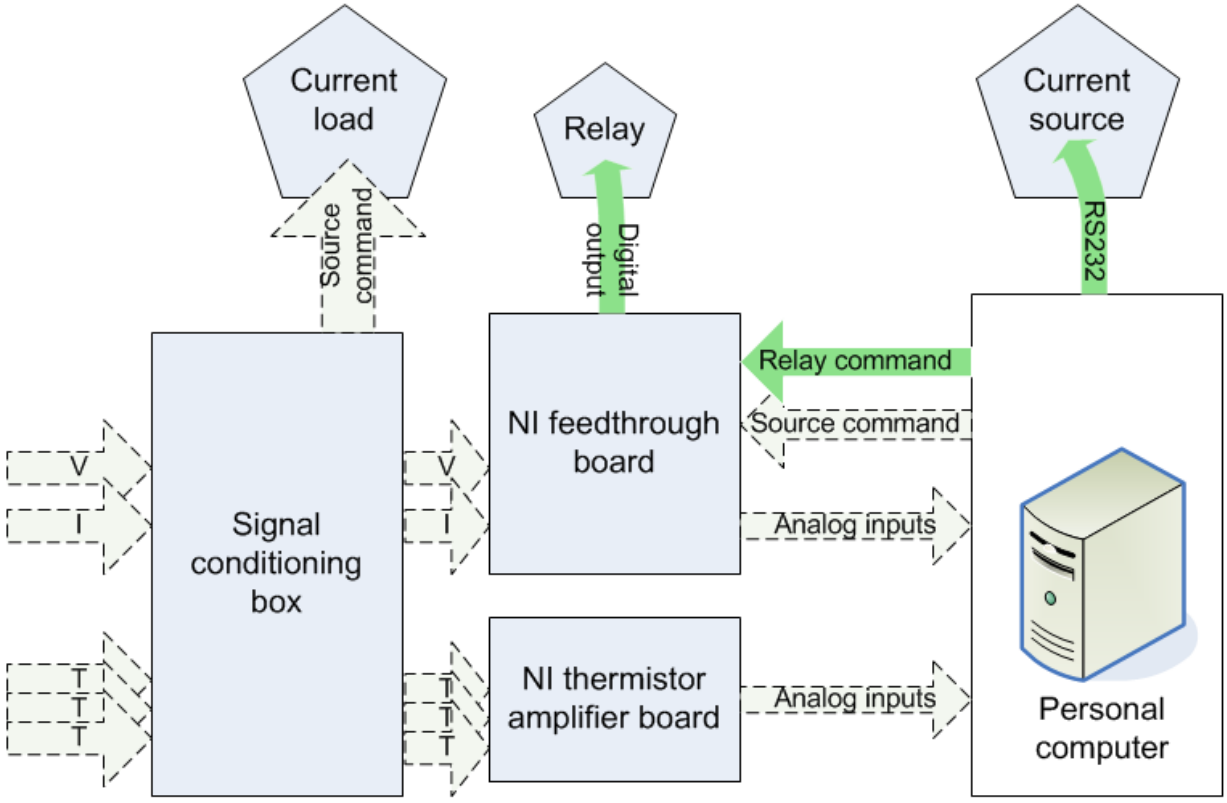

Figure 20: Experimental bench data flow (analog and digital inputs and outputs)

3.2.2 Software

The software controlling the system involves MATLAB and LabView (from The Mathworks and National Instruments, respectively). Matlab is used to create control command files for the hardware. These files are input to a LabView visual interface (VI). The VI, in a nutshell, controls the electronic supply, load, and battery isolation relay, while simultaneously collecting current, voltage, and temperature data into an ASCII text file. The VI was extended beyond that of [4] in order to perform RS232 control of the new load (see the previous section on hardware) and to isolate the battery when it was not being charged or discharged.

The VI can accept any sample rate. 320 Hz was chosen as an optimal between noise immunity and PC speed. (This rate is extremely high and allowed significant amounts of noise to enter the system.) The actual use of the software will be detailed in an appendix that will be

deposited with the Battery group at the Center for Automotive Research, and will not accompany this thesis.

3.3 Battery modeling methodology

Recall from Section 3.1 that the battery model is an LTI system over a window of time for which the electrical circuit elements remain constant (the battery SOC and temperature may vary over this window, because they are dynamic states of the system). In this section, the experiments done to uncover the values of these circuit elements at different operating points will be detailed.

3.3.1 Experimental methodology

Using the experimental bench described in the previous section, the battery was subjected to a sequence of discharge pulses, designed to remove 5% of the SOC from the battery to 50% SOC, and followed by a similar sequence of charge pulses to take the battery to nearly 100% SOC. The pulses comprised a set of step voltages, constructed as per Figure 21. The voltage responses to the sequence of increasing step inputs, followed by relaxation, can be analyzed to yield the circuit values at various SOCs and temperatures, as illustrated in [41], and derivable from the analysis from Section 3.1.1, and as detailed in the next section. This was repeated at multiple temperatures. The data was sampled at 320 Hz. With this serving as introduction, a detailed methodology will be presented.

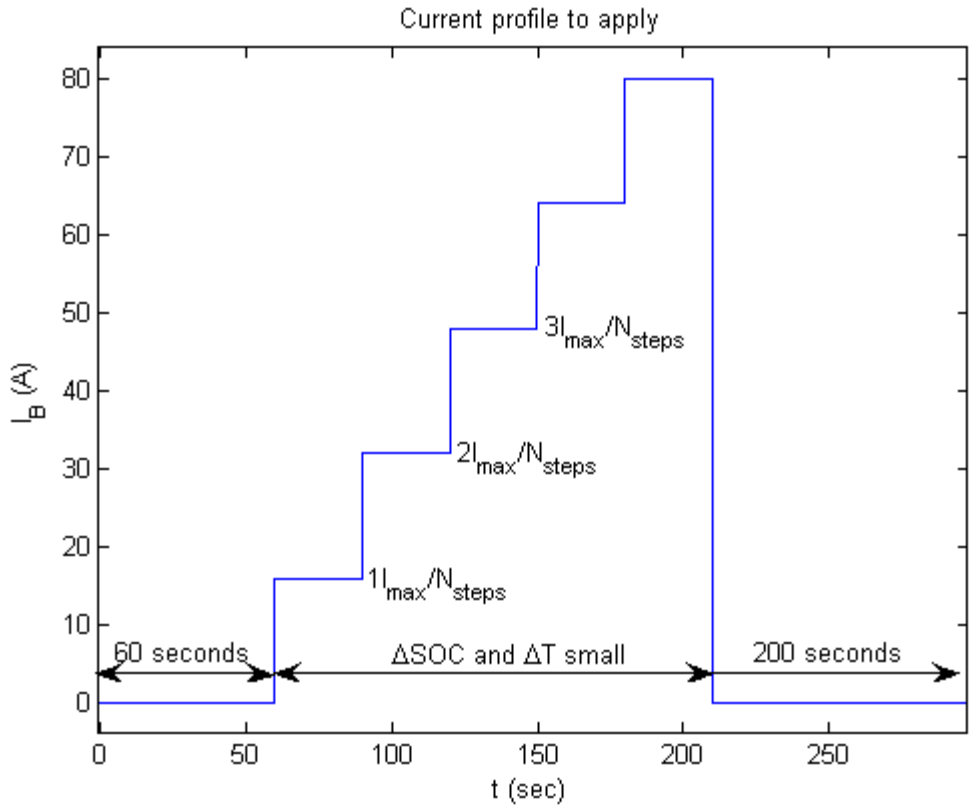

Figure 21: Construction of one current pulse for parameter estimation

The first step in constructing the current profiles to yield the circuit parameterization desired is deciding the independent variables of the model, and the domain over which they need to span. As Section 3.1 described, the model's circuit parameters are expected to vary with *state of charge, battery temperature,* and *battery current* (direction being important — the values are expected to be different when charging and discharging). The domains are given in Table 1.

Table 1: Restriction of battery model's domain

Variable	***Minimum***	***Maximum***	***Resolution***
Charge current	0 A	20 A	N_{steps} = 6 steps
Discharge current	0 A	80 A	N_{steps} = 5 steps
State of charge	50%	100%	5% increments
Temperature	5 °C	35 °C	5, 20, and 35 °C

The charging current was restricted to maximally 20 A because initial data acquired from

a commercial passenger car indicated that a properly functioning alternator and voltage regulator rarely charges a battery above 10 A after cranking. (Immediately after cranking, the alternator can dump up to 45 A into the battery, but this is for less than 15 seconds.)

An important aspect of charging profiles was that the LabView VI would cut off charging current for one set of plateaus if the battery voltage rose above a set point of 14.5 V. That is, as one set of plateaus (comprising one "pulse") was progressing, if the battery voltage rose above 14.5 V, that set of plateaus would be terminated until the current requested 0 A, after which the desired current profile would resume. This was done to simulate the fact that in a vehicle, the voltage regulator will modulate charging current to maintain the battery at such a set voltage (although in the vehicle, this varies by temperature). This is very important to avoid overcharging the battery and causing it to vent, but does have some ramifications for parameterization: we will not have circuit parameters for high charging currents at high SOC.

The discharging current was restricted to 80 A because one of the tasks of the battery is to provide support for a failing alternator. An average size for an alternator is 80 A. In normal car operation, however, the battery almost never sees currents this high for more than a few seconds, as the alternator field control detects the drop in voltage accompanying battery discharge and produces more current.

Because state of charge increments of 5% was deemed sufficient resolution to adequately characterize the battery, the resolution of current (both charging and discharging) was chosen to preclude extremely lengthy test times. It had been our experience that during very lengthy current profiles (more than 3 hours), the probability that the personal computer would encounter a software malfunction increases, and anomalies begin creeping into the acquired data (such as oddly varying voltages that are impossible in real life, such as battery voltages sagging by 1 V for 15 seconds during a capacity test, etc.). One of the major points of incompleteness of this

thesis is that the battery was not more finely characterized at lower currents, where more details could be observed, and where the battery spends most of its time.

(Note that during cranking, the battery will see discharges of more than 600 A for a few seconds. Unfortunately, this exceeds the capacity of the electronic supply, and there isn't a safe way to extract this much current from the battery for a controlled period of time. However, diagnostics can be restricted to post-crank operation of the vehicle, so this point was not deemed as terribly critical.)

After an initial set of battery tests at 25 °C, it was noticed that the battery temperature (as measured at its conductive terminals) changed little over a 1 hour sequence (jumping up some 4 °C during discharge, and overall less than 1 °C from ambient). Therefore, to characterize the battery at nominally "cold" and "hot" temperatures, a ±15 °C test regime was adopted.

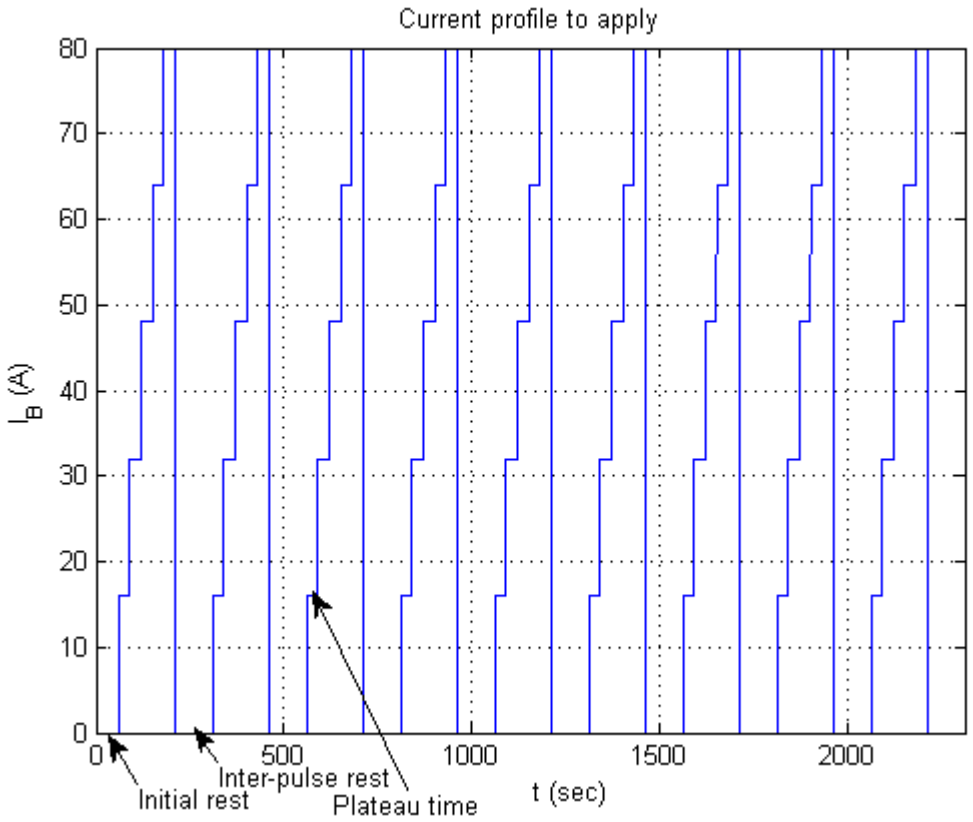

Figure 22: Example current profile, with three secondary experimental variables

With these conditions determined, a current profile such as the one in Figure 22 was

constructed. Three remaining parameters for experimentation remain to be described:

- *Initial rest*: this is a minor time, to ensure that enough samples of the starting voltage have been collected. This was chosen to be either 200 or 60 seconds.
- *Inter-plateau rest*: chosen to be 200 seconds for both charging and discharging curves, this is needed for the open-circuit voltage to settle. 200 seconds is on the lower end of adequate for discharging at these currents, but proved to be inadequate during charging. Open-circuit voltage had to be estimated using curve-fitting techniques.
- The *plateau time* is computed directly from the amount of SOC to remove from the battery. For charging sequences, each current plateau was held for 100 seconds, and for discharging, 30 seconds.

This made total charging and discharging experimental test times 117 minutes and 53 minutes long, respectively.

Once these current profiles had been constructed in MATLAB, they were exported to the Labview VI for executing. This process consisted of the following steps.

1. Using a commercial car battery charger, the battery was charge to 100% SOC.
2. The battery was allowed to relax for 2 hours while soaking in the environmental chamber at a set temperature.
3. The environmental chamber temperature control was disabled (because it interfered with the temperature measurements at the battery's terminals), and the discharge sequence was initiated.
4. After the sequenced completed and the battery was at approximately 50% SOC, the battery was given another 2 hours to relax with the temperature control reinitiated.
5. The charging sequence was initiated (with the current .
6. Once the charging profile completed, step 1 was immediately executed for another temperature, or the batter was left overnight before resuming another run the next day.

3.3.2 Data analysis methodology

Three methods were investigated to extract circuit parameters from the input-output current-voltage curves at various SOCs, temperatures, and currents outlined previously. The first method, widely used [41], relies on solution of the circuit's differential equation assuming a step

input. The voltage profile will therefore be an instantaneous drop across the series resistance R_0, followed by an exponential curve that saturates at some final terminal voltage.

The problems with this method will be delineated in the following section. A parametric estimation method based on function minimization was subsequently utilized; this involved using the MATLAB function `fmincon`, in conjunction with a Simulink model of the battery differential equations modeling a simply LTI system, with a specified cost function (a specific norm between the experimental and simulated voltages). The technique requires a set of initial guesses for the parameters of the model (nominal values for open-circuit voltage, resistances, and capacitances) and nonlinearly iterates on the initial guess vector to find a set of parameters that minimizes the discrepancy between the output of the simulated model and the actual battery. This method is very sensitive to initial guesses, as in the previous method. (`fminsearch` and `fmincon` are quite similar in operation, but the latter can be bounded.)

3.3.2.1 Feature-extraction parameter estimation

This section will explain one method to extract circuit parameters from the input-output curves that involves identifying and extracting certain features in the output voltage profile, such as instantaneous rise and exponential, and deducing from these functions' mathematical forms the underlying circuit parameters.

In Section 3.1.1, the battery terminal voltage for the circuit in Figure 17 was expressed as

$$V_B = E_0 - I_B(R_0+R_1) + (I_B R_1 - V_c(0))\,\mathrm{e}^{-\frac{t}{R_1 C_1}} \tag{18}$$

and its simplifications for steady-state were derived. This expression reveals that there is always a base voltage, the open-circuit voltage E_0, which is modified instantaneously by a current. Such a current will charge the capacitor C_1, and until it is fully charged will have a decaying exponential at some time constant τ. Once the capacitor is fully charged, the terminal voltage

will be the open-circuit voltage with a simple ohmic drop across the two resistors.

A pictorial representation of these equations will readily explain how this is utilized: Figure 23. The following considerations will be noted before a step-by-step outline of the analysis programs is given.

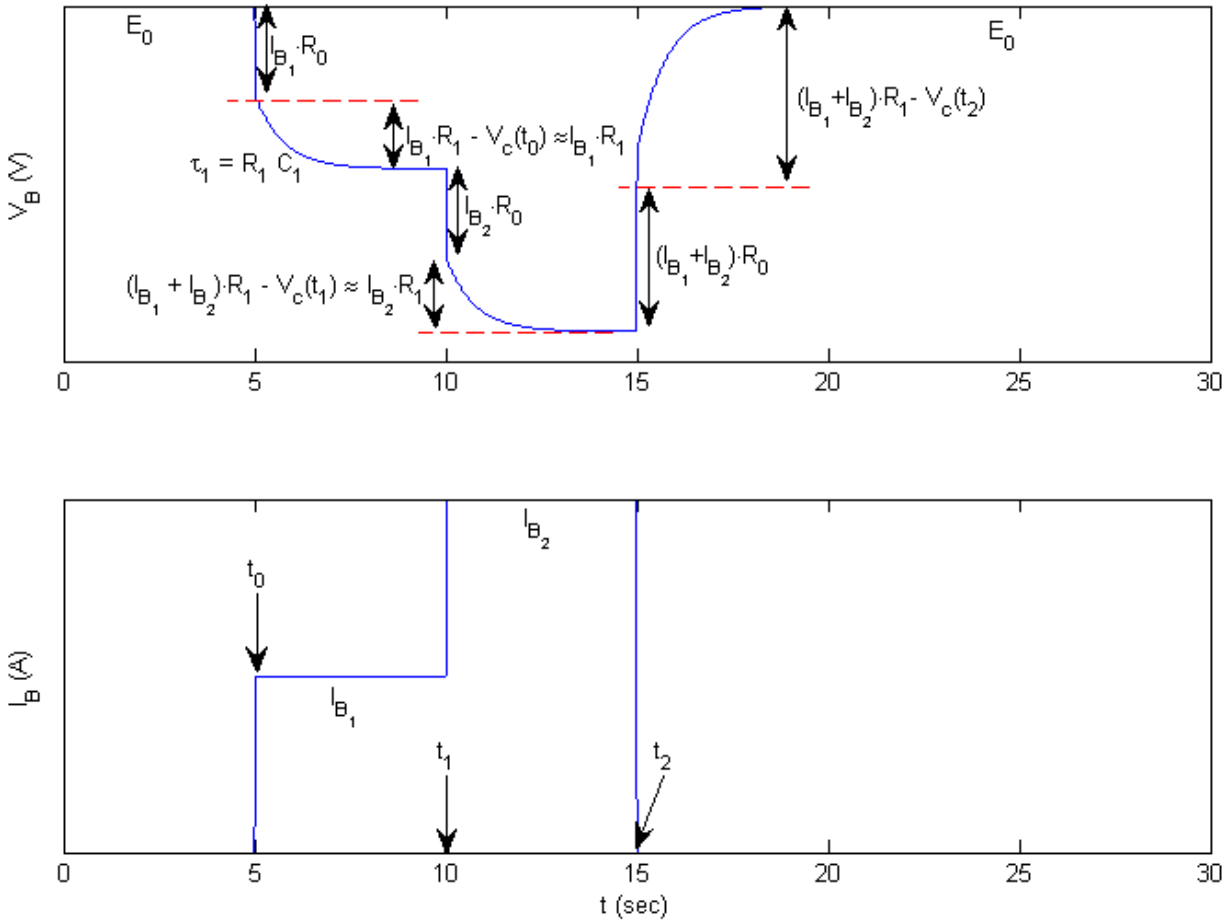

Figure 23: Circuit parameter extraction from battery voltage response

Recall from Section 3.1.1 that the open-circuit voltage E_0, two resistances R_0 and R_1, and the capacitance C_1 were all expected to be some function of SOC, temperature, and current level.

The *open-circuit voltage* E_0 is well-known to be a function of only SOC and temperature [3], as it is defined for an unloaded battery. Therefore, this is only a 2-dimensional function, and data points for it can be gathered during rest periods. The data gathered at 20 °C is shown in Figure 24, both the charge and discharge case. The effect of surface charge is very clear for the

discharge case: the experiment was begun with the battery fully charged, and therefore the first open-circuit voltage is elevated. This is useful because the battery model will certainly operate at high SOCs, due to voltage regulation in the vehicle (and in the larger automotive electrical network simulator that it will run in), during which the effects of surface charge must not be ignored.

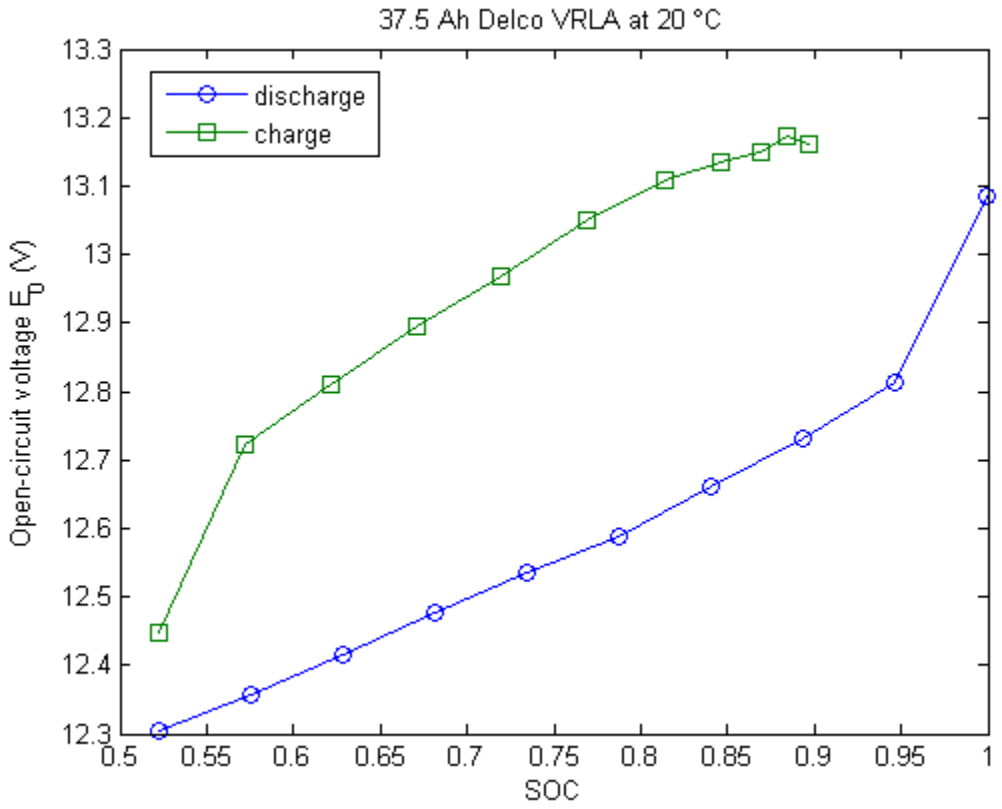

Figure 24: Open-circuit voltage as a function of SOC at 20 °C. Note the effect of surface charge at high SOC, where the experiment began.

A second point to note about the open-circuit voltage is that there is a strong hysteresis between open-circuit voltages in the charging and discharging cases, at the same SOCs. This is due to surface charge. The lengthy relaxation time required to measure the actual open-circuit voltage during charging (4 hours at minimum, many recommend 8 or more hours) precluded this measurement, and therefore a calorimetric efficiency could not be computed for every voltage step. It is therefore neglected; future experiments may enable us to determine this value by

testing at the beginning and end of a complete experimental cycle. (The clustering of points in the charge curve at higher SOCs is due to truncating parts of the charging current profile depending on battery voltage, to avoid overcharging. See the previous section.)

Another major point is regarding the non-variability of the capacitor C_1. It was noticed when examining the voltage responses that at all but the lowest currents, either charging or discharging, that the steady-state voltage after a current step was applied was not a constant voltage but a linearly decreasing or increasing voltage (depending on charging or discharging). An example is shown in Figure 25. The trend of this linear-sloping voltage profile strongly resembled the 0.1C discharge profile obtained by a capacity test, and the Peukert effect was immediately suspected (see Figure 3 and Section 1.3.5).

Once a parameter estimation algorithm was written, several of these individual voltage responses were analyzed for various lengths of time. Consistently, the time-constant of the exponential decay indicated *a constant capacitor value*, on the order of 200 F. This result is the same as found by [3] for dry cell lead-acid batteries. Therefore, the parameter estimation program was extended to isolate the exponential transient part of the voltage response and ignore the linear slope by considering varying lengths of the voltage response that yielded a time-constant amenable to this set value of C_1.

With these notes in mind, we proceed to a broad but fine step-by-step outline of the parameterization algorithms. These were implemented in MATLAB.

1. Load current, voltage, and temperature data acquired from LabView.
2. Filter current and voltage data using multi-stage median filtering.
3. Locate the discrete jumps in the current profile by differentiating the filtered voltage (for discharge experiments) or current profile (for charging experiments). Using the voltage signal is preferred to best isolate the samples that comprise the instantaneous voltage change, but the PowerTen supply used for charging injects noise into the voltage reading with a standard deviation at the same order of magnitude as the jumps being examined.

Therefore, for charging, the measured current curve is used, as its derivatives are much cleaner.

4. With the discrete plateaus isolated, determine the instantaneous voltage change ΔV, by examining the samples of the voltage for which the derivative of the current or voltage is above a threshold. This threshold is adjusted for each experiment, based on the filtering done for each one.
5. Begin looking for the exponential transient part of the voltage response by subjecting successive clips of the voltage to the nonlinear curve fit in the form of

$$V_B = a + b\ \mathrm{e}^{ct} \tag{19}$$

This is done using `fminsearch()`, with initial values set to the simple ohmic drop expected (see Figure 23).

6. Extract circuit parameters from each plateau's curve fit. Defining ΔV as the instantaneous voltage drop, I_B as total current through the battery, and $I_{Bi} = i\, I_{max} / N_{steps}$

$$R_0 = \frac{\Delta V}{I_{Bi}} \tag{20}$$

$$R_1 = \frac{b + V_c(0)}{I_B} \tag{21}$$

$$C_1 = -1/\left(c\, R_1\right) \tag{22}$$

If C_1 is not near the expected value of C_1, 200 F, discard this truncation of the voltage response and continue searching for a more isolated exponential transient. Build a map of circuit values at all available SOCs, temperatures, and current levels.

7. Once a relaxation curve is reached, record the open-circuit voltage as the final value of the curve-fit.
8. Once all the plateaus have been analyzed, proceed to the next experiment (be it the charging experiment at the same temperature or the discharge experiment at a new temperature).
9. Once all experiments have been analyzed and circuit value maps generated over the domain of the model, find a polynomial curve fit for each circuit parameter as a function of the model variables. Find separate polynomials for charging and discharging cases.

Results of these procedures have been given in the next chapter, including the results of the curve fitting, and the experimentally obtained circuit values. (The polynomial fits for the

circuit parameters is a simple exercise, and while the code has been written to compute it using a least-squares fit, the results are not presented as the actual circuit parameters are of more interest at the present moment than arbitrary functions modeling them.)

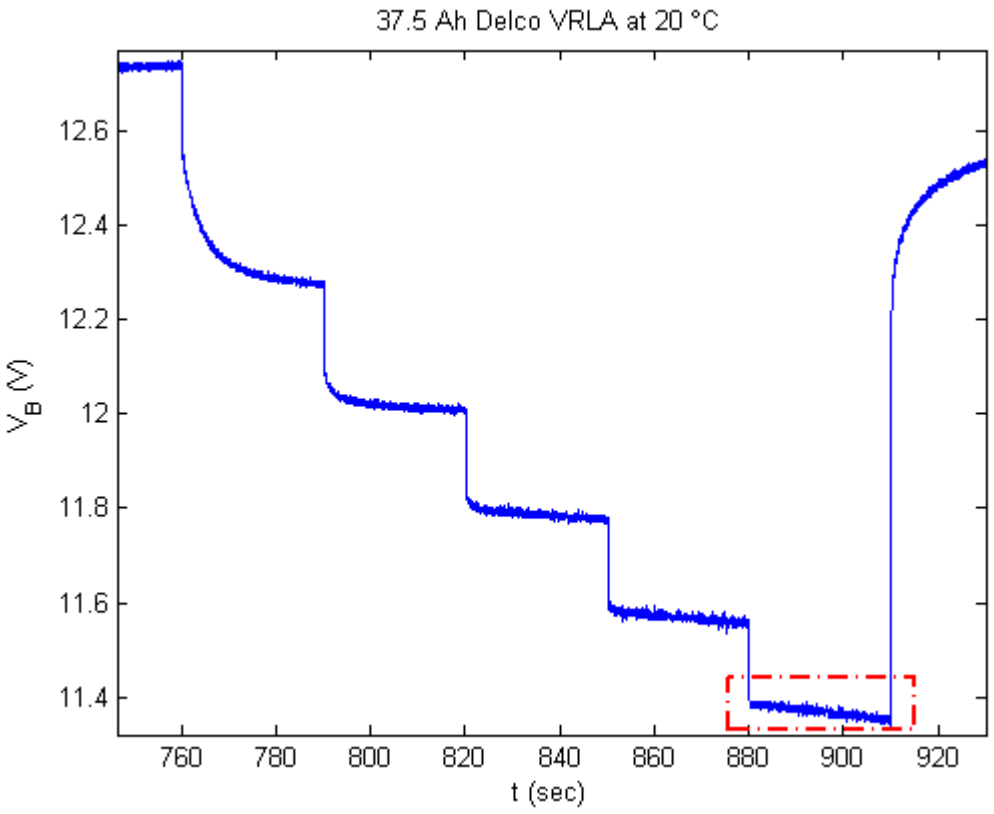

Figure 25: Battery voltage's linear steady-state due to Peukert effect

The files for this method are included in the data store, but will not be detailed here because the method was not used for parameter estimation. Only the plateau isolation functionality was used, and the algorithm does this by simply loading a highly filtered version of a voltage or current curve and thresholding its derivative to find the discontinuous jumps.

3.3.2.2 Nonlinear minimization parameter estimation

While the technique outlined above has been used successfully in many studies ([22], [41]), it has been usually applied without transient isolation. Without transient isolation, simple fitting of the curve as described above yields quite high circuit resistances, which may mean that this method is unsuitable for the lead-acid battery over this particular domain.

A computationally simpler by more costly approach involves modeling the system's dynamic equations over the small time window that it is assumed to be linear, and then searching for the set of parameters that engender an output most similar to the input. This task is frequently done in system identification. The MATLAB toolchain contains both Simulink (for creating and simulating systems) as well as optimization routines such as `fminsearch` and `fmincon` (in the optimization toolbox), which provide a complete framework to perform such a parameterization.

This method does not rely on assuming the form of the voltage profile, and therefore non-idealities may be acknowledged instead of being assumed to be unimportant. Essentially, the method involves breaking up the experiment into small windows where the battery may be assumed to be a linear time-invariant system. The circuit parameters of the system are then found using numerical optimization.

The algorithm consists of the following steps:

1. For each experiment, filter the voltage or current profiles so that it becomes easy to isolate each current plateau. This step is the same as in the previous method. However, very precise isolation of the plateaus is not necessary with this procedure, and indeed, the results are better (that is, are more realistic and the final simulated output using estimated parameters have less error) if several samples from the previous plateau are included in the current-voltage window.
2. For each of these isolated plateaus, use `fmincon`, in conjunction with a cost function which accepts possible circuit parameters, runs a Simulink model to obtain simulated system output, and finds the norm-error between the output of the Simulink model and the experimental results. `fmincon` will also be given initial guesses for all circuit parameters estimated, and it will search the phase space to determine the best set of values.
3. Once the numerical method has found the “best” set of parameters, save the states of the system (for the electrical system, the capacitor voltage) for the next plateau.

For discharge experiments, because exists a very accurate SOC-temperature map for the open-circuit voltage E_0, only the circuit element values of R_0, R_1, and C_1 were left as free

variables. For the charge case, however, due to the hysteresis in open-circuit voltage between the charging and discharging case, E_0 was also estimated.

Some notes about this parameter estimation. Both first- and second-order models were implemented for estimation. For the discharge case, a specialized cost function was used that weighted the beginning of the voltage profile more than the tail; this would force the minimization to emphasize the transient more than the steady-state, due to poor initial guesses. For the charging case, a simple norm (between the simulated and experimental curves) was taken as the cost function, and this worked well because initial guesses were better.

A good initial guess vector is vital for successful minimization; with up to 6 dimensions being searched (e.g., for the second order model, charging experiment: E_0, R_0, R_1, C_1, R_2, C_2), most of the variable spaces will not be searched very thoroughly.

All files implementing this algorithm, and results, are in the `'fmincons/'` directory of the thesis datastore. Each experiment is placed in a different directory. The MATLAB script `nonlinear_plant_run.m` in each directory will load the appropriate experimental data files and run the minimization, and save the results. In the parent directory `fmincons`, there is another script `plot_curvefitting.m` which, given an experiment and model (first order, second order, etc.), will load the results of the estimation and plot the variable surfaces.

The algorithm utilizes the results of plateau isolation done using the previous method; if new experimental data is gathered and this method is utilized without using that curve-based method, a simpler plateau isolation (time-based isolation) may be used.

3.3.2.3 ARMA-based estimation

Because the system is assumed to be linear and time-invariant, a simple dynamic model may be set up for the electrical circuit with the only state being the capacitor voltage. During the discharge case, the open-circuit voltage is a known coefficient.

$$\dot{V}_c = \left[\frac{-1}{R_1 C_1}\right] V_c + \left[\frac{1}{C_1}\right] I_B \tag{23}$$

$$-V_B + E_0 = [1] V_c + [R_0] I_B \tag{24}$$

For charging, the state and output equations may be altered to make the open circuit voltage E_0 an unknown parameter to be estimated:

$$\dot{V}_c = \left[\frac{-1}{R_1 C_1}\right] V_c + \begin{bmatrix} \frac{1}{C_1} & 0 \end{bmatrix} \begin{bmatrix} I_B \\ 1 \end{bmatrix} \tag{25}$$

$$-V_B = [1] V_c + \begin{bmatrix} R_0 & -E_0 \end{bmatrix} \begin{bmatrix} I_B \\ 1 \end{bmatrix} \tag{26}$$

Given these systems with their LTI ***A***, ***B***, ***C***, and ***D*** matrices containing known and unknown parameters, an ARMA model can be constructed. There exist simple but powerful algorithms that can, given input and output data (in the form of time series), robustly estimate the ***A***, ***B***, ***C***, and ***D*** matrices. Unlike `fmincon`, MATLAB implementations of ARMA-model parameterization such as `pem` (in the System Identification toolbox), form a specific cost function based on least-squares analysis. The cost function constructed describes a quadratic surface in all unknown dimensions with one minimum, so instead of a nonlinear search like the one that `fmincon` implements, a simple gradient descent is employed to find the set of parameters that leads to minimum least-squares error (the minimum of the cost function).

Estimation of the open-circuit voltage E0, using both this method and the previous one, may reveal the effects of surface charge more clearly (see next chapter).

Therefore, the input-output curves are separated again into individual current plateaus, and these segments of the curves are fed into the algorithm. The files `ltisysid.m` and `ltisysid_e0.m` implement the discharge and charging cases respectively, in the `'arma/'` directory of the datastore. The script `plot_armax.m` will plot the results of these scripts.

This method proves to be much less sensitive to initial guesses, runs much faster than

`fmincon`, and also gives assurance of optimality of the estimates produced: they are precisely matched to the system described, and second- or higher-order systems may be defined as easily as the first-order one. The only clearly visible drawback is that it can only be used with LTI models.

The method, despite its attractiveness, was not used for the final parameterization because, although it gave very satisfactory results for loaded conditions (during discharge or charge), *it yielded negative resistances and/or capacitances during relaxation* for the first-order model. For the second-order model, the second RC pair was assigned negative values. Although the output curves produced numerically using these circuit parameter values closely resemble the experimental curves, the negative-valued elements make no sense. Clearly the algorithm works because of its performance during load; therefore, it is surmised that there exists some error in the model description as presented above (although the equations were derived from the same understanding that produced the Simulink model used in the `fmincon`-based method). Therefore, the method is mentioned here and the code is attached in the datastore because of its simplicity and power, but its results were not suitable for use in this work.

4 Modeling results

The parameterization method described in Section 3.3.2.2 was utilized for final modeling and parameterization for the experimental data collected. The results will be presented in this chapter, with some analysis. Recall that experiments were conducted to characterize the battery for a first-order series-parallel RC electrical circuit at various temperatures (5, 20, and 35 °C, states of charge (100% to approximately 55% in 5% increments), and currents as described in Section 3.3.1. The code to perform similar characterization for the second-order model exists, but the results for these will not be included here.

The first point to note is the high variability in the datapoints observed. In some graphs, no single unifying trend is visible, and this is attributed to some significant factors:

1. Nonlinearity of the system.
2. High noise power due to extremely high sample rate (320 Hz).

Preliminary work using electrochemical impedance spectroscopy (EIS) on lead-acid batteries indicates a strong nonlinearity at high and low frequencies, well-modeled by a Warburg impedance (see page 28). Therefore, even the best-fitting simulated voltage curves presented below have slightly different patterns than the experimental curves; this is not solely a limitation of the first-order model as the problem persisted in the second-order curve fits.

The major note is that circuit parameters obtained immediately after rest and during rest are discontinuous from the rest of the surface described by the circuit parameter, as it varies over the SOC-T_B-I_B planes. A glance at any of the subsequent maps illustrate this: the curves obtained for 0 A and the first non-zero current load (16 A for discharge, -3.3 A for charge) are noticeably different than the other curves. This is even more clearly visible on surface plots (best viewed on an interactive screen, and therefore not reproduced here).

Another point to note is how little the `fmincon` algorithm attempted to tune the

capacitance C_1. This is because it is essentially fitting time-constants, and therefore tunes R_1 more aggressively.

Also, the plots of the open-circuit voltage during charging (Figures 39, and especially in 44 and 49) clearly indicate the effect of surface charge: clusters of six points are fairly linear, but are followed by a significant discontinuous jump to the next set of pulses. This happens during the 200 second rest period between each set of plateaus, and the open-circuit voltage rises as the charge permeates the electrodes.

One note on experimental results that has only recently been considered is the resistance of the cables connecting the battery to the experimental setup. To keep the battery inside the environmental chamber, approximately 2 meter long cables connect the battery to the load and source; the resistance of this cable may be significant when compared to the series resistance of the battery, R_0, and therefore should be measured. This enables one to see that points in a certain part of the domain may not fit the rest of the points, and this is most often due to bad fitting (minimization did not converge).

One may remark that the curves presented here are more more jagged when compared to the fitted data from other works, such as [3]. An important point to note is that this work attempted to develop an algorithm that would work without fine-tuning the initial guesses or cost functions for every single part of every experiment. Once reasonable initial guesses have been identified for a battery type, given the model type, the `fmincon` approach converges quite satisfactorily, and it is left to a human to examine the curves and locate the trends. From these curves, outliers may be eliminated for an arbitrary polynomial fit, for example.

With these notes in mind, we present the latest results of modeling of a single automotive lead-acid battery.

4.1 Discharging results

4.1.1 20 °C (discharging)

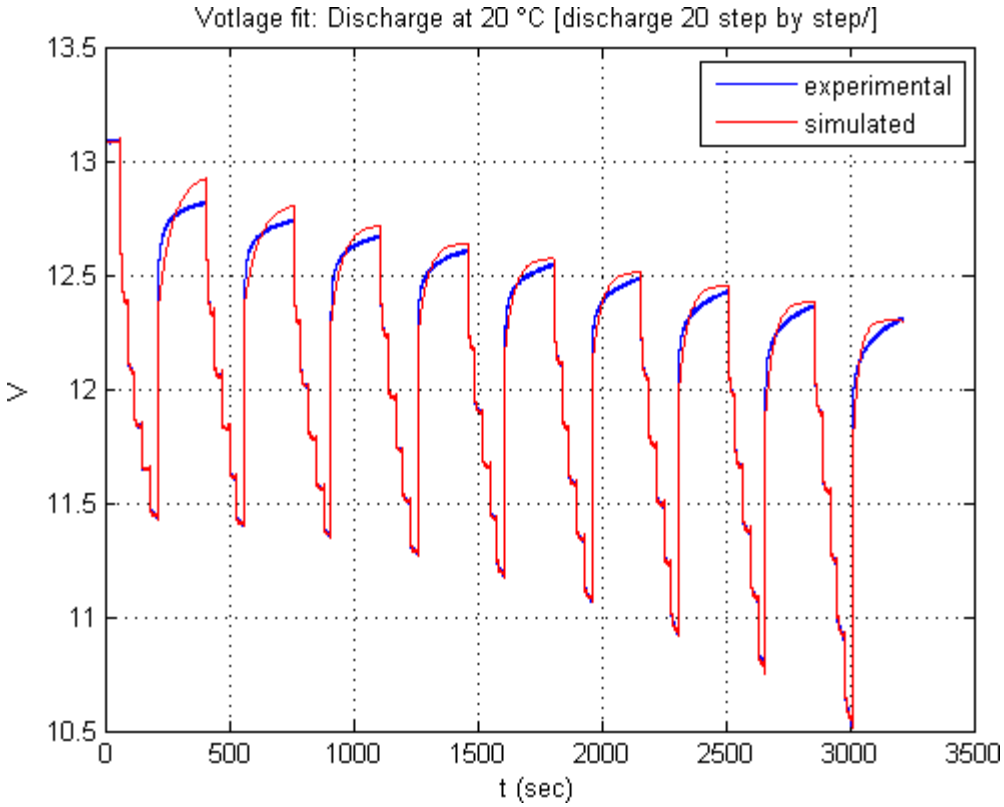

Figure 26

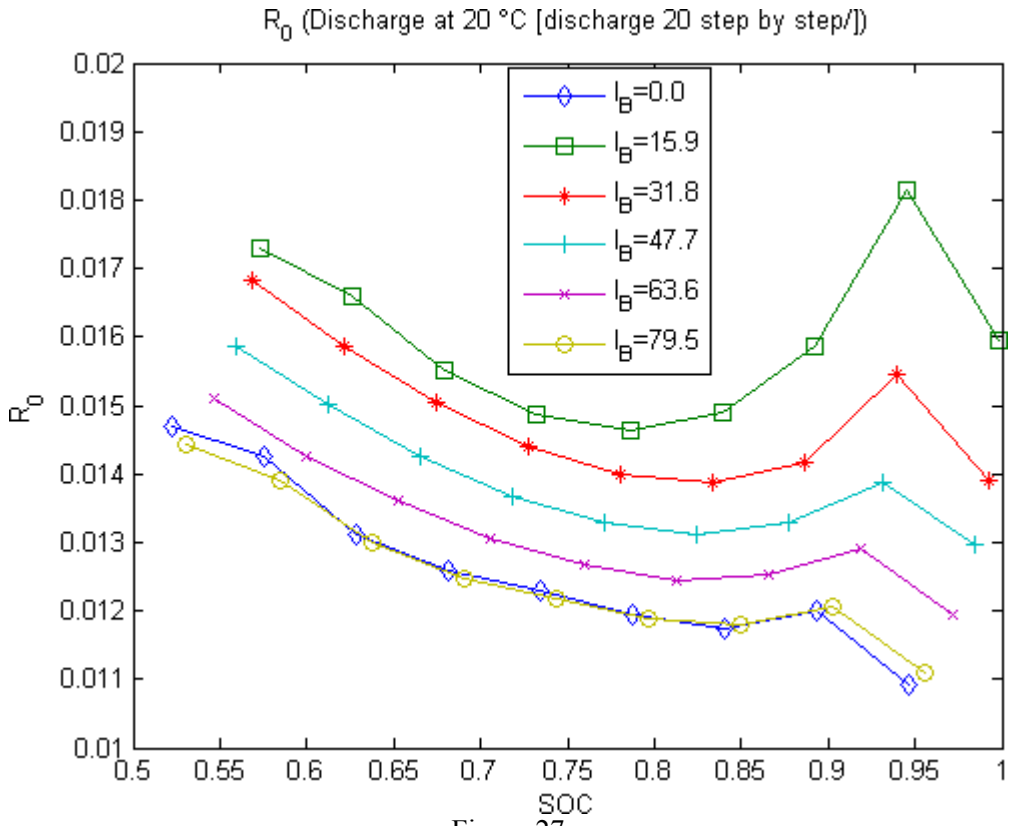

Figure 27

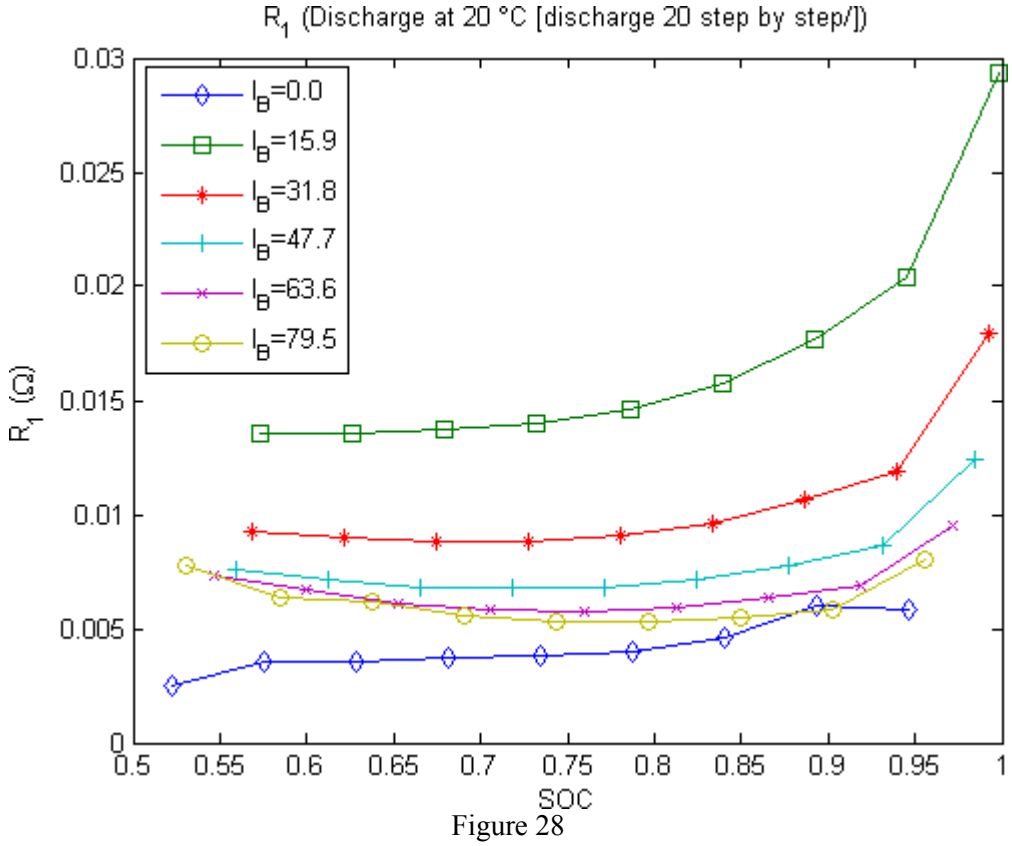

Figure 28

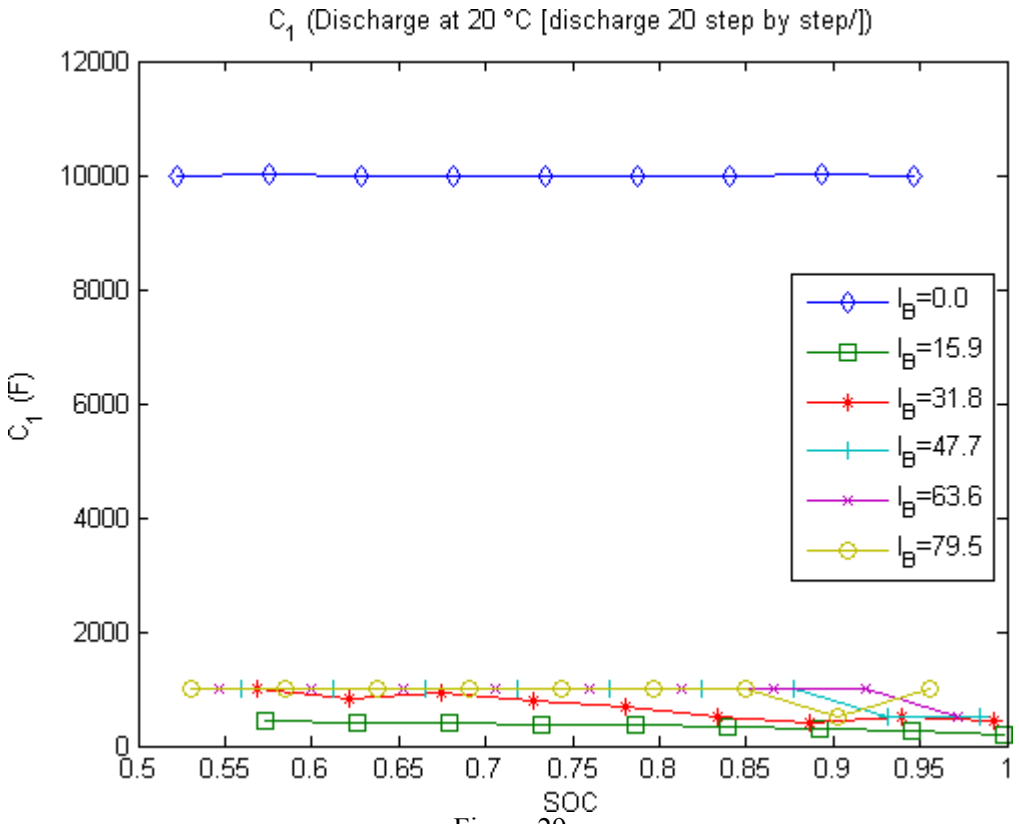
C1 (Discharge at 20 °C [discharge 20 step by step/])
12000
10000
8000
6000
4000
2000
0
C1 (F)
0.5
0.55
0.6
0.65
0.7
0.75
0.8
0.85
0.9
0.95
1
SOC
IB=0.0
IB=15.9
IB=31.8
IB=47.7
IB=63.6
IB=79.5
Figure 29

4.1.2 35 °C (discharging)

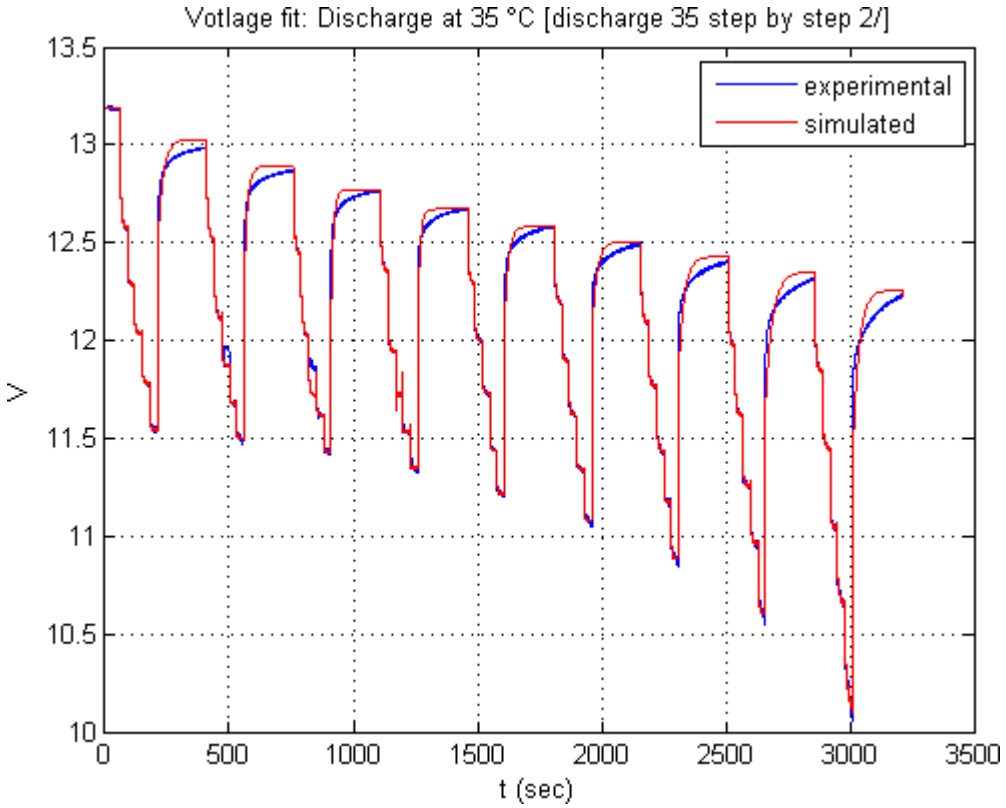

Figure 30

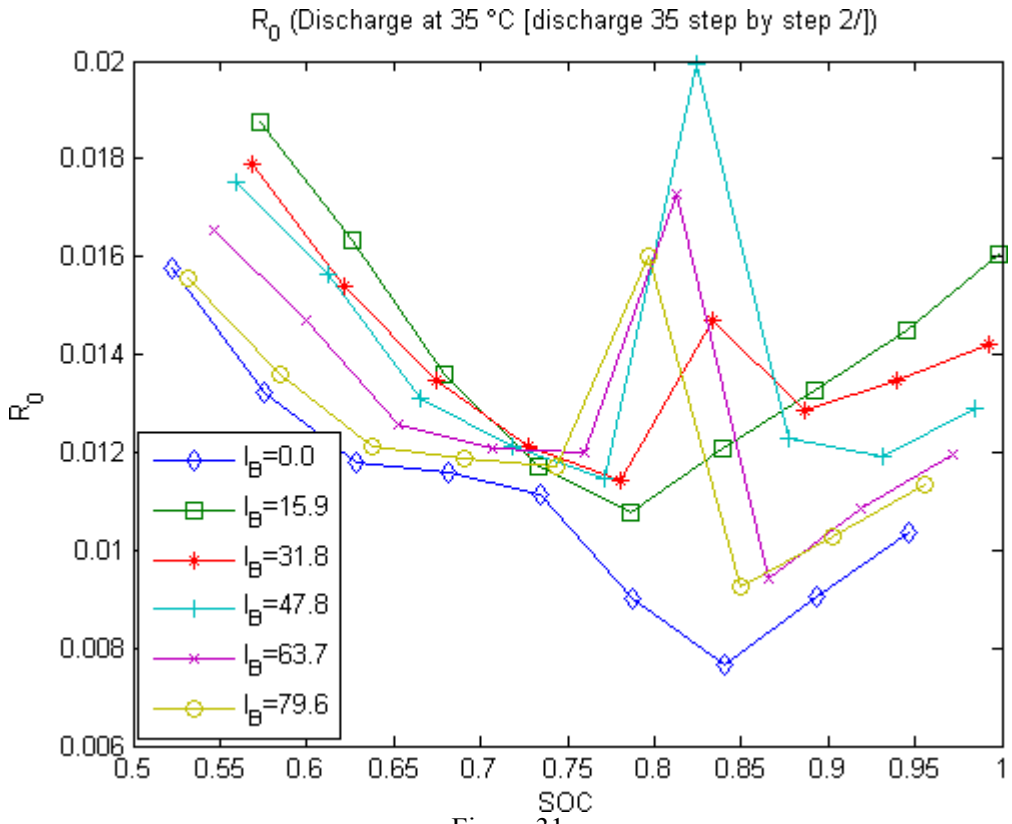

Figure 31

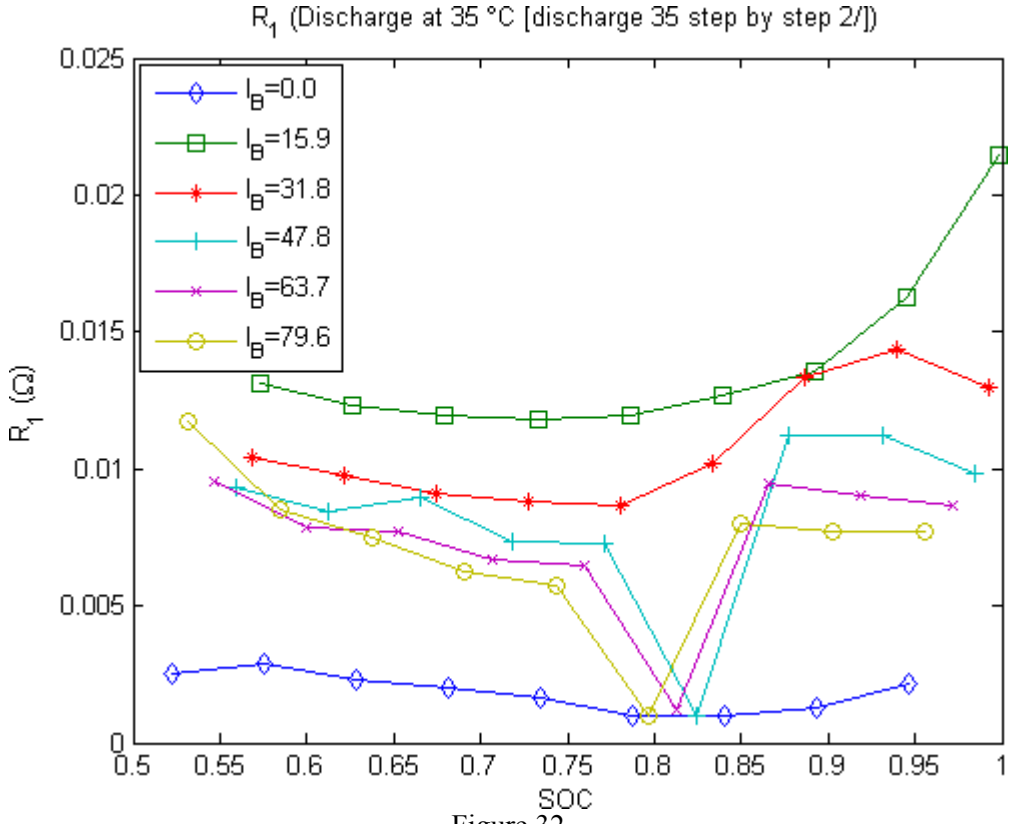

Figure 32

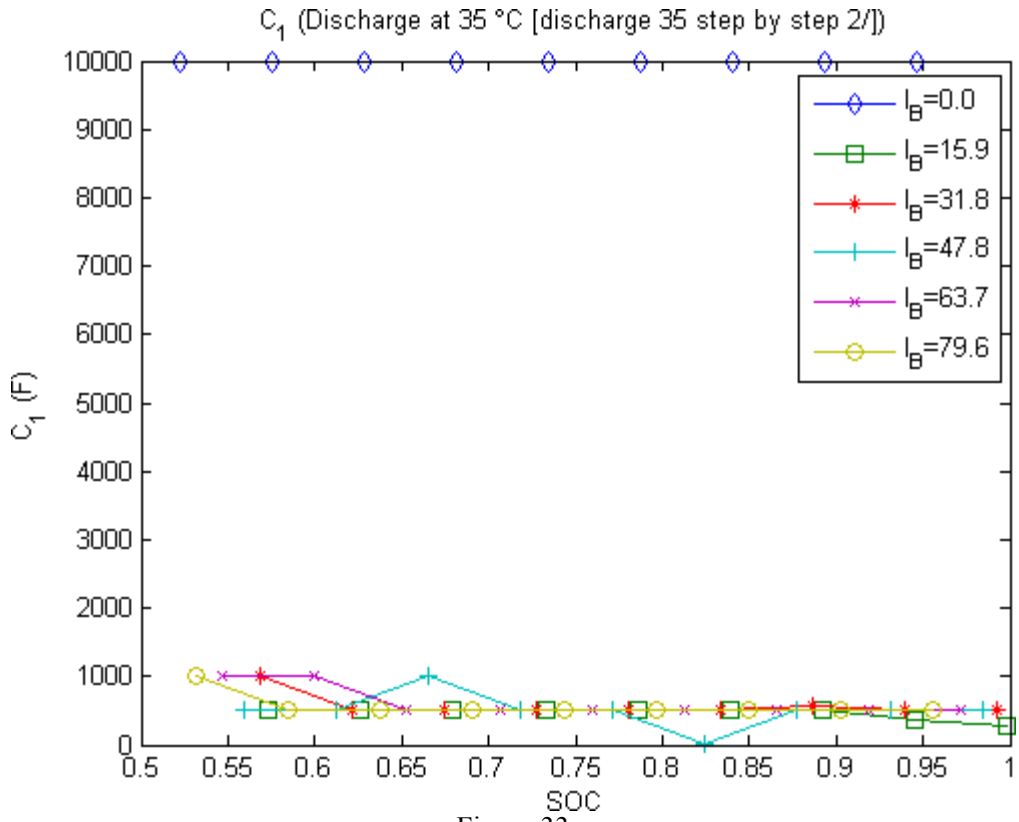
C1 (Discharge at 35 °C [discharge 35 step by step 2/])
C1 (F)
SOC
IB=0.0
IB=15.9
IB=31.8
IB=47.8
IB=63.7
IB=79.6
10000
9000
8000
7000
6000
5000
4000
3000
2000
1000
0
0.5
0.55
0.6
0.65
0.7
0.75
0.8
0.85
0.9
0.95
1
Figure 33

4.1.3 5 °C (discharging)

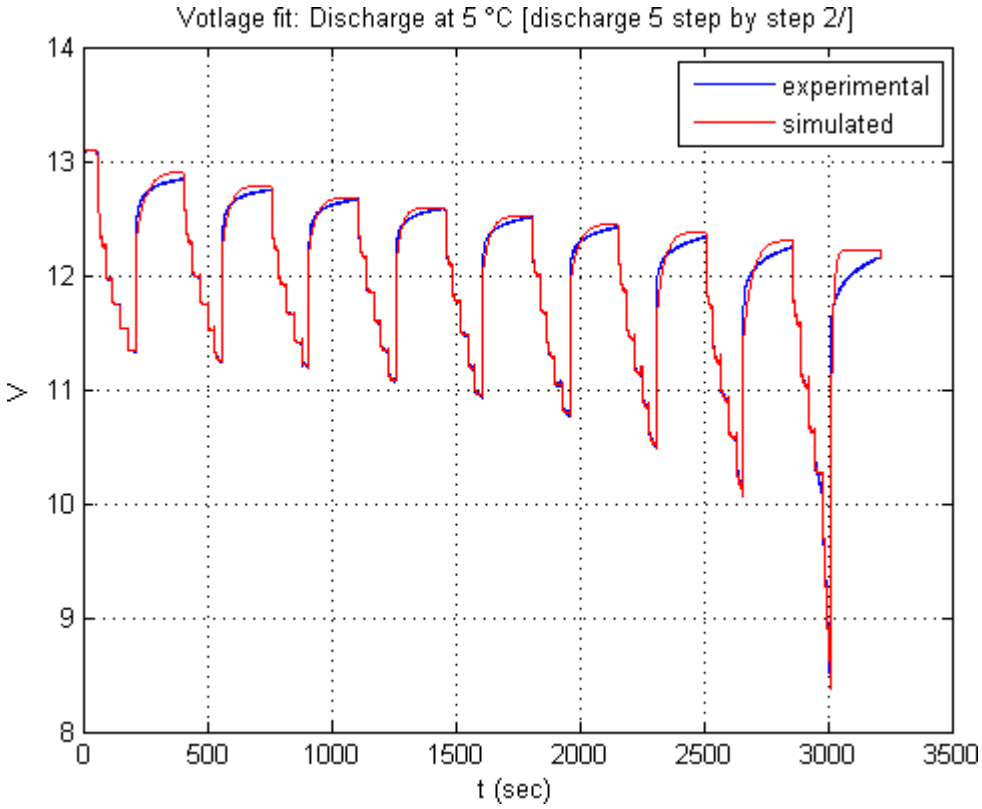

Figure 34

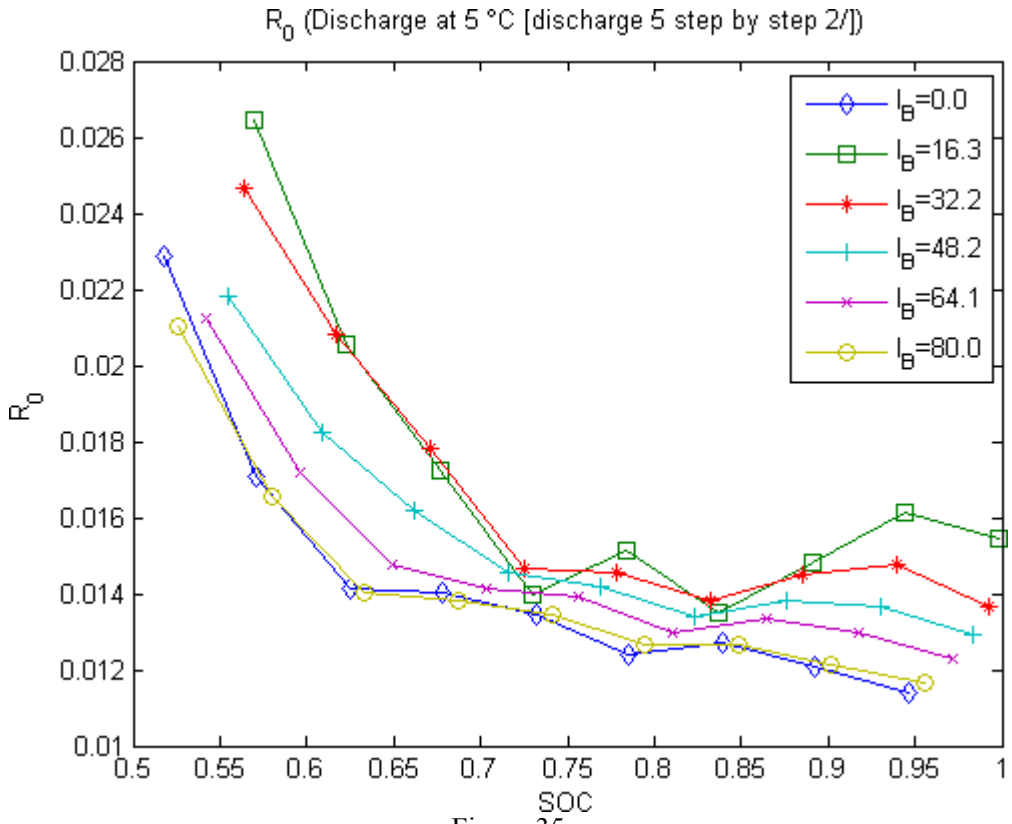

Figure 35

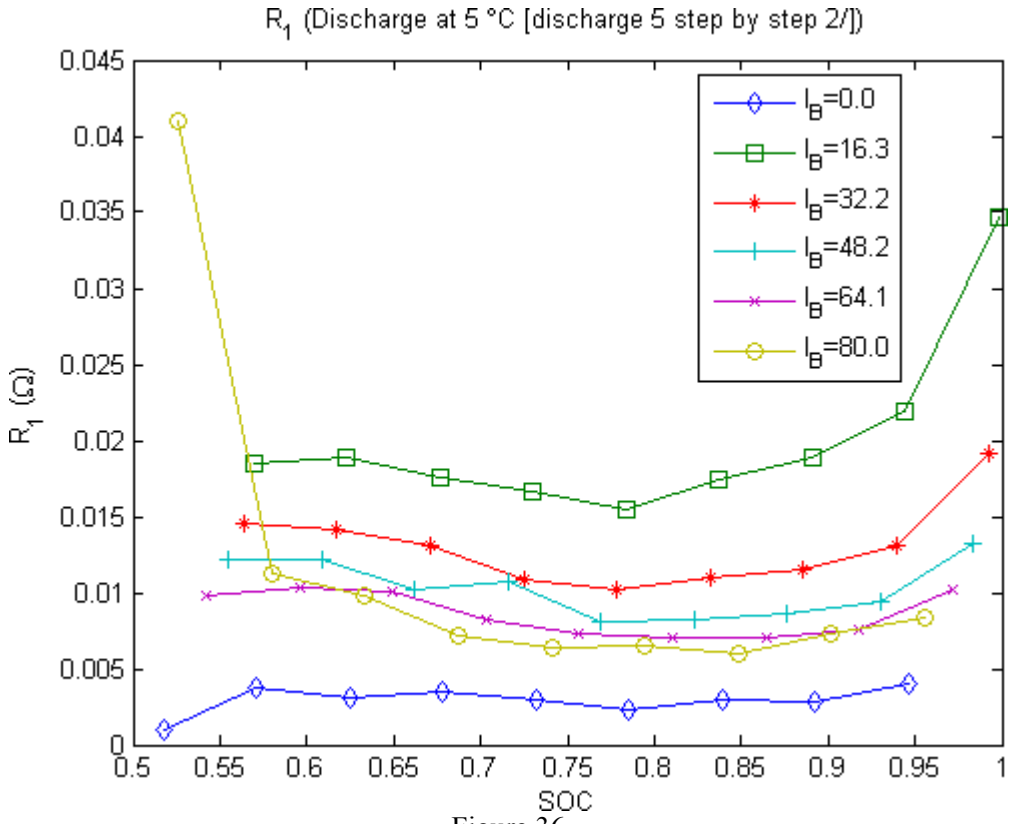

Figure 36

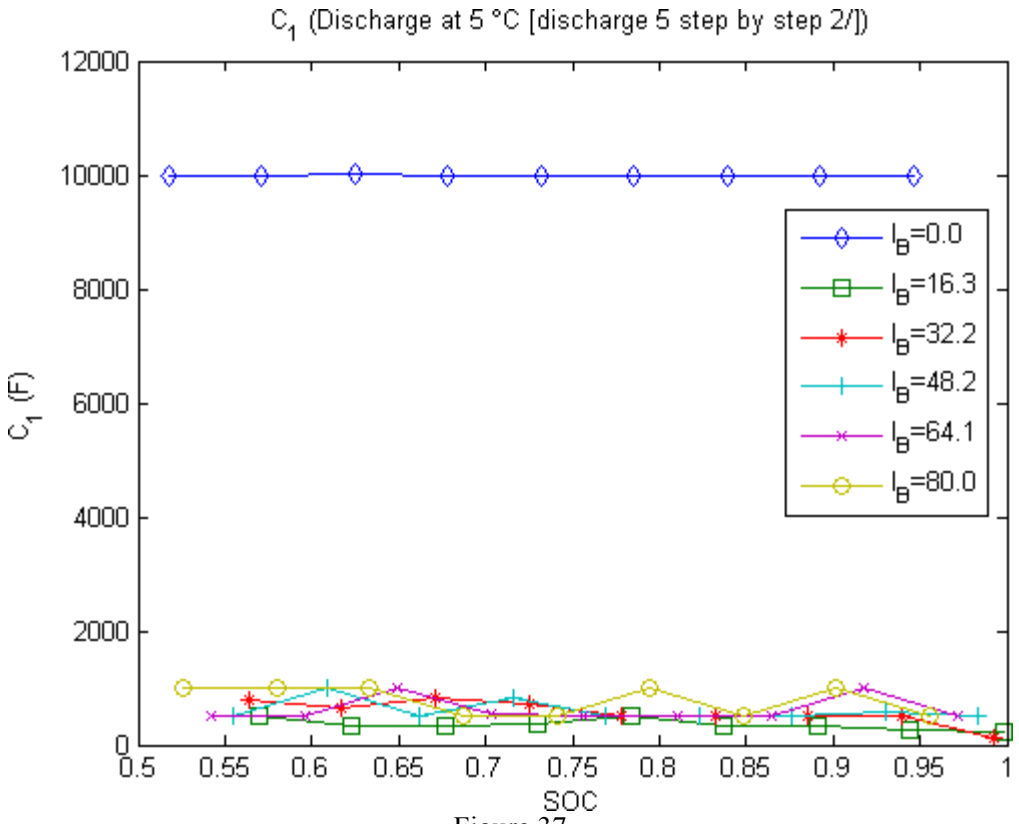
C1 (Discharge at 5 °C [discharge 5 step by step 2/])
12000
10000
8000
6000
4000
2000
0
C1 (F)
0.5
0.55
0.6
0.65
0.7
0.75
0.8
0.85
0.9
0.95
1
SOC
IB=0.0
IB=16.3
IB=32.2
IB=48.2
IB=64.1
IB=80.0
Figure 37

4.2 Charging results

4.2.1 20 °C (charging)

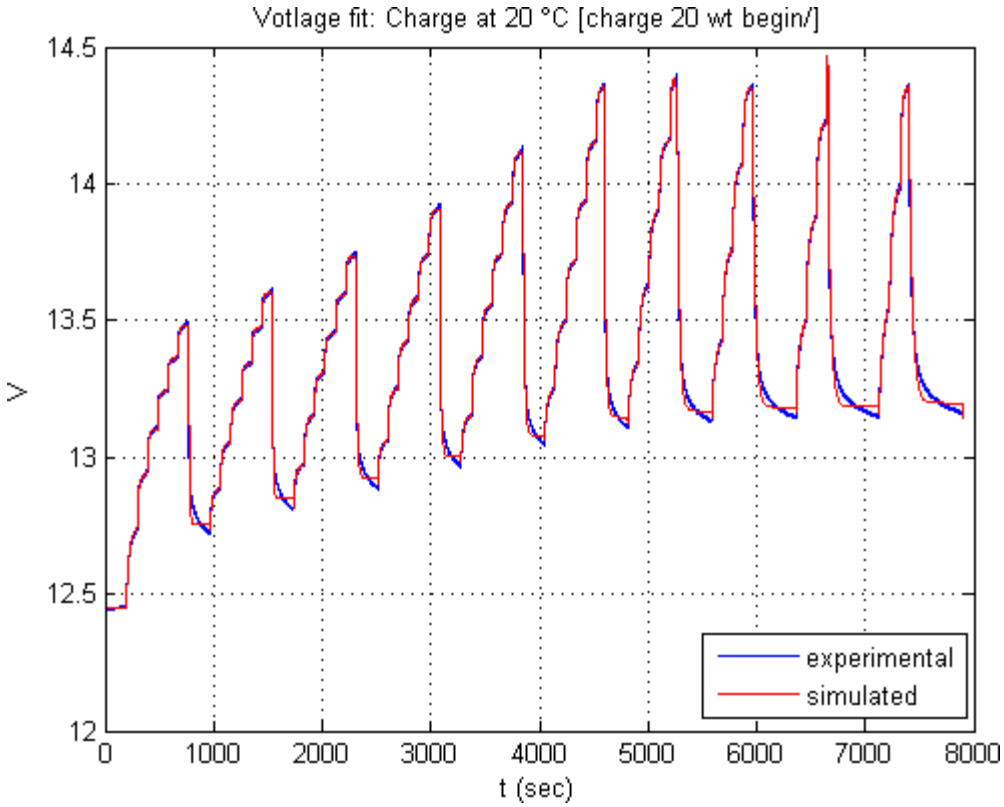

Figure 38

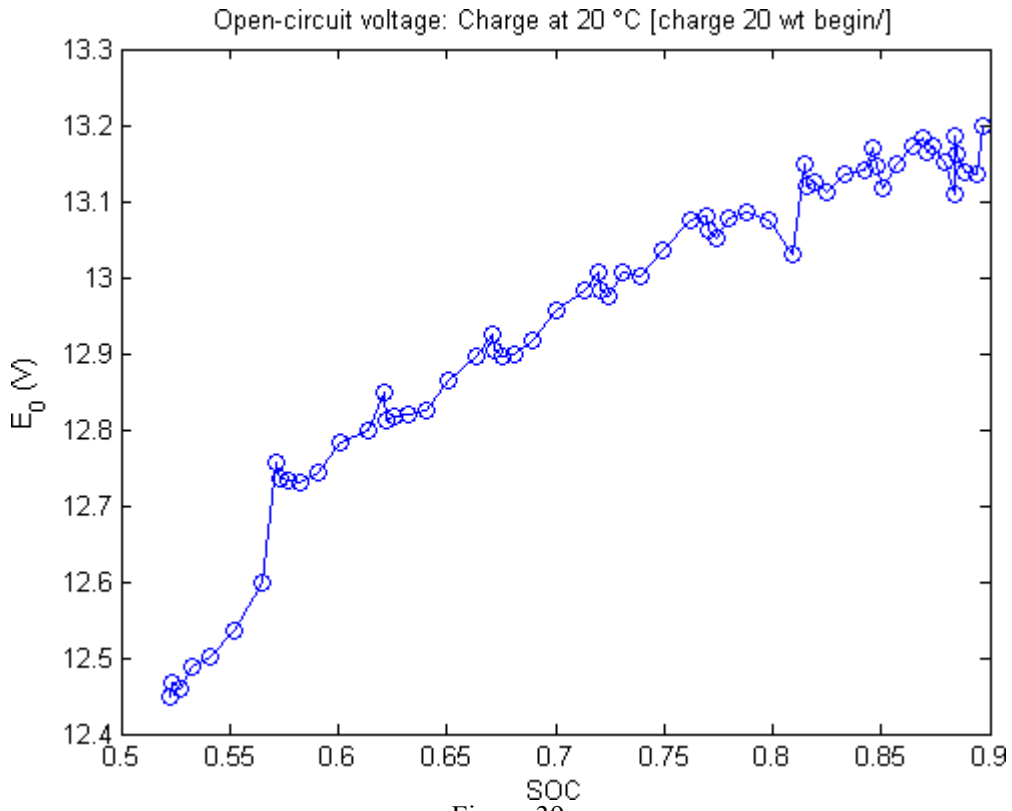

Figure 39

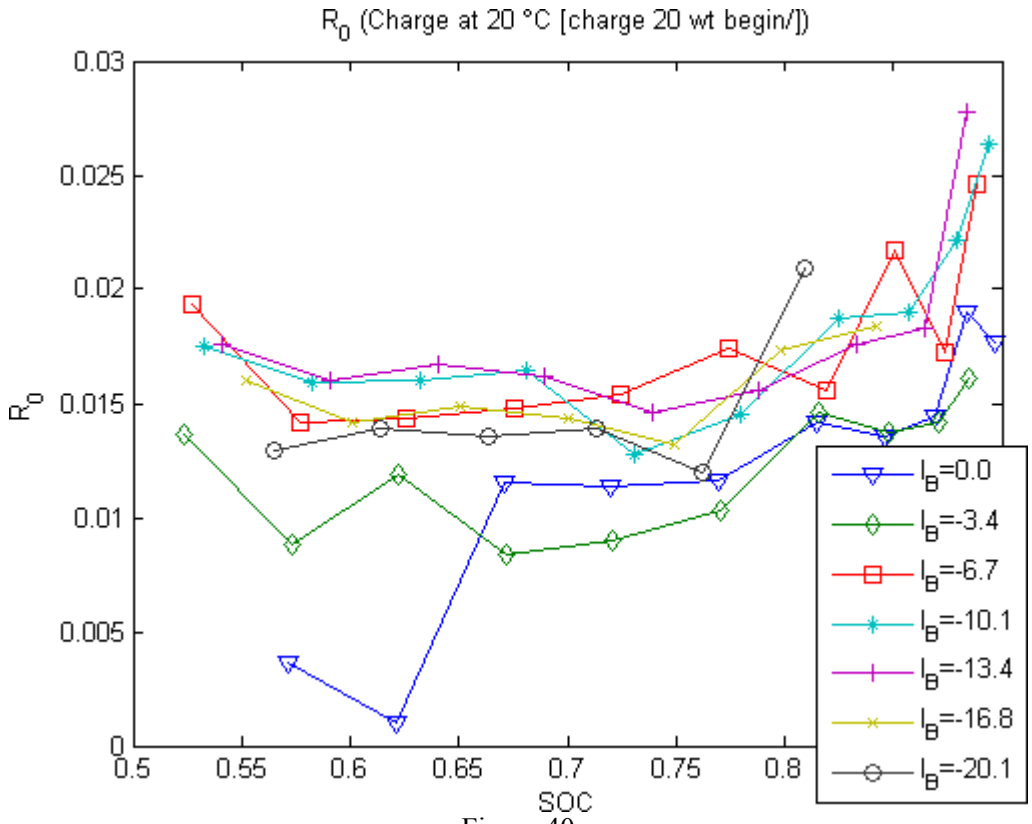

Figure 40

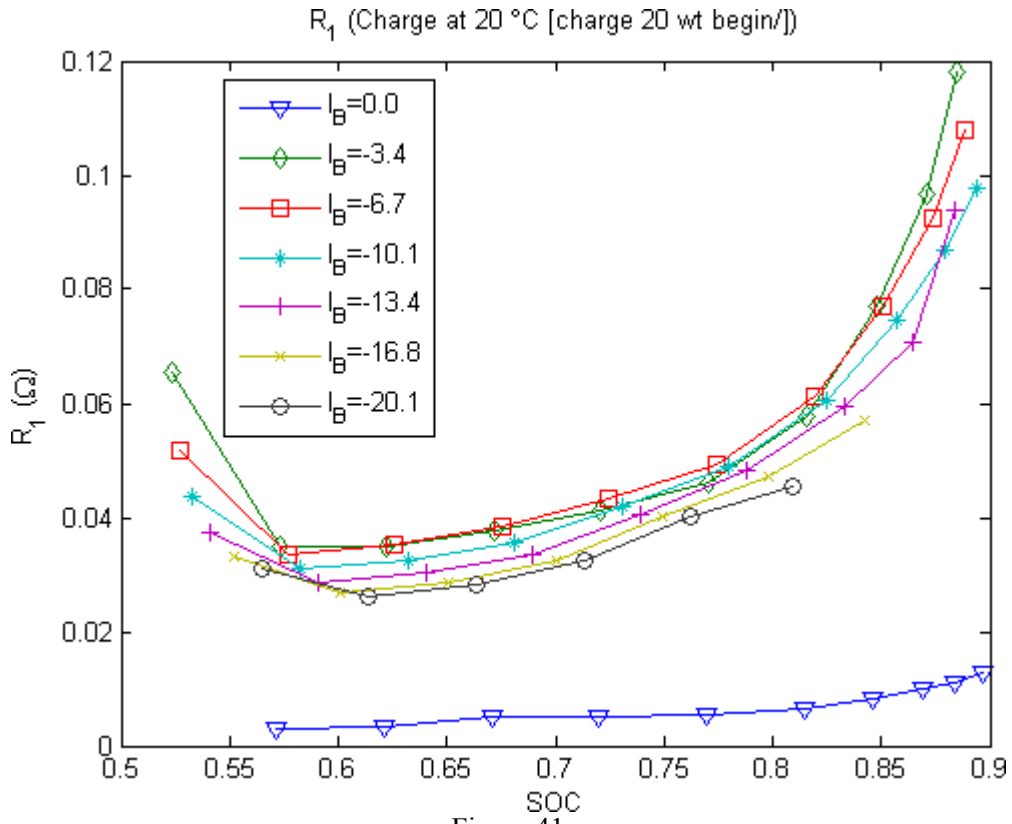

Figure 41

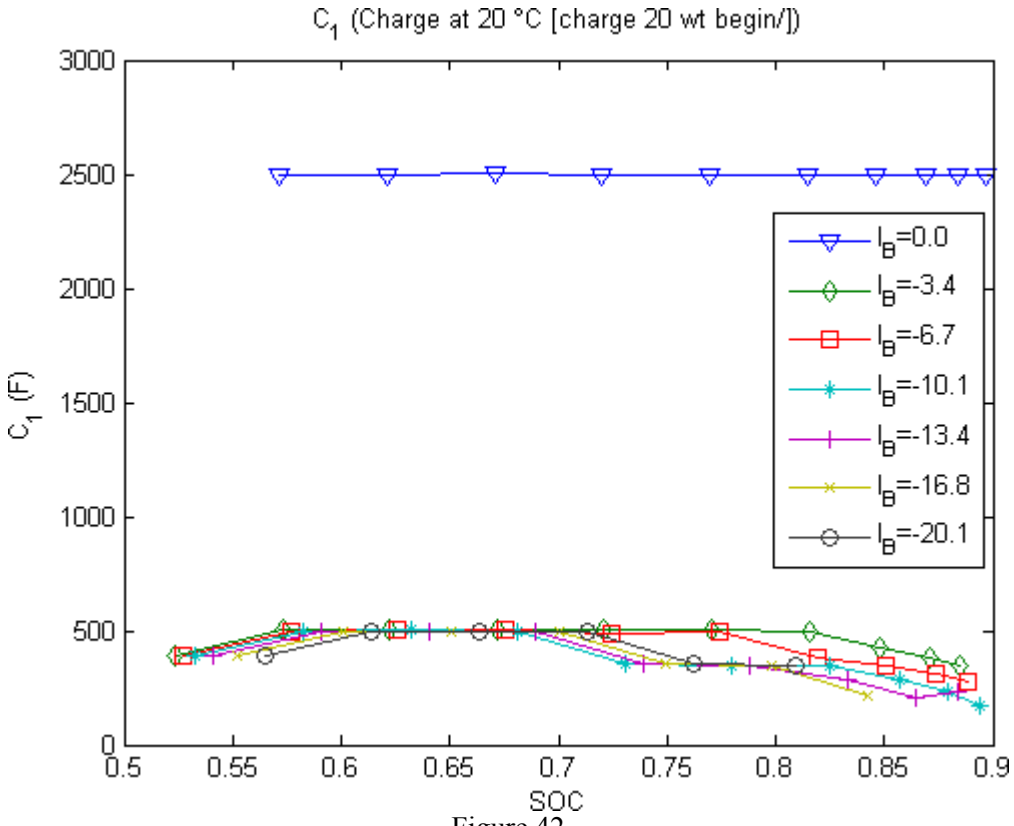

Figure 42

4.2.2 35 °C (charging)

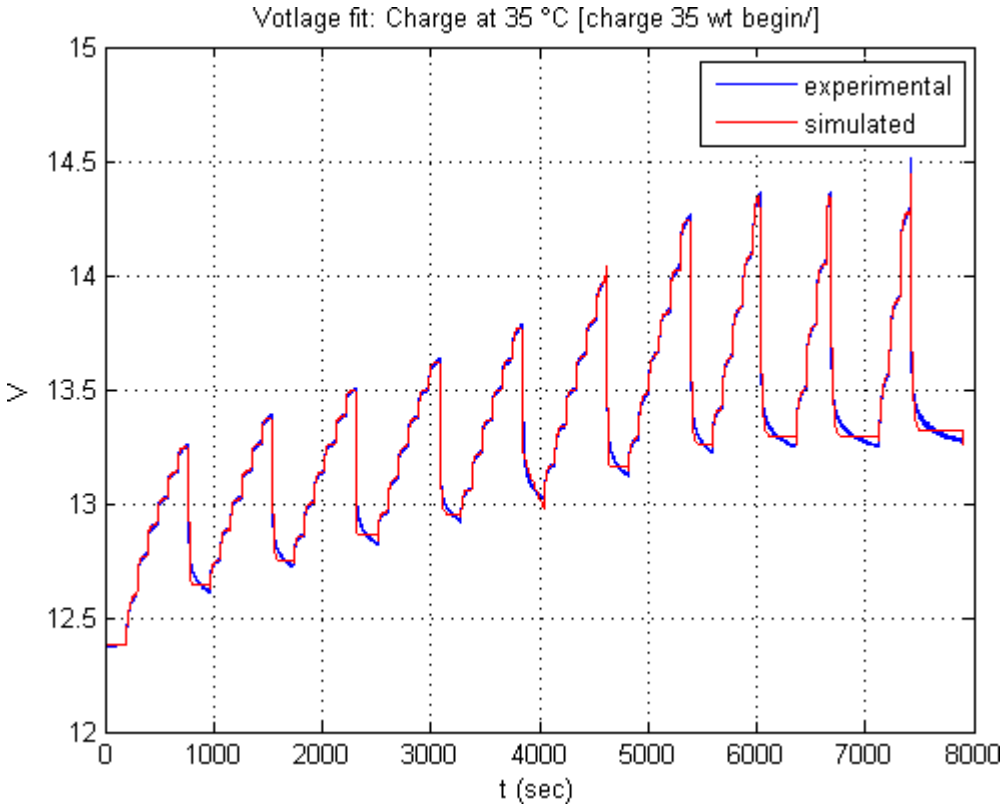

Figure 43

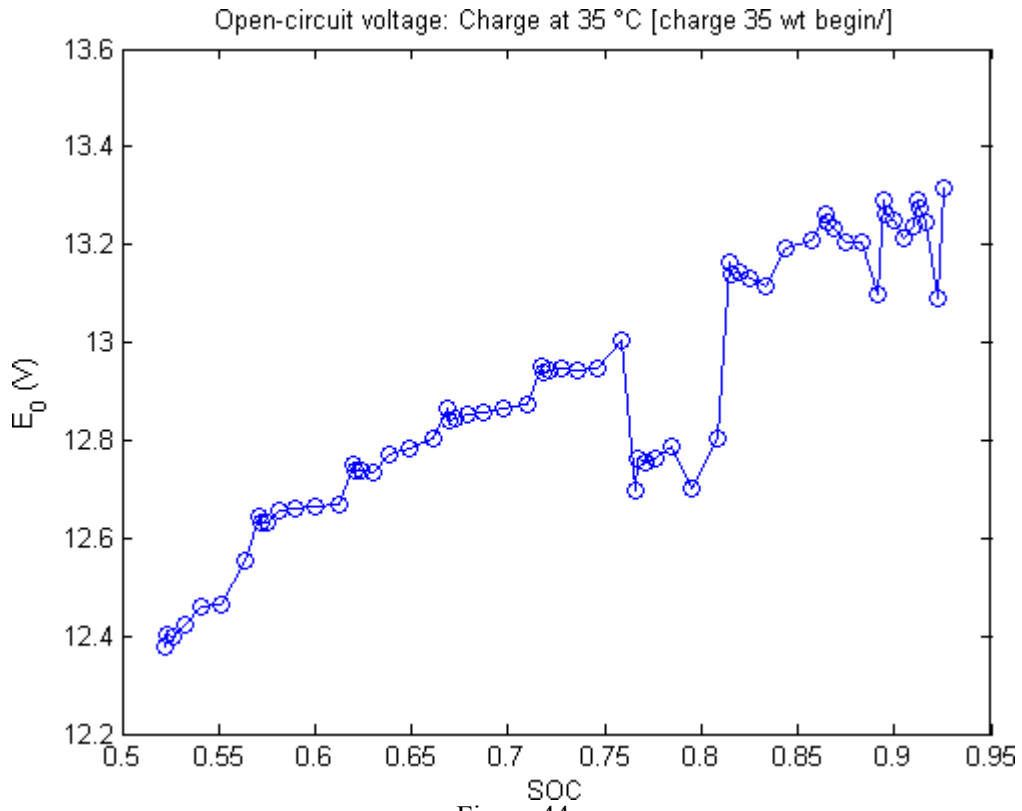

Figure 44

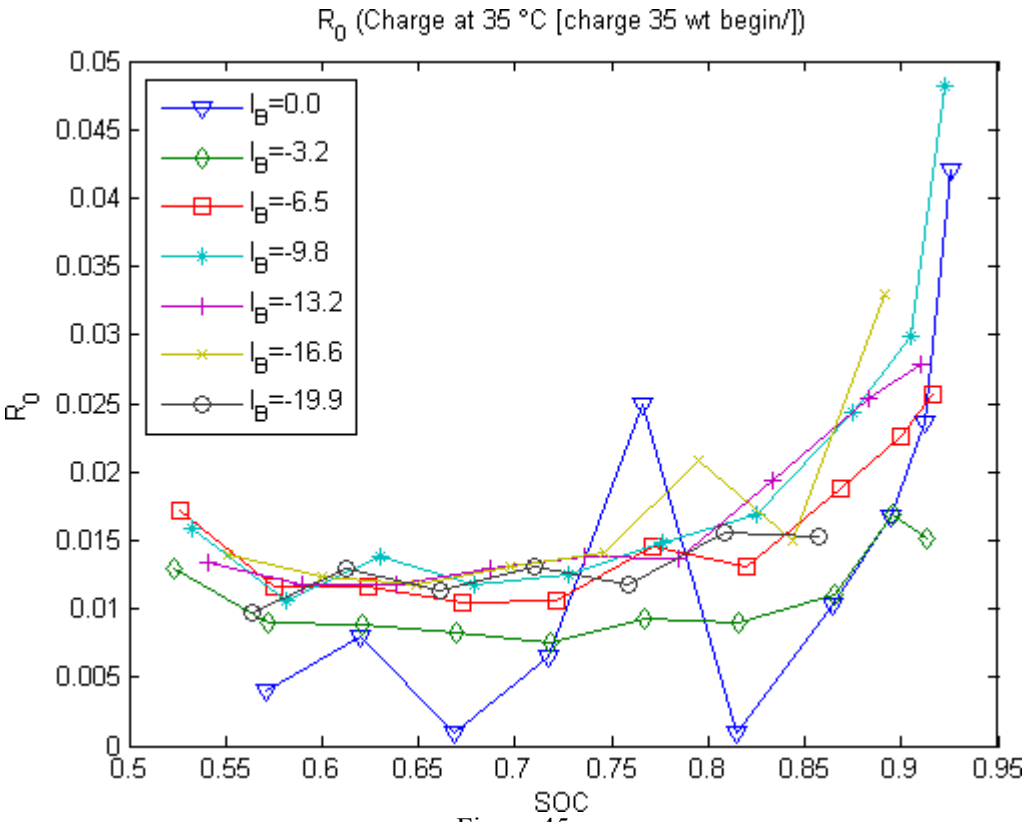

Figure 45

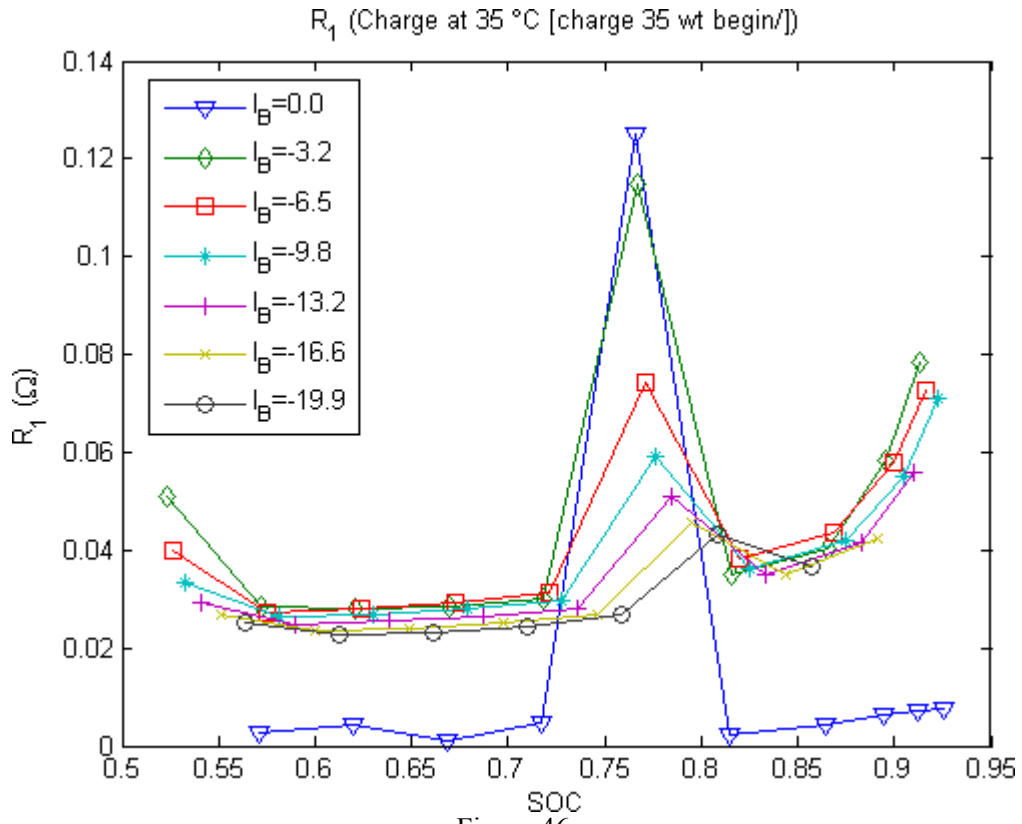

Figure 46

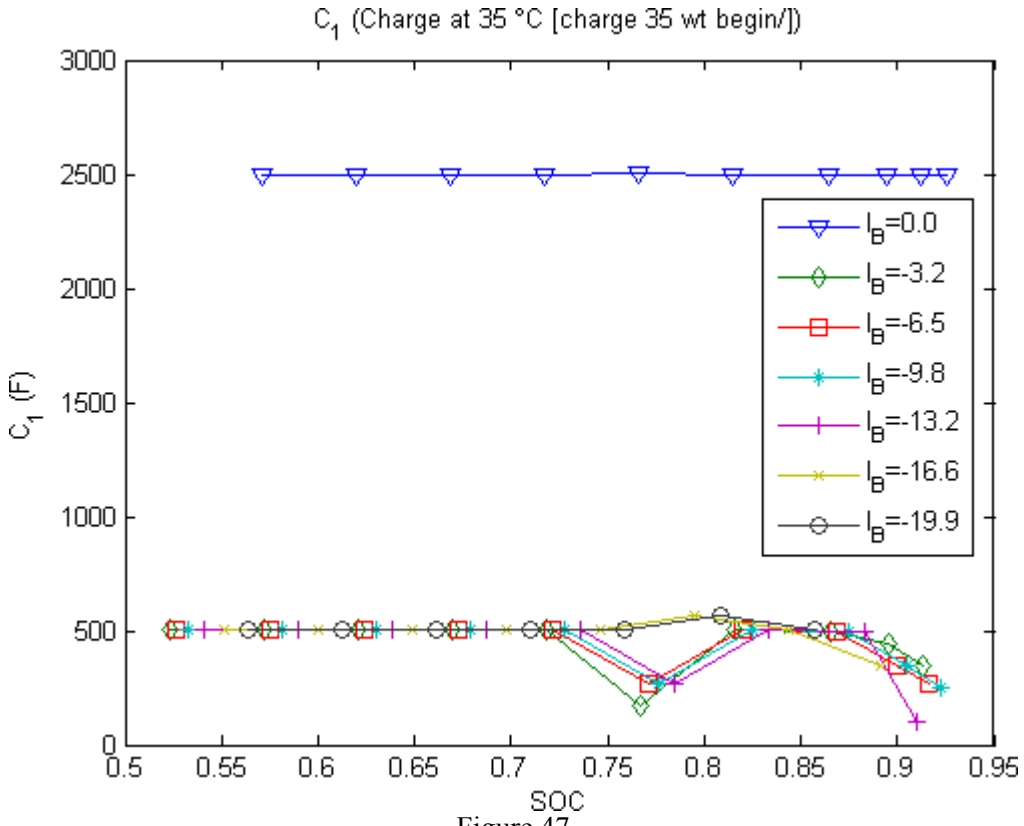

Figure 47

4.2.3 5 °C (charging)

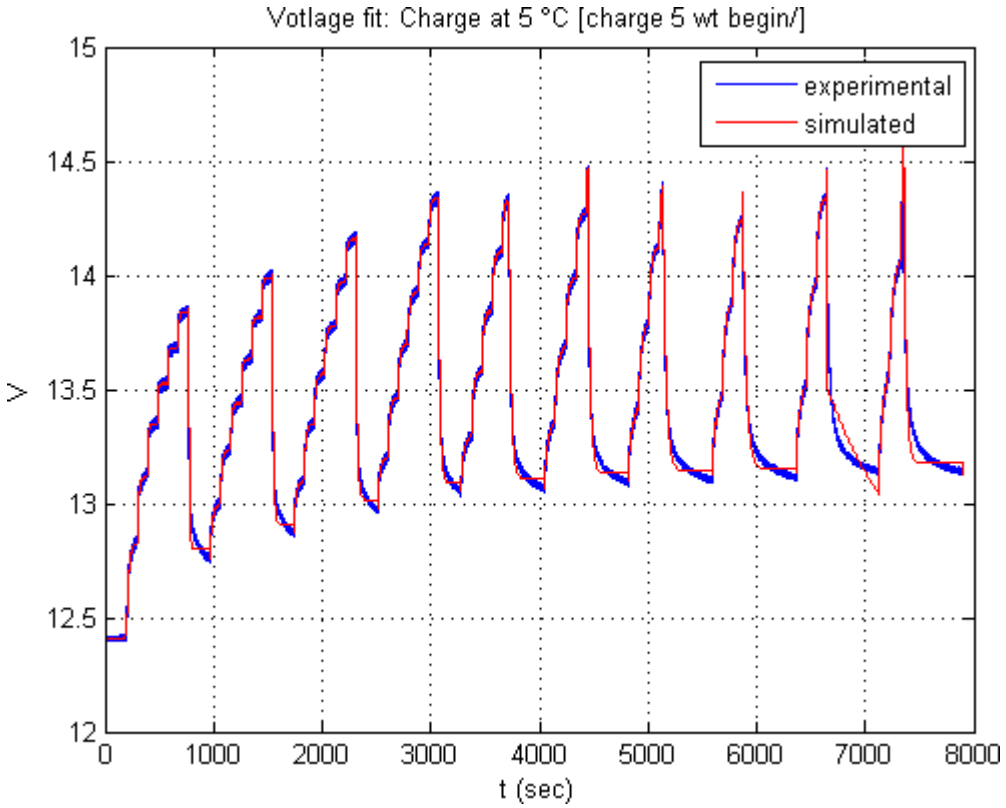

Figure 48

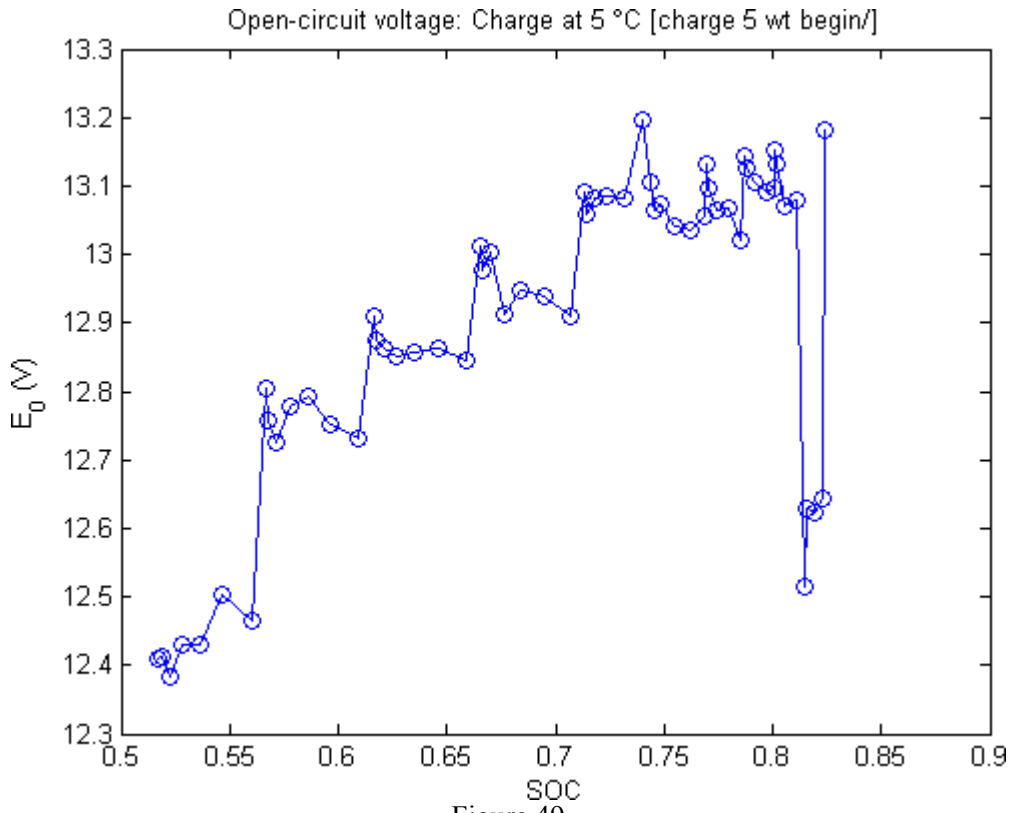

Figure 49

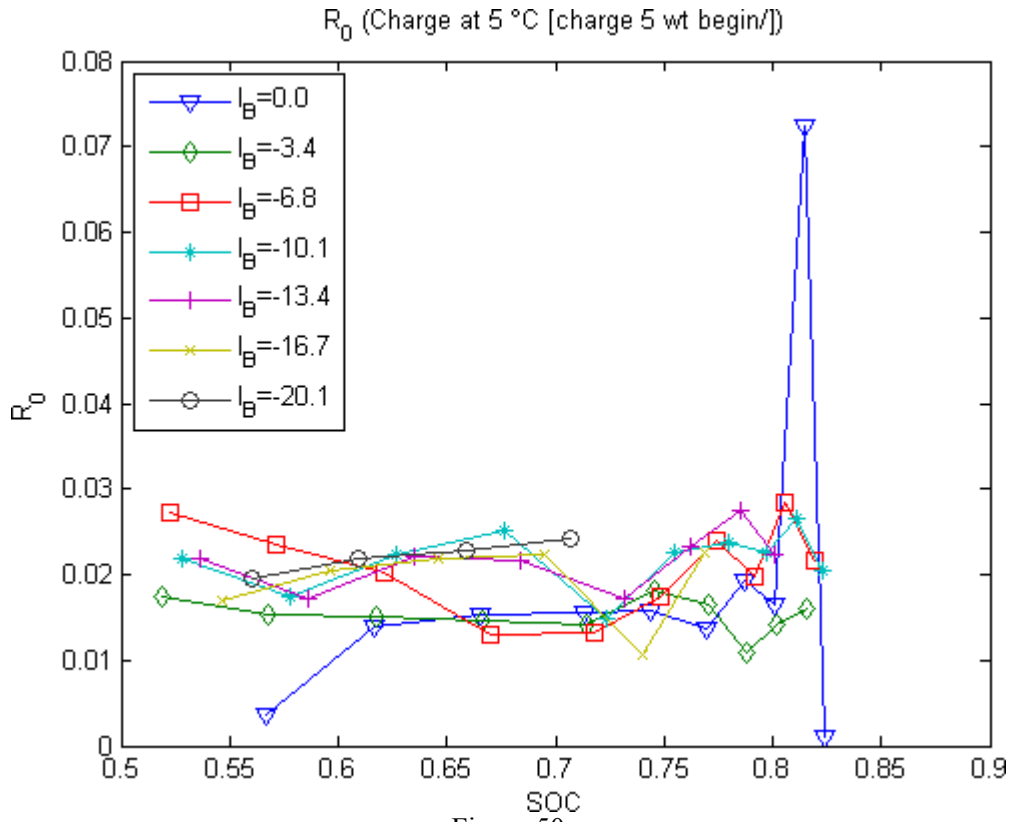

Figure 50

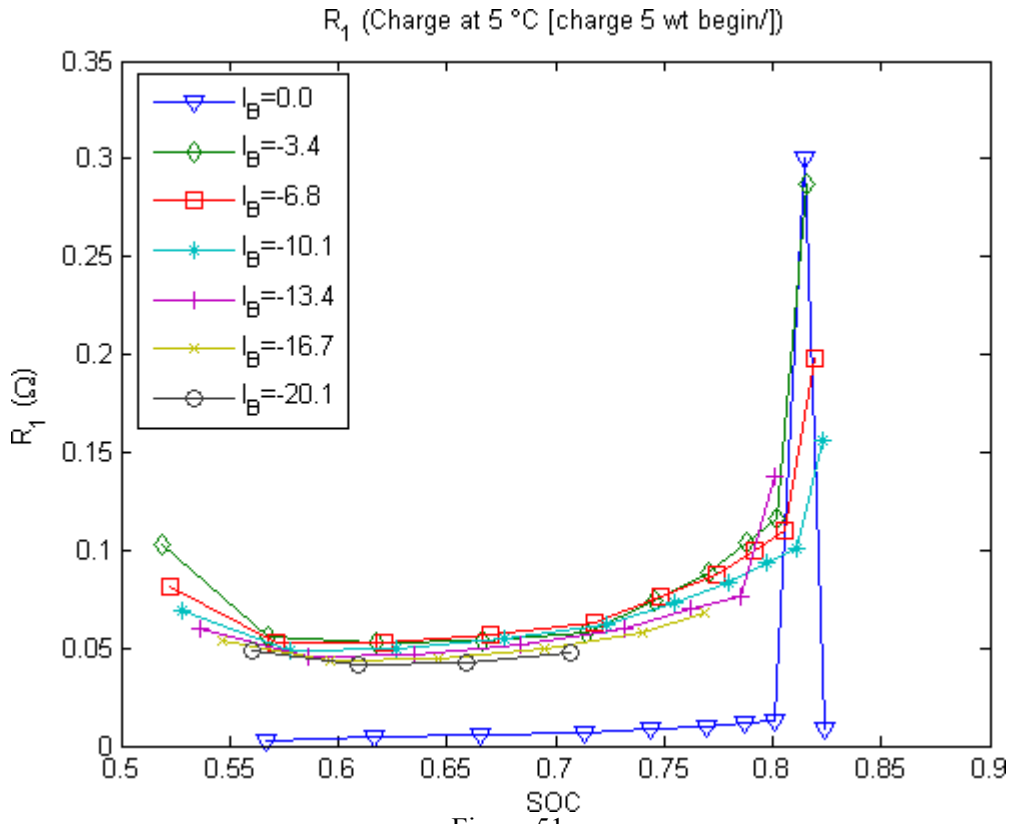

Figure 51

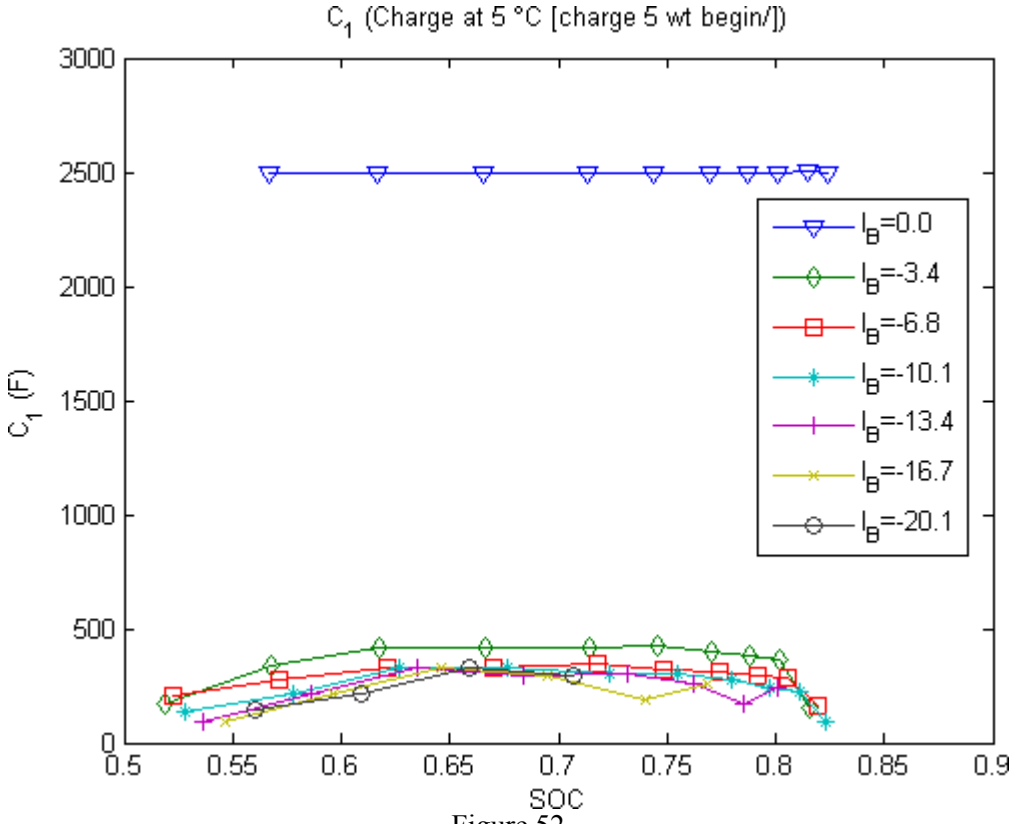

Figure 52

5 Conclusion and nomenclature

5.1 Conclusion and future work

The work here presents a common battery modeling methodology and the results of its application to modeling automotive lead-acid batteries over the range of environmental conditions that it is expected to operate in. The two major portions of the work, and the biggest contributions, was the experimental methods (excitation currents used) and parameter estimation. Both of these have appeared previously, and were applied successfully to the specific task of automotive battery modeling.

The work of this thesis presents an incomplete picture of the full process of modeling and fault-diagnosis of these batteries. The modeling was done separately from fault diagnosis; the fault modes were investigated and presented as a literature review, but no batteries were aged to validate or quantify these highly variable processes. The modeling also cannot be considered complete as it was based only on one battery.

A number of improvements could be made to the experimental methodology and analysis techniques presented in this work.

5.1.1 Experimental methodologies suggestions

The data acquisition (DAQ) hardware is quite adequate for battery modeling. However, the signal conditioning electronics designed for the [4] work are mysterious and not expandable. For example, it remains unclear exactly what kind of anti-aliasing is performed by the entire system on the signals that it samples. This is clearly a major area for future improvement; with proper anti-aliasing filters, a much lower sample rate may be selected (e.g., 20 Hz instead of 320), yielding less noisy data.

The software controlling the National Instruments DAQ hardware is written in LabView.

We reiterate the suggestion in [4]: it may be very beneficial for future users of the system to invest one or two weeks in rewriting the DAQ software in MATLAB, using the Data Acquisition Toolbox. This would allow much faster tuning of the experimental process and could enable sophisticated testing patterns. These can of course be implemented in LabView, but the majority of electrical and mechanical engineers working on battery technology at the Center for Automotive Research are much more familiar with the language-based programming style of MATLAB than the graphical style of LabView.

Also, the battery exercise experiments were done only on a single battery. The manufacturing variability of automotive batteries is known to be extremely high; the battery will ensure a certain minimum Ampere-hour capacity, but specimen may have much higher capacities. Therefore, a number of batteries should be tested.

The excitation current profile used here seems quite suitable for automotive batteries, and allows a battery to be characterized as such in three days.

5.1.2 Modeling work

The major concern that the excitation profile raises is the issue of surface charge. Clearly, this causes the open-circuit voltage hysteresis seen between the charge and discharge cases, and one can also clearly see the sharp rise in open-circuit voltage between pulses (during the 200+ seconds of rest) in the figures for charging above (Figures 44 and 49). It remains unclear how one can model these effects.

A second point about the modeling was raised in the previous chapter as well: the nonlinearity of the battery may not be reducible, for large currents, to local LTI models. Very preliminary EIS experimentation on automotive lead-acid batteries indicates that the effect of a nonlinear Warburg impedance (see page 28) is significant in the high and low frequency regions.

The effectiveness of the ARMA battery model (a simple IIR filter that implements the

system's differential equations) would be immense if the extraneous (negative) circuit parameters could be eliminated. The strength of using the form of the desired system itself, instead of the form of an input or output, is very attractive, without having to utilize exotic genetic algorithms or particle swarm optimizations.

Finally, we address the issue of a thermal model. All the work on parameter estimation done here assumes an isothermal environment, but during loading of the battery, there is certainly temperature changes. The question of how these microchanges affect battery characteristics remains open.

5.2 Nomenclature

5.2.1 Variables

Variable	*Name*	*Comments*
E_0, V_{oc}	Open-circuit voltage	In Volts.
R_0	Low-frequency resistance	In Ohms.
R_1	1st high-frequency resistance	In Ohms.
C_1	1st high-frequency capacitance	In Farads.
R_2	2nd high-frequency resistance	In Ohms.
C_2	2nd high-frequency capacitance	In Farads.
I_B	Battery current	In Amperes. >0 is discharge.
V_B	Battery terminal voltage	In Volts.
Q	State of charge	$0 \leq Q \leq 1$
ΔT	Temperature from ambient	In Celsius.
Q_0	Nominal capacity	In Ampere-hours.
C	Unit of current, equivalent to Q_0 in A.	In Amperes. E.g., 2C for a 50 Ah battery is 100 A.
Zw	Warburg impedance	A frequency-dependent complex impedance.

5.2.2 Acronyms

Acronym	*Explanation*
SOC	State of charge.

Acronym	*Explanation*
OCV	Open-circuit voltage.
A-h	Ampere-hours (measure of capacity).
SLI	Starting, lighting, ignition (automotive batteries).
VRLA	Valve-regulated lead-acid (maintenance-free batteries).
DTC	Diagnostic trouble code.
OBD	On-board diagnostics.
SOH	State of health (degradation due to aging).
KF	Kalman filter(ing).
EKF	Extended Kalman filter(ing).
NLTV	Nonlinear time-varying.
LTV	Linear time-varying.
LTI	Linear time-invariant.

6 References

[1] D. Berndt, E. Meissner, W. Rusch., "Aging effects in valve-regulated lead-acid batteries", Telecommunications Energy Conference, 1993. INTELEC '93. 15th International, Volume 2, 27-30 Sept. 1993, pp. 139-145.

[2] D. Linden, T.B. Reddy, *Handbook of batteries*, New York: McGraw-Hill, 2002.

[3] H.-S. Kim, *Dynamic Battery modeling in hybrid electric vehicles*, Masters thesis, The Ohio State University, 2002.

[4] K. Do, *A Dynamic electro-thermal model of double layer "supercapacitors' for HEV powertrain applications*, Masters thesis, The Ohio State University, 2004.

[5] Security Sales & Integration, "Minimum VRLA battery voltage." Online. http://www.securitysales.com/t_ci_articleView.cfm?aid=1263&sid=18

[6] HyperPhysics, "Lead-acid batteries." Online. http://hyperphysics.phy-astr.gsu.edu/Hbase/electric/leadacid.html

[7] ev-list-archive, Yahoo mailing list post, 2005. Online. http://autos.groups.yahoo.com/group/ev-list-archive/message/39454

[8] HowStuffWorks, "What is the difference between a normal lead-acid car battery and a deep cycle battery?" Online. http://auto.howstuffworks.com/question219.htm

[9] Smart Gauge Electronics, "A simple explanation of surface charge (and surface discharge)." Online. http://www.smartgauge.co.uk/surf_chg.html

[10] R. Somogye, *An aging model of NI-MH batteries for use in hybrid-electric vehicles*, Master's thesis, The Ohio State University, 2004.

[11] Panasonic Corporation, "HHR650D nickel metal hydride batteries: individual data sheet." Online. http://www.panasonic.com/industrial/battery/oem/images/pdf/hhr650d.pdf

[12] California Motors, "Hybrid systems: glossary of terms." Online. http://www.calmotors.com/faqs_glossary.html

[13] SmogSite.com, "On board diagnostics II theory." Online. http://www.smogsite.com/obd2.html

[14] Ramohalli, G., "The Honeywell on-board diagnostic and maintenance system for the Boeing 777", Digital Avionics Systems Conference, 1992. Proceedings, IEEE/AIAA 11th, 5-8 Oct 1992, pp. 485-490.

[15] John Neal, personal interviews: March 2005 – May 2006.

[16] Stobart, R., "Observers in engine control systems: What is the potential?" Automotive Applications of Advanced Modelling and Control, IEE Colloquium on, Vol., Iss., 16 Nov 1994. Pages:5/1-5/3.

[17] P. Pudney, *Optimal energy management for solar-powered cars*, Masters thesis, University of South Australia, 2000. Online. http://www.library.unisa.edu.au/adt-root/uploads/approved/adt-SUSA-20030403-114302/public/03part2.pdf

[18] S. Liu, R. Dougal, J. Weidner, L. Gao, "A simplfied physics-based model for nickel hydrogen battery", Journal of Power Sources, Vol. 141, Issue: 2, March 1, 2005. pp. 326-339.

[19] C.C. O'Gorman, D. Ingersoll, R.G. Jungst, T.L. Paez, "Artificial neural network simulation of battery performance", System Sciences, 1998., Proceedings of the Thirty-First Hawaii International Conference on Volume 5, 6-9 Jan. 1998, pp. 115-121, vol.5.

[20] E. Barsoukov, J.H. Kim, C.O. Yoon, H. Lee, "Universal battery parameterization to yield a non-linear equivalent circuit valid for battery simulation at arbitrary load", Journal of Power Sources, Vol. 83, Issue: 1-2, October, 1999. pp. 61-70.

[21] A. Jossen, "Fundamentals of battery dynamics", Journal of Power Sources, Vol. 154, Issue: 2, March 21, 2006. pp. 530-538.
[22] Zakaria Chehab, “Aging characterization of NIMH batteries for hybrid electric vehicles, Masters thesis, Ohio State University, 2006.
[23] Gamry Instruments, “Electrochemical Impedance Spectroscopy Theory: A Primer.” Online. http://www.gamry.com/App_Notes/EIS_Primer/EIS_Primer.htm
[24] S. Piller, M. Perrin, A. Jossen, "Methods for state-of-charge determination and their applications", Journal of Power Sources, Vol. 96, Issue: 1, June 1, 2001. pp. 113-120.
[25] J. Chiasson, B. Vairamohan, "Estimating the state of charge of a battery", Control Systems Technology, IEEE Transactions on, Volume 13, Issue 3, May 2005, pp. 465 – 470.
[26] B.S. Bhangu, P. Bentley, D.A. Stone, C.M. Bingham, "Nonlinear observers for predicting state-of-charge and state-of-health of lead-acid batteries for hybrid-electric vehicles", Vehicular Technology, IEEE Transactions on, Volume 54, Issue 3, May 2005, pp. 783-794.
[27] S. Sato, A. Kawamura, "A new estimation method of state of charge using terminal voltage and internal resistance for lead acid battery", Power Conversion Conference, 2002. PCC Osaka 2002. Proceedings of the, Volume 2, 2-5 April 2002 pp. 565-570.
[28] S. Pang; J. Farrell, J. Du, M. Barth, "Battery state-of-charge estimation", American Control Conference, 2001. Proceedings of the 2001, Volume 2, 25-27 June 2001, pp. 1644-1649.
[29] A. Kawamura, T. Yanagihara, "State of charge estimation of sealed lead-acid batteries used for electric vehicles", Power Electronics Specialists Conference, 1998. PESC 98 Record. 29th Annual IEEE, Volume 1, 17-22 May 1998 Page(s):583-587.
[30] J. Mendel, *Lessons in Estimation Theory for Signal Processing, Communications, and Control*, Englewood Cliffs, N.J.: Prentice Hall PTR, 1995.
[31] Steven Kay, *Fundamentals of Statistical Signal Processing, Volume I: Estimation Theory*, Englewood Cliffs, N.J.: Prentice Hall PTR, 1993.
[32] P.E. Pascoe, H. Sirisena, A.H. Anbuky, "Coup de fouet based VRLA battery capacity estimation", Electronic Design, Test and Applications, 2002. Proceedings. The First IEEE International Workshop on, 29-31 Jan. 2002, pp. 149-153.
[33] C.S.C. Bose, F.C. Laman, "Battery state of health estimation through coup de fouet", Telecommunications Energy Conference, 2000. INTELEC. Twenty-second International, 10-14 Sept. 2000, pp. 597-601.
[34] F. Badin, O. Briat, S. Olivier, B. Jeanneret, R. Trigui, B. Malaquin, “The use of batteries in hybrid vehicles”, IEEE International Symposium on Vehicular Power and Propulsion, Paris, France, October 6-8, 2004.
[35] R. Wagner, "Failure modes of valve-regulated lead/acid batteries in different applications", Journal of Power Sources, Vol. 53, Issue: 1, January, 1995. pp. 153-162.
[36] P. Ruetschi, "Aging mechanisms and service life of lead-acid batteries", Journal of Power Sources, Vol. 127, Issue: 1-2, March 10, 2004. pp. 33-44.
[37] H.A. Catherino, F.F. Feres, F. Trinidad, "Sulfation in lead-acid batteries", Journal of Power Sources, Vol. 129, Issue: 1, April 15, 2004. pp. 113-120.
[38] Mega Pulse Battery, “Frequently asked questions”. Online. http://www.megapulse.net/FAB/faq.htm
[39] Magna Labs, “Magna Labs 6, 12, 24, and 36Volt "Tuned Frequency" Pulse De-Sulfation Units”. Online. http://www.magnalabs.com/desulfate1.htm
[40] Battery Pulse, “MAXI-Life Pulse”. Online. http://www.batterypulse.com/
[41] Energizer Holdings, “Nickel-metal hydride: application manual”. Online.

http://data.energizer.com/PDFs/nickelmetalhydride_appman.pdf